LARS Technical Report 091487

Spatial Filtering of Shuttle Imaging Radar-B Data

by

Paul W. Mueller

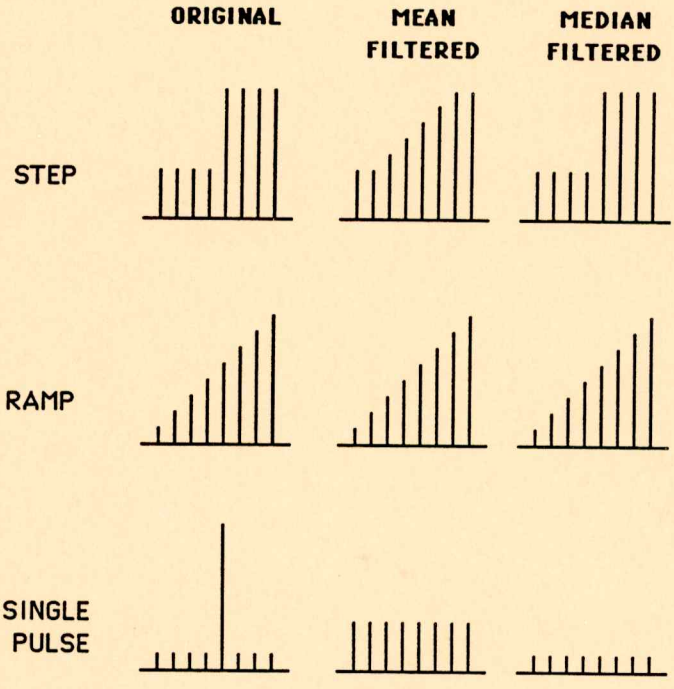

Department of Forestry and Natural Resources

in cooperation with

Laboratory for Applications of Remote Sensing

Purdue University West Lafayette, Indiana 47907

LARS Technical Report 091487

SPATIAL FILTERING OF SHUTTLE IMAGING RADAR-B DATA

by

Paul W. Mueller

Department of Forestry and Natural Resources
in cooperation with
Laboratory for Applications of Remote Sensing
Purdue University
West Lafayette, Indiana 47907

Research Supported by JPL Subcontract 956952
under NASA Contract NAS7-918

This report is dedicated to the memory of the crew of the Space Shuttle Challenger who lost their lives in January 1986 while pursuing increased knowledge and understanding of our planet and universe. May we learn from their sacrifice and continue the utilization of space for such peaceful purposes as remote sensing of our earth. The SIR-B data utilized in this study were obtained from Challenger during Flight 41-G in October 1984.

ACKNOWLEDGMENTS

This research was supported by Subcontract 956952 from the Jet Propulsion Laboratory (JPL) under NASA contract NAS7-918. Martin Ruzek and the JPL staff are acknowledged for their efforts in the acquisition and correlation of the SIR-B data and also the registration of these data to the Thematic Mapper data. Champion International Corporation, Owens-Illinois Incorporated, Southern Resin and Chemical Company, and the USDA-Forest Service, are acknowledged for providing forest stand information and maps and also access to their landholdings in the study site area. Additionally, acknowledgment is made of Dr. Roger Hoffer, who is the SIR-B Principal Investigator for this subcontract and also my major professor, for his guidance, help, and support of this research. Finally, Fabian Lozano and my other colleagues and professors at Purdue University are gratefully acknowledged.

TABLE OF CONTENTS

Page

LIST OF TABLES

LIST OF FIGURES

Figure Page

ABSTRACT

Mueller, Paul William. M.S.For., Purdue University, December 1987. Spatial Filtering of Shuttle Imaging Radar-B Data. Major Professor: Roger M. Hoffer.

In the past few years, interest in assessing and mapping forest resources with synthetic aperture radar (SAR) data has been steadily increasing. Many of the digital analysis techniques and procedures developed and tested for use with optical (multispectral scanner) data do not work as well with SAR data, due to the distinctly different inherent characteristics of SAR data, such as speckle. Radar speckle increases the variance within SAR data, and increased variance adversely affects the ability to discriminate different cover types when using various pattern recognition techniques. Although spatial filters have often been used with SAR data for reducing speckle effects, no study to determine the most effective filter treatment for improving classification results was found when conducting the literature search.

The purpose of this study was to determine the most appropriate low-pass spatial filter treatments for reducing speckle effects in Shuttle Imaging Radar-B (SIR-B) digital

data that is to be utilized for assessing forest resources. The SIR-B data set utilized consisted of a L-band HH polarized multi-angle data collected during Space Shuttle Flight 41-G at center incidence angles of 28.4°, 45.3°, and 58.4°. The study site was located in northeastern Florida. The pixel size of the unfiltered data was 28.5 meters.

Thirty-four filter treatments were applied to the data. These treatments included the use of square mean, separable mean, square median, and separable recursive median algorithms implemented at 1 to 3 iterations with window sizes ranging from 1 x 3 to 1 x 9 (separable filters) and 3 x 3 to 7 x 7 (square filters).

Both quantitative and qualitative evaluation techniques were utilized. Four specific evaluation studies were conducted: Cover Type Differentiation Study, Edge/Boundary Retention Study, Cover Type Classification Study, and Visual Assessment Study. Distinct differences resulting from algorithm, window dimension, and iteration were found. Based on all tests, the 3 x 3 square median filter implemented twice (2 iterations) provided the best overall results based on all tests. This study clearly demonstrated the benefits of filtering SAR data.

CHAPTER 1

INTRODUCTION

Satellite-acquired remote sensor data offers a synoptic view of earth resources, and through the use of computer-aided analysis techniques, digital remote sensor data can be classified according to resource cover types. The majority of these analysis techniques have been utilized with optical data obtained by the Landsat Multispectral Scanner (MSS) sensor and recently the Landsat Thematic Mapper (TM) sensor. Numerous studies have shown that MSS and TM data can be utilized effectively to classify forest cover. The use of MSS data is reviewed by Cihlar (1986), while studies involving TM data include those by Lillesand and Lo (1985) and Mueller et al. (1985a).

There has been increased interest in the utilization of data acquired beyond the optical portion of the electromagnetic spectrum (i.e. microwave) and the majority of this interest has focused on radar data. Although radar systems produce imagery somewhat similar to that generated by optical-region sensors, radar imagery must be

interpreted very differently due to the unique characteristics of radar systems and microwave signal-target interactions. Radar systems involve active sensors, and therefore they can acquire image data of the earth's surface independent of solar illumination or weather conditions such as clouds. Radar can penetrate cloud cover, whereas clouds frequently hinder the acquisition of timely data with optical systems. The radar backscatter (portion of signal that is returned to sensor) is influenced by both system and target parameters. System factors include the operating wavelength, viewing geometry, and polarization of both the signal and backscatter. Characteristics of the target influencing backscatter include surface slope and roughness, electrical properties, and the target orientation and structure. Modeling the complex interactions of these factors is a topic of much current research.

From an applications standpoint, relatively little research has been conducted to quantitatively analyze digital satellite-acquired radar data to evaluate its usefulness for identifying forest vegetation and determining forest cover type characteristics. The potential utility of SAR data for forestry studies is recognized by researchers and applications scientists, but its level of effectiveness has yet to be fully determined (ERIM 1986). Research in the 1960's was concentrated on

the use of relatively short wavelength Ka-band radars flown from aircraft altitudes (Morain and Simonett 1967). During the late 1960's and early 1970's, relatively little research was conducted with imaging radars. However, one of the most ambitious operational radar mapping projects ever was conducted in Brazil's Amazon Basin with X-band (3 cm) aircraft radar to survey and map the natural resources of the region (van Roessel and de Godoy 1974; de Azevedo 1971).

During the late 1970's, interest in forest mapping with aircraft radar imagery increased (Goodenough et al. 1980; Knowlton and Hoffer 1981). With the launch of Seasat in 1978, and the Shuttle Imaging Radar-A (SIR-A) and SIR-B in 1981 and 1984, respectively, satellite radar data became available. SIR-B was a synthetic aperture radar (SAR) that had the capability to orient its antenna at various angles relative to the Earth's surface--a first from space altitudes. For land areas that were imaged more than once at different angles of measurement, the resulting multi-angle SAR data sets provided unique opportunities to quantitatively study the advantage of multi-angle data and differences between the individual angle data sets. In addition to the multi-angle data obtained by SIR-B, this radar system provided the first true digital satellite SAR data (Curlander 1986). Since hardware restrictions on digital recording and processing of SAR have only recently

been overcome (ERIM 1986), all radar data sets used in forestry studies prior to SIR-B had been optically recorded. Although such optically recorded output film products can be digitized by electronic scanning, this process does not provide the dynamic range nor geometric fidelity that the recently developed digital correlation procedures can provide.

The research described in this thesis is part of a larger study entitled "Microwave and Optical Remote Sensing of Forest Vegetation" coordinated by Dr. Roger M. Hoffer who is a SIR-B Investigation Team Member. The purpose of the larger study, as described by Hoffer (1984), is to determine the utility of multi-angle SAR data for identifying forest cover and characterizing forest stand conditions (e.g. inventory parameters) when used singly and in combination with Landsat Thematic Mapper data.

Although digital analysis techniques and procedures developed and tested for use with multispectral scanner (optical) data have proven to be very effective, there was concern that such techniques might not work as well with SAR data, due to the distinctly different inherent characteristics of SAR data, including speckle noise and complex signal-target interactions. Speckle noise, caused by the radar return randomly fluctuating across extended targets, increases the variance within SAR imagery which can adversely affect the ability to discriminate different

cover types with pattern recognition techniques. Although spatial filters have been used with SAR data in the past (Brisco et al. 1983; Goodenough et al. 1980; Knowlton and Hoffer 1983; Sader 1987; Wu 1984), no study to determine the most effective filter treatment for improving classification results has been published, to the best of the author's knowledge. Theoretical development and evaluation of several filters are available (Chin and Yeh 1983; Gallagher and Wise 1981; Huang 1981; Nodes and Gallagher 1982, 1983), but there is a void of practical results from actual image data sets being filtered as a preprocessor to classification. The purpose of this study, therefore, is to evaluate various preprocessing techniques as an aid to further digital processing of SIR-B digital data. To achieve this goal, several low-pass spatial filter treatments will be evaluated. As the variance is reduced with low-pass spatial filters, there is a trade-off in that image sharpness decreases and narrow linear features tend to be lost. Therefore, both quantitative and qualitative evaluation techniques will be necessary to identify the most appropriate filter treatment(s).

Objectives

The overall objective of this research is to identify the most appropriate low-pass spatial filter treatment(s)

for reducing speckle effects in SIR-B digital data that is to be utilized for assessing forest resources.

Specific sub-objectives are:

1) Define methods for evaluation of the filtered images.
2) Compare the relative effectiveness of four spatial filtering algorithms, namely, square mean, separable mean, square median, and separable recursive median, using quantitative and qualitative evaluation methods.
    a) Determine the most effective window dimensions.
    b) Determine the most appropriate number of iterations.

CHAPTER 2

LITERATURE REVIEW

Remote Sensing with Imaging Radar

Radar is an acronym for Radio Detection and Ranging which refers to operation in the microwave portion of the electromagnetic spectrum and also the inherent capability to measure distances (range) to targets. To effectively utilize any type of remote sensing data, the analyst must understand fundamentals of the sensor system, energy-matter interactions, and appropriate analysis techniques. These will be discussed for imaging radar systems.

Imaging Radar

Imaging radar sensors are active systems, meaning that the energy measured is also provided by the radar instrumentation. Figure 2.1 illustrates a highly simplified radar system consisting of transmitter, receiver, transmit-receive (T-R) switch, antenna, electromagnetic wave, and target. A radar transmits a pulsed microwave signal at a specific frequency and

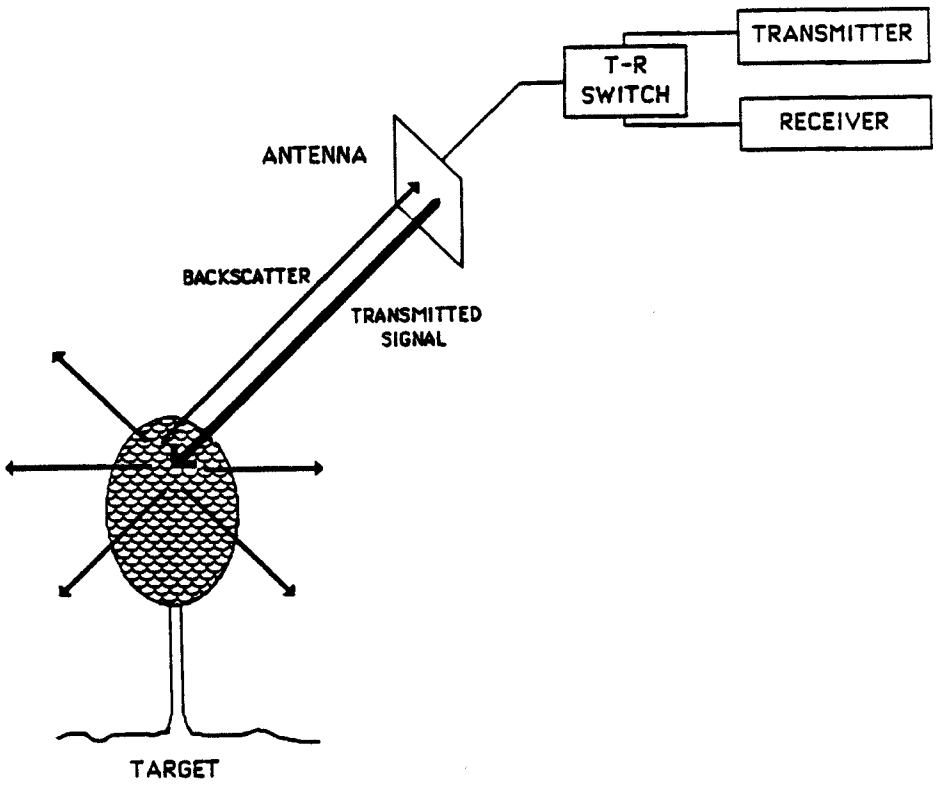

Figure 2.1 Simplified imaging radar system.

measures both the time for the signal to return and the quantity of the backscattered (returned) signal. Other active microwave sensors used in remote sensing include scatterometers, and altimeters (Ulaby et al. 1981). Both of these sensors are non-imaging instruments. The former quantitatively records the radar signal returned from terrain as a function of the viewing geometry, while the latter is used to determine altitude.

The T-R switch is needed when the same antenna is used for both transmitting and receiving microwave signals, as is commonly the case for imaging radars used for remote sensing purposes. The transmitter generates the pulsed microwave signal which generally has a specific wavelength ranging approximately between 1 mm and 1 m (Lillesand and Kiefer 1987). Letter designations, which were assigned by the military to specific wavelength regions during the period when radar systems were classified for security reasons, are still used today by civilians. The actual ranges of wavelengths or associated frequencies are not absolute; several different schemes are listed in the literature. Table 2.1 lists the radar band designations according to Long (1975).

Imaging radar systems utilized for remote sensing of the earth's surface are side-looking sensors which have an antenna oriented perpendicular to the line of flight of the aircraft or satellite platform. The signal beam is wide

Table 2.1 Radar band designations. Adapted from Long (1975).

Band	Frequency (f)[1] GHz	Wavelength (λ) cm
P	0.3 - 1.0	30 - 100
L	1.0 - 2.0	15 - 30
S	2.0 - 4.0	7.5 - 15
C	4.0 - 8.0	3.75 - 7.5
X	8.0 - 12.5	2.4 - 3.75
Ku	12.5 - 18.0	1.67 - 2.4
K	18.0 - 26.5	1.1 - 1.67
Ka	26.5 - 40.0	0.75 - 1.1

1. **Frequency:** $f = c\,\lambda^{-1}$

Where: c = Velocity of light (3×10^8 m sec^{-1})

λ = Wavelength

GHz = Gigahertz (10^9 cycles sec^{-1})

vertically and narrow horizontally (Ulaby et al. 1981). The vertical angle of the beam determines the swath width and thus the range dimension (across-track) of the resulting imagery, while the forward motion of the platform accounts for the azimuth (along-track) dimension.

Figure 2.2 illustrates the viewing geometry of a side-looking radar system. The distance from the sensor to the object can be measured in two ways -- slant range and ground range. The former is the line of sight distance from the sensor to the target, while the ground range is the ground distance measured from nadir to the target. The vertical component of the radar beam can be described by the incidence angle, depression angle, or look angle. Incidence angle is measured on the ground between the incident radar beam and vertical at the target. The depression angle and look angle are complementary angles with the latter being measured relative to vertical. Figure 2.3 from Lillesand and Kiefer (1987) illustrates the concept of how a radar measures distance. The radar signal energy propagates in air at approximately the speed of light (c). Therefore, the slant range, R, to any target is given by (Lillesand and Kiefer 1987):

$$R = \frac{ct}{2} \qquad (2.1)$$

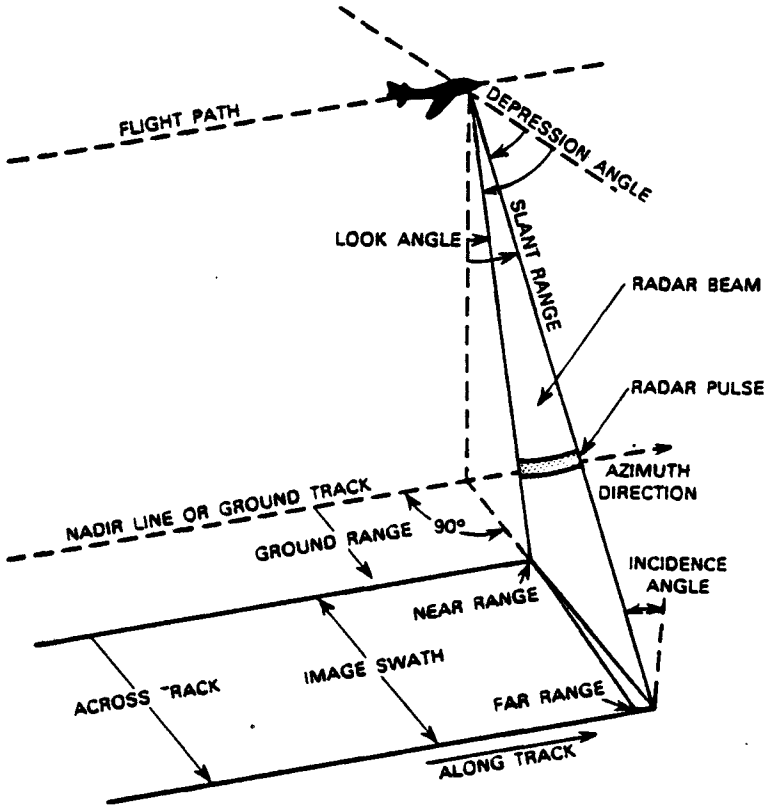

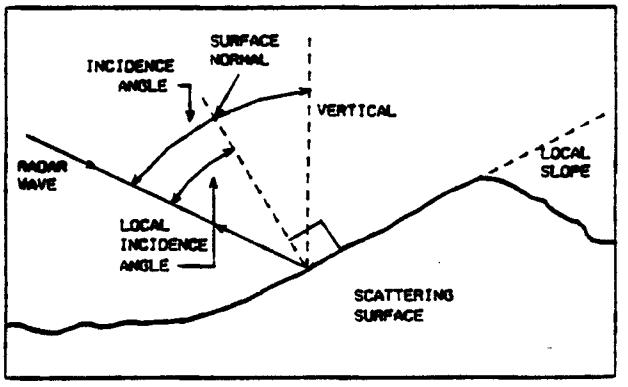

Figure 2.2 Viewing geometry of a side-looking radar system. (From Avery and Berlin 1985.)

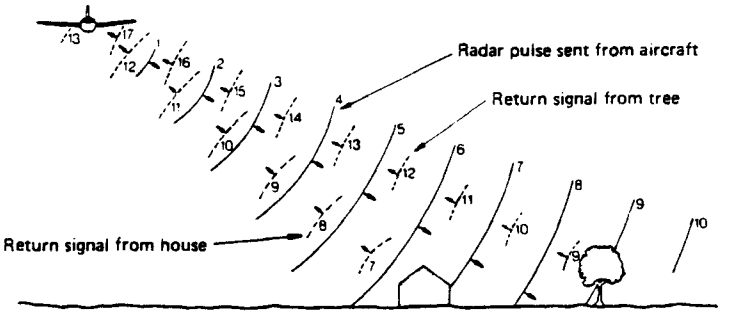

(a) Propagation of one radar pulse (indicating the wavefront location at time intervals 1-17)

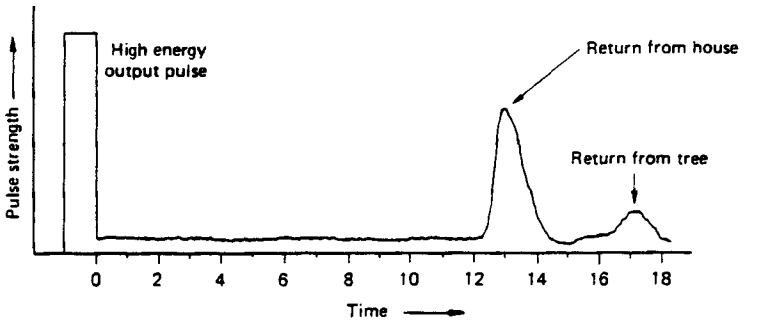

(b) Resulting antenna return

Figure 2.3 Operating principle of side-looking radar. (From Lillesand and Kiefer 1987.)

Where:

R = Slant range (m),

c = Speed of light (3 x 10^8 m/sec),

t = Time between pulse transmission and return reception (s).

Radar System Types

Side-looking radars can be divided into two categories: real aperture systems and synthetic aperture systems (Lillesand and Kiefer 1987; Long 1975; Moore 1983; Ulaby et al. 1981). The principal difference between these two systems is their resolving power and the means whereby this is achieved. The beamwidth (azimuth direction) of a real aperture system is defined by the physical size of the antenna, while synthetic aperture systems depend on complex signal processing techniques in which a coherent phase history of the pulsed return signal is used to obtain a much narrower beamwidth in the azimuth direction than is possible with the real antenna (Tomiyasu 1978; Ulaby et al. 1981). The pixel resolution for a real aperture radar is determined by the antenna beamwidth according to (Moore 1983; Tomiyasu 1978; Ulaby et al. 1981):

$$\beta h = \lambda / l \qquad (2.2)$$

Where:

β_h = Beamwidth (rad),

λ = Wavelength (m),

l = Horizontal length of antenna (m).

The resulting azimuth (along-track) resolution is:

$$r_A = \beta_h R \tag{2.3}$$

Where:

r_A = Azimuth resolution (m),

R = Slant range.

However, the range (across-track) resolution is dependent on the pulse length which can be thought of in units of time or distance. The range resolution is given (in terms of time) by:

$$r_R = \frac{\tau c}{2 \sin\theta} \tag{2.4}$$

Where:

r_R = Range resolution (m),

c = Velocity of light (m s^{-1}),

τ = Pulse duration (s),

θ = Angle of incidence (rad).

If two targets in the same range direction are to be detected separately (resolved), it is necessary for their returned signals to be received at separate times by the antenna (Henderson 1985; Jenson et al. 1977). One can think of the pulse length in terms of distance L and then it can be seen intuitively that for two objects in the same

range direction to be resolved, the slant range distance separating them must be at least L/2. If there is no difference in time between the two returns or the slant range distance separating them is less than L/2, then the two objects will be recorded as one entity in the data. Figures 2.3 and 2.4 from Lillesand and Kiefer (1987) illustrate this concept.

It can be seen from the above discussion that with a real aperture radar (RAR) system, the ground resolution element dimensions increase in both the range and azimuth directions as the distance from sensor increases. Fortunately, this problem of geometric distortion can be avoided by using a synthetic aperture radar (SAR) system.

SAR Techniques

As was discussed previously, SAR sensors have higher resolution capabilities than RAR systems. The high-resolution capability of SAR is independent of the platform altitude because the doppler history and differential time delays of the returning signal are utilized, none of which is a function of the slant range from the radar to the target (Elachi et al. 1982b). Thus, SAR can be utilized from either satellite or aircraft platforms.

Consider the case of a satellite platform several hundred kilometers from the target. To achieve fine

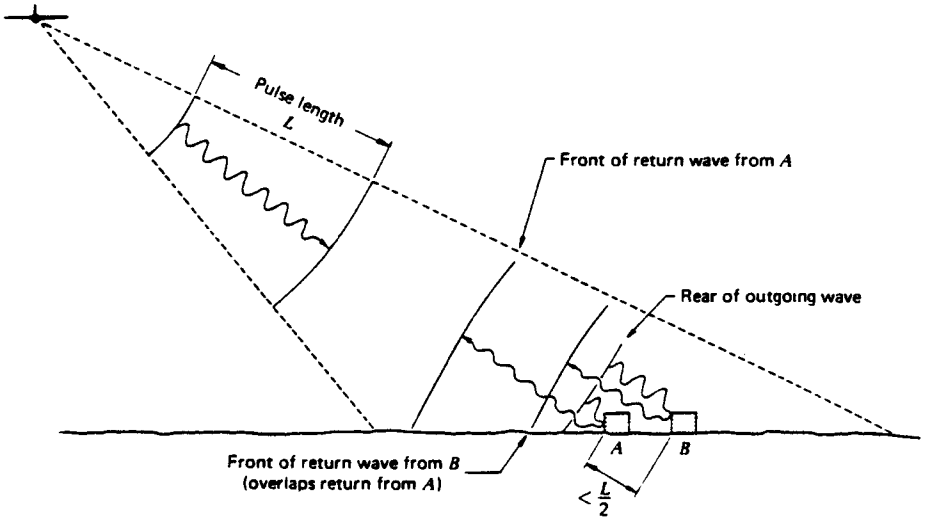

Figure 2.4 Dependence of range resolution on pulse length. (From Lillesand and Kiefer 1987.)

azimuth resolution with a real aperture radar system, a very short wavelength or very long (several kilometers) physical antenna would have to be utilized according to Equation 2.2. With synthetic aperture techniques, a long antenna array is simulated. According to Tomiyasu (1978):

> . . . the array need not necessarily be continuous, but can be composed of numerous small elemental radiators . . . [also] it is not necessary for all elements to radiate simultaneously since each of the elements can be excited in sequence provided an orderly coherent phase relationship is maintained.

Therefore, a physically small antenna can be carried aboard a platform moving at a constant velocity with the radar transmitting pulses of microwave energy at regular intervals as the antenna is laterally displaced. The length of this long antenna array is synthesized from a number of pulses transmitted and integrated coherently (Tomiyasu 1978).

The synthesized effective length of the antenna array (or aperture) is the ground distance over which the target is illuminated by the radar beam (Moore 1983). This length is analogous to the azimuth resolution of a real aperture radar with the same beamwidth according to Equation 2.2, such that:

$$L_{SA} = \beta_h R \qquad (2.5)$$

Where:

L_{SA} = Length of synthesized antenna (m).

This concept is illustrated according to Ulaby et al. (1981) in Figure 2.5. Thus, the length L_{SA} varies linearly as the slant range distance varies, while the azimuth resolution remains constant. The length L_{SA} is also related to the time the target is illuminated, the dwell time T_D, and the velocity V of the platform as follows (Tomiyasu 1978):

$$L_{SA} = VT_D \tag{2.6}$$

Where:

T_D = Dwell time (s),

V = Velocity of platform (m s^{-1}).

It can be shown (Elachi et al. 1982b; Moore 1983; Tomiyasu 1978; Ulaby et al. 1981) that for a SAR, the one-look azimuth resolution r_A can theoretically be as small as

$$r_A = D/2 \tag{2.7}$$

where D is the true along-track (azimuth) length of the physical SAR antenna, in meters. In direct opposition to the case of real aperture radar, Equation 2.7 indicates that for a SAR, the azimuth resolution r_A can actually be improved when the length of the physical antenna is reduced. It would seem that an infinitesimally fine resolution could be achieved. However, the above explanation is highly simplified and in reality other factors come into play such as pulse repetition frequency, signal to noise ratio, antenna area, and power requirements. For instance, the pulse repetition frequency

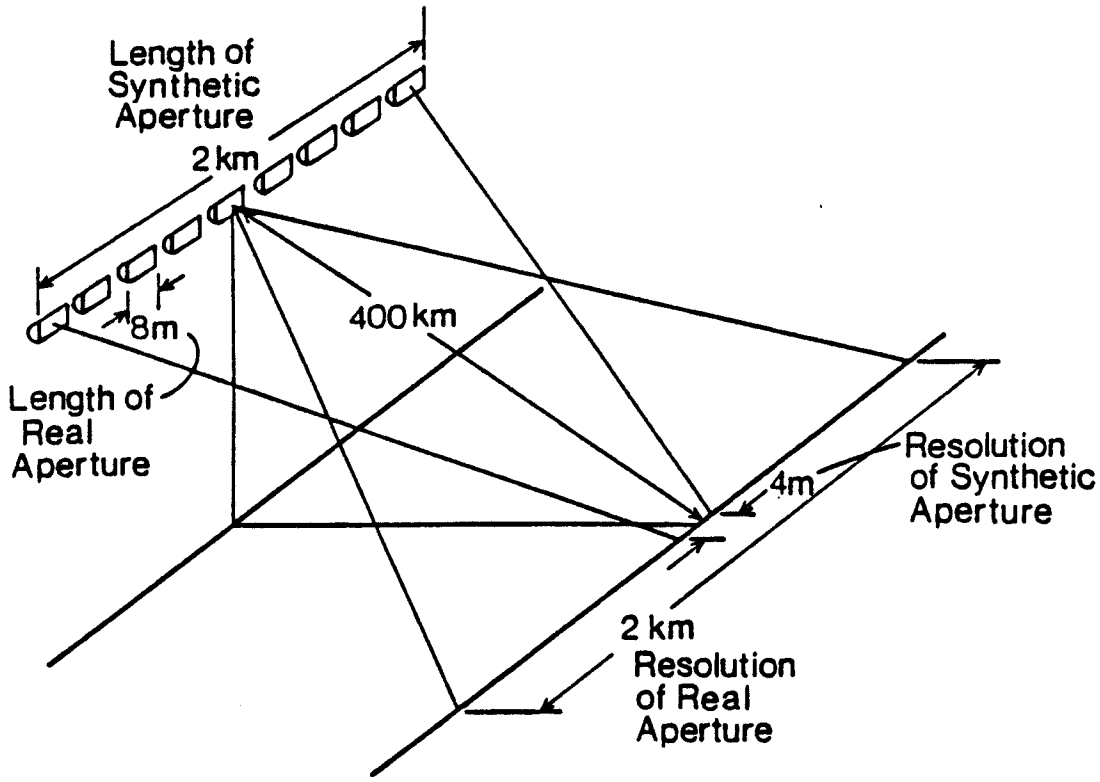

Figure 2.5 Differences in resolution between real aperture radar and synthetic aperture radar systems. This illustration is an example of a 4 cm wavelength spaceborne radar. (From Knowlton 1982, after Ulaby et al. 1981.)

must be sufficiently high so that the transmitter is pulsed again by the time the antenna moves one half of its length (Tomiyasu 1978). To illustrate the complexities of the situation, Moore (1983) states:

> Although r_A [azimuth resolution] is independent of range R, the complexity and accuracy requirements imposed on the radar, the storage element, and the processor increase with range for fixed values of r_A and wavelength; likewise, the complexity and accuracy requirements increase with wavelength for fixed values of r_A and range; and furthermore, the radiated RF power requirement grows sharply as D [physical antenna length] is decreased, thereby leading to a tradeoff between resolution and image S/N at long operating ranges.

More detailed and comprehensive discussions of these aspects of SAR systems are included in Elachi et al. (1982b) and Tomiyasu (1978).

The range resolution for all radars (RAR and SAR) depends on an effective transmitted pulse length or alternatively, on signal bandwidth (Tomiyasu 1978). The latter is utilized with a SAR system, where high resolution in the range direction is usually achieved through pulse compression techniques (Kovaly 1977). Usually a frequency-modulated pulse with bandwidth B is utilized to achieve fine resolution in the range direction. Therefore, the system range resolution, r_R, is (Ulaby et al. 1981):

$$r_R = \frac{c}{2B \sin\theta} \qquad (2.8)$$

Where:

B = Bandwidth (Hz),

c = Velocity of light (3 x 10^8 m/sec),

θ = Incidence angle (rad).

Radar Equation

The radar equation describes the performance of a radar by relating the power of the returning signal received by the sensor to the target and radar sensor parameters (Fung and Ulaby 1983; Long 1975). The generalized radar equation, using conceptual terms, is given in Figure 2.6.

Power Received	=	Power Density at a Distance R	X	Target Backscatter Cross Section	X	Space Attenuation on Return Path	X	Antenna Collecting Area

Figure 2.6 Generalized radar equation depicted in conceptual terms. (Based on Considine, 1983).

Assuming that the transmitter and receiver are in the same location, the radar equation, disregarding atmospheric path losses, can be written as follows (Fung and Ulaby 1983; Long 1975; Skolnik 1980):

$$P_r = \frac{P_t G_t}{4 \pi R^2} \sigma_{rt} \frac{A_r}{4 \pi R^2} \qquad (2.9)$$

Where:

P_r = Received power at polarization r (W),

P_t = Transmitted power at polarization t (m),

G_t = Gain of transmitting antenna in the direction of the target at polarization t,

R = Distance between radar and target (m),

σ_{rt} = Radar cross-section; the area intercepting that amount of incident power of polarization t which, when scattered isotropically, produces an echo at polarization r equal to that observed from the target (m^2),

A_r = Effective area of the receiving antenna aperture at polarization r (m^2).

According to Fung and Ulaby (1983), most geoscience applications involve extended targets, meaning that the actual target is larger than the resolution cell of the radar system. They consider a corn field to be an extended target. Therefore, one might consider a forest stand which has much more spatial variation than an agricultural field, to be an extended target, especially since stand inventory parameters are averaged over stand areas. For an extended target, it is more convenient to deal with an average return power (P_{AR}) and define a radar cross-section per unit area known as the scattering coefficient σ_{rt}. The effective size of the antenna aperture is related to the antenna gain by:

$$Ar = \frac{Gr\ \lambda^2}{4} \qquad (2.10)$$

Where:

Gr = Gain of the receiving antenna in the direction of the target at polarization r,

λ = Radar operating wavelength (m).

Therefore, the radar equation in terms of average power received can be rewritten (Fung and Ulaby 1983) as:

$$P_{AR} = \frac{\lambda^2}{(4\pi)^3} \int_{A_o} \frac{Pt\ Gt\ Gr}{R^4}\ \sigma^{\circ}_{rt}\ dS \qquad (2.11)$$

Where:

S = Surface; the surface integral is taken over the irradiated area Ao,

σ°_{rt} = Scattering coefficient ($m^2\ m^{-2}$).

Since Pt, Gt, Gr, and λ are radar system parameters that are constant, for a given range, the factor affecting the average power returned is the scattering coefficent σ°_{rt}. Fung and Ulaby (1983) state that the scattering coefficient σ°_{rt} is generally a function of wavelength, polarization, look angle, and interaction properties of the target which include geometric, dielectric, and conductive properties. These parameters are discussed below.

Influences on Radar Backscatter

The signal transmitted by a radar is scattered by the target and only a portion will return and be received by

the radar. The strength of the radar return (i.e. backscatter) is influenced by the properties of both the target and the system. Target parameters affecting radar backscatter are surface slope and roughness, target orientation, and complex dielectric constant, while system parameters include operating wavelength, antenna depression angle, polarization, and antenna look direction (Avery and Berlin 1985).

Target Parameters. The surface slope, sometimes referred to as macrorelief, is due to local topography. It affects the angle of incidence of the incoming radar signal. As the surface slope approaches normality to the radar signal path (i.e., incidence angle is 0^0), independent of wavelength and surface roughness, the radar return increases (Avery and Berlin 1985; Jenson et al. 1977). The return due to macrorelief may be so strong that it dwarfs any contribution due to the surface roughness or other characteristics of the target.

Radar backscatter (return) is also greatly affected by the surface roughness, sometimes referred to as microrelief, of the target. Based on the surface roughness there are two major categories of radar signal reflection--specular and diffuse. The former occurs when the target is smooth relative to the radar operating wavelength while the latter occurs when the surface is rough relative to the

wavelength. According to Avery and Berlin (1985), a smooth surface reflects the incident radar signal in a single direction away from the antenna (as long as the angle of incidence is not approaching zero). According to Snell's Law, the pulse will be reflected at an angle equal to and in the direction opposite that at which it strikes the surface (i.e. the Fresnel-reflection direction). However, a rough surface scatters the radar signal in many directions and thus some is reflected back (backscattered) toward the radar antenna. An isotropic scatterer, or Lambertian surface, represents maximum surface roughness and will provide strong backscatter regardless of the angle of incidence. It has microrelief several times the wavelength of the radar signal (Avery and Berlin 1985).

Surface roughness is related to the wavelength and depression angle of the radar system. If a height difference h exists between two points on a surface, then the waves reflected at these two points will be shifted in phase with respect to each other. Lord Rayleigh developed a criterion which gives a qualitative indication as to the roughness of a surface in the electromagnetic sense (Long 1975). According to the Rayleigh criterion, a surface is smooth if (Avery and Berlin 1985; Long 1975; Sabins 1987):

$$h < \frac{\lambda}{8 \sin\gamma} \quad (2.12)$$

Where:

h = Average vertical height (Δ h) of microrelief (m),

λ = Operating wavelength (m),

γ = Grazing angle between the terrain and incident radar signal (rad).

The Rayleigh criterion considers a surface to be either smooth or rough as if there were no gradient between the two textures. Peake and Oliver (1971) modified the Rayleigh criterion to define the upper and lower bounds of h for a surface of intermediate roughness. The smooth criterion considers a surface to be smooth if:

$$h_S < \frac{\lambda}{25 \sin\gamma} \quad (2.13)$$

The rough criterion considers a surface to be rough if:

$$h_R > \frac{\lambda}{4.4 \sin\gamma} \quad (2.14)$$

Smooth surfaces will cause the radar signal to be specularly reflected away from the radar sensor and therefore the return will be minimal. The low return means a low digital number (DN) for that pixel and is represented in radar imagery by a dark tone. Rough surfaces cause the radar signal to be diffusely scattered, therefore causing some of the radar signal to be backscattered (returned) to the radar sensor. In this case, the DN value for the

corresponding pixel will be relatively high and the image tone will be relatively bright. Surfaces of intermediate roughness would fall between these two categories and would have gray tone in radar imagery.

Smooth surfaces can produce a high amount of backscatter when the surface is oriented perpendicular to the incident radar signal or when the smooth surface is part of a corner. When planar surfaces intersect at right angles (called a corner), the radar signal can be reflected back toward the sensor, thus causing a high return (backscatter) which is often anomalous. The prevalence of corner reflectors in urban settings often causes urban scenes to be represented by a bright tone on radar imagery.

The electrical properties of target materials can have a strong influence on the intensity of radar backscatter. The complex dielectric constant is a measure of an object's electrical characteristics and is an indication of its reflectivity and conductivity. At microwave wavelengths, most natural materials have a dielectric constant ranging from 3 to 8 when dry. Since water has a dielectric constant of approximately 80, the presence of moisture in soil or vegetation can significantly increase radar reflectivity (Lillesand and Kiefer 1987).

It should be noted that it is the synergistic effects of all these target characteristics combined with radar system parameters that determine the radar backscatter from

an object. As an example, water has a high dielectric constant. Despite this, if a body of water has a calm surface, the smooth surface will cause most of the incident signal to be specularly reflected away from the sensor.

System Parameters. As mentioned earlier, system parameters that influence radar backscatter include operating wavelength, polarization, antenna depression angle, and antenna look direction. The antenna look direction determines the target orientation which was discussed previously. The operating wavelength and antenna depression angle (or the related local incidence angle) influence the backscatter greatly. Table 2.2 illustrates the relationships between incidence angle, operating wavelength and target roughness characteristics.

Imaging radars transmit pulsed energy with a defined polarization and also receive the returned energy at a specific polarization. The electric field vector (E vector) for a uniform plane wave must lie in the plane perpendicular to the forward motion of the plane wave (Ulaby et al. 1981). Polarized microwave energy has the entire E vector oriented in a particular direction. Standard transmit/receive combinations of polarizations for remote sensing purposes are: HH (horizontal send-horizontal receive), HV (horizontal send-vertical receive), VH, and VV. Like-polarized radar systems have a HH or VV

Table 2.2 Definition of radar surface roughness categories for three local incidence angles at three different wavelengths. This table is based on a modified Rayleigh criterion. From Lillesand and Kiefer (1987).

Roughness Category	Root-mean-square surface height variation (cm)		
	K_a Band (λ = 0.86 cm)	X Band (λ = 3.2 cm)	L Band (λ = 23.5 cm)
(a) Local Incidence Angle of 20°			
Smooth	< 0.04	< 0.14	< 1.00
Intermediate	0.04 - 0.21	0.14 - 0.77	1.00 - 5.68
Rough	> 0.21	> 0.77	> 5.68
(b) Local Incidence Angle of 45°			
Smooth	< 0.05	< 0.18	< 1.33
Intermediate	0.05 - 0.28	0.18 - 1.03	1.33 - 7.55
Rough	> 0.28	> 1.03	> 7.55
(c) Local Incidence Angle of 70°			
Smooth	< 0.10	< 0.37	< 2.75
Intermediate	0.10 - 0.57	0.37 - 2.13	2.75 - 15.6
Rough	> 0.57	> 2.13	> 15.6

configuration, while cross-polarized radar systems operate with HV or VH polarizations.

From the above discussion, it can be seen that the interactions between system and target parameters are complex. When interpreting radar imagery, these various influences should be considered. Modeling the complex interactions of these factors is a topic of much current and ongoing research (see Lang et al. 1987; Murata et al. 1987; Richards 1986; Ulaby and Dobson 1986).

Speckle

An inherent characteristic of SAR imagery is speckle. It is caused by the instantaneous radar return randomly fluctuating (or fading) widely as the radar beam passes over an extended target (Fung and Ulaby 1983; Ulaby et al. 1982). Target features normally consist of a large number of randomly distributed scatterers and it is this randomness that is responsible for image speckle (JPL 1986). Skolnik (1980) states that constructive and destructive interference result in a breakup of distributed scatterers causing the speckled appearance of radar imagery, i.e. random variability in image tone among pixels corresponding to different pixels of a uniform target. The randomly distributed scatterers of the target cause the transmitted coherent radar signal to become a

non-coherent return, and the resulting random constructive and destructive interference patterns create relatively high and low returns (i.e., high variability). Thus, speckle is caused by the coherent imaging process of SAR systems and is not a result of spatial variability in the physical or electromagnetic properties of the the target feature (JPL 1986).

Speckle noise inhibits interpretation and digital analysis of SAR data. Therefore, techniques are utilized to reduce the speckle present in SAR imagery. One method to reduce speckle is to use multiple looks at the same ground pixel by not using the entire synthesized antenna length L to achieve an azimuth resolution r_A, but to break up the synthesized length into n subsections and look at the scene from slightly different aspects each with range resolution r_R (Skolnik 1980). These independent samples are then combined incoherently into a single image. The speckle noise is reduced by a factor of the square root of n, where n is the number of images used, or the "looks" (Keyte and Pearson 1983). Based on previous discussion, however, one sees that as the number of looks is increased, the portion of the synthesized antenna used becomes smaller and the azimuth resolution becomes larger. Skolnik (1980) reports: "It has been suggested that the noncoherent combining of images of lesser resolution produces a better image with less speckle than a single image of greater

resolution." Figure 2.7, adapted from Moore (1983), illustrates how the resolution is degraded as the number of independent looks increases. Although the spatial resolution is reduced through such an operation, the apparent resolution may be improved due to the speckle reduction. Using this method, the reduction of speckle by a factor of the square root of n reduces the resolution by a factor of n. Multi-look averaging is conducted during the digital correlation process of the SAR data.

A second method of speckle reduction that has been commonly employed is digital spatial filtering. Multi-look processing smoothes in the azimuth direction, only, whereas spatial filters can be chosen to filter in both the azimuth and range dimensions. Digital filtering will be discussed in detail in a later section.

Signal Correlation

The conversion of the original radar signal returns (Doppler phase histories) to image data is known as correlation. Both optical and digital correlation techniques are utilized. Most correlation has been accomplished optically by initially recording the radar signal returns on photographic film. This signal film is then optically processed with a Precision Optical Processor which passes a collimated coherent light beam through the

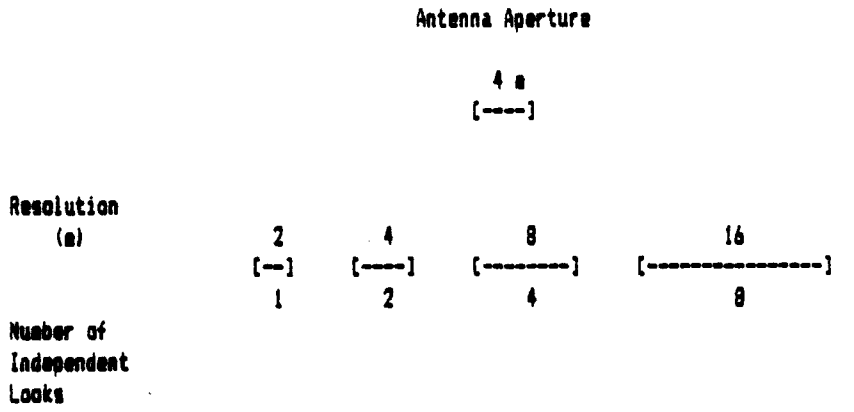

Figure 2.7 Example of a 4 meter SAR antenna showing potential number of independent looks and the effect on resolution. (Adapted from Moore 1983.)

signal film and through a series of lenses, the resultant collimated beam of light then being recorded on photographic image film (Jenson et al. 1977; Moore 1983). To obtain a digital format of optically processed signal film, the image film is replaced with a photosensitive detector (Moore 1983) or the image film can be digitized with a microdensitometer. Although this produces a digital product, this process does not yield the dynamic range nor geometric fidelity that digital correlation precedures can provide.

Digital correlation of SAR data involves a large number of complex calculations for each output pixel. Due to the high volume of calculations necessary to generate SAR imagery, high-speed digital processors for airborne SAR sensors became possible only after computing systems began utilization of integrated circuits in the early- to mid-1970's (Elachi 1982b). This was two decades after the development of optical SAR processors. Therefore, more of the optically correlated images have been available for interpretation. More detailed discussions of optical processing techniques are given by Curtis (1977), Moore (1983), and Tomiyasu (1978). Digital processing is discussed in several papers including those by Bennett et al. (1981); Curlander (1986); Elachi et al. (1982b); English (1984); Guignard (1981); Kirk (1975); Liu (1982); and Raney (1982).

Spaceborne Imaging Radar

On three occasions to date, L-band radar data of the Earth's surface has been obtained from a space platform. In 1978, the free-flying Seasat satellite operated for just over three months. The L-band (23.5 cm) HH-polarized SAR onboard Seasat provided optically correlated data (Ford et al. 1980). In November 1981, aboard the Space Shuttle orbiter Columbia, the Shuttle Imaging Radar-A (SIR-A) acquired optical L-band (23.5 cm) HH-polarized SAR data (Elachi et al. 1982a; Ford et al. 1983). In October 1984, SIR-B, also a 23.5 cm HH-polarized L-band SAR, was operated aboard the Space Shuttle orbiter Challenger, acquiring both digital and a limited amount of optical data (Ford et al. 1986; NOAA 1984). The SIR-B experiment enabled the acquisition of multiple-incidence angle data for the first time from space altitudes. The nominal ground resolution for both the Seasat SAR and SIR-B was 25 meters, while SIR-A had a ground resolution of 40 meters.

Many additional spaceborne SAR systems are being planned (Elachi 1986). NASA is planning for the SIR-C and SIR-D missions (each will have L-band, C-band, and X-band, multi-polarization, multi-angle capabilities) to be launched in the early 1990's. These experiments will culminate in the deployment of a SAR sensor aboard the Earth Observation System (EOS) polar platform scheduled for

launch in 1994. Satellite SAR's scheduled for deployment by other countries in the early 1990's include the L-band JERS-1 SAR (Japan), the C-band ERS-1 (ESA), and the C-band Radarsat SAR (Canada).

Digital Filtering

Introduction

A digital filter is an arithmetic procedure that operates on a digital data set to eliminate irrelevent data or noise (Swain and Davis 1978). Filtering can be done in one of two domains, the frequency-transform domain or the spatial domain (Gonzalez 1986). The spatial domain is used when removing speckle noise from SAR image data. The spatial domain refers to the aggregate of pixels constituting an image. Spatial filters utilize digital values of many adjacent image pixels to derive a new value for a particular pixel (usually central to the group). Terminology associated with digital filters follows.

A window is the image area (sub-array) considered in a single filtering (i.e. arithmetic) operation. The window shape can be one-dimensional (1 x n, n x 1), square (n x n), rectangular (m x n), circular, cross, or virtually any other shape. The first three shapes are the most common. Normally, the dimensions of the window are such that an odd

number of pixels are involved in the operation. The window location is shifted (incremented) between each filtering operation. The window is incremented until the entire image has been filtered.

A recursive filter utilizes output feedback. After a filtering operation is completed on a particular window area, the output value replaces the original value in the image. Then the window is incremented and the next filtering operation is implemented, utilizing the previously calculated (filter output) values. The normal (non-recursive) procedure is that each new calculated value is placed in a separate image file and only the original image pixel values are considered in each filtering calculation.

A separable filter utilizes successive applications of a one-dimensional window, first along the rows and then along the columns (or vice versa) of an image array to simulate a two-dimensional window (Narendra 1981).

There are basically four types of spatial filters: low pass, high pass, directional, and textural (Holdermann et al. 1978). Each has a different function as illustrated in Table 2.3.

It is the low pass filter that is of use in reducing the effects of speckle noise. A low pass filter enhances (or passes) low spatial frequencies -- features that are larger than the window size, at the expense of high spatial

Table 2.3 Types of digital spatial filters and their functions.

Type	Function
Low-Pass	Smoothing
High-Pass	Edge-enhancement
Directional	Smoothing or edge enhancement in a particular direction
Textural	Assigns a texture measure

frequencies (which are attenuated) that are smaller than the window size (Curran 1985; Duda and Hart 1973). Spatial frequency refers to the changes in digital number values over a given distance (Lillesand and Kiefer 1987). When the digital numbers change abruptly over a relatively small number of pixels, the spatial frequency is considered to be high. Edges and impulse noise are high frequency features. Low spatial frequency areas have digital numbers that vary gradually over a relatively large number of pixels. The data of a typical image is concentrated primarily in the low frequency component due to the high spatial correlation among neighboring pixels (Lim 1984).

High pass filters enhance high spatial frequencies (features that are smaller than the window used), while low spatial frequencies (features larger than the window) are attenuated. This type of filter is used for edge enhancement. Directional filters utilize either high or low pass operations that enhance particular spatial frequencies in their direction of travel. Textural filters are used to assign a value to a point that is indicative of the texture of the surrounding area based on some measure of variance such as range, kurtosis, or standard deviation (Curran 1985).

Low Pass Arithmetic Operations

As stated previously, it is the low pass filter that is of use in smoothing or reducing the effects of speckle in SAR image data. The most common arithmetic operations utilized for smoothing are mean and median. The mean filter is a neighborhood averaging operation where the digital numbers within the window are averaged. This linear operation is easy to implement using convolution techniques. One of the main difficulties is that it blurs edges and other sharp details (Gonzalez 1986; Chin and Yeh 1983).

The median filter is a non-linear operation in which the digital numbers within the window are ranked and the median or mid-value is selected. This type of filtering was first suggested by Tukey (1971) in time series analysis. Gonzalez (1986) reports: "The principal function of median filtering is to force points with very distinct intensities to be more like their neighbors, thus actually eliminating intensity spikes that appear isolated in the area of the filter mask [i.e. window]."

The major advantage of the median filter over a mean filter is that smoothing is accomplished with much less blurring; edges are retained (Chin and Yeh 1983; Gonzalez 1986; Heygster 1982; Rosenfeld and Kak 1982). This property allows for the filter to be iterated without

compounded blurring. Median filters are effective in removing salt and pepper (high and low intensities) and spike noise (Huang 1981; Justusson 1981). It is important to note that the edges that are retained may not be analogous to cover type boundaries or edges found in actual images. To better understand the properties of these filters, some signal processing terminology will be defined (Gallagher and Wise 1981):

> A constant neighborhood is a region of at least N + 1 consecutive pixels, all of which are identically valued (where window width = 2N + 1).
>
> An edge is a monotonically rising or falling set of pixels surrounded on both sides by constant neighborhoods.
>
> An impulse is a set of N or less pixels whose values are different from the surrounding regions and whose surrounding regions are identically valued constant neighborhoods.
>
> A root is a signal which is not modified by filtering.

Figure 2.8 illustrates the differences in performance of the one-dimensional mean and median filters. In (a) the distinct edge (or step) is preserved by the median filter while it is converted to a ramp function (gradual edge) by the mean filter. Both the mean and median filters effectively preserve ramp functions. When impulses are present, the mean filter does not retain the value of the surrounding constant neighborhoods as is seen in (c), (d), and (e). Rather the neighborhood value is raised due to the impulse. In the case of the median filter, pulse

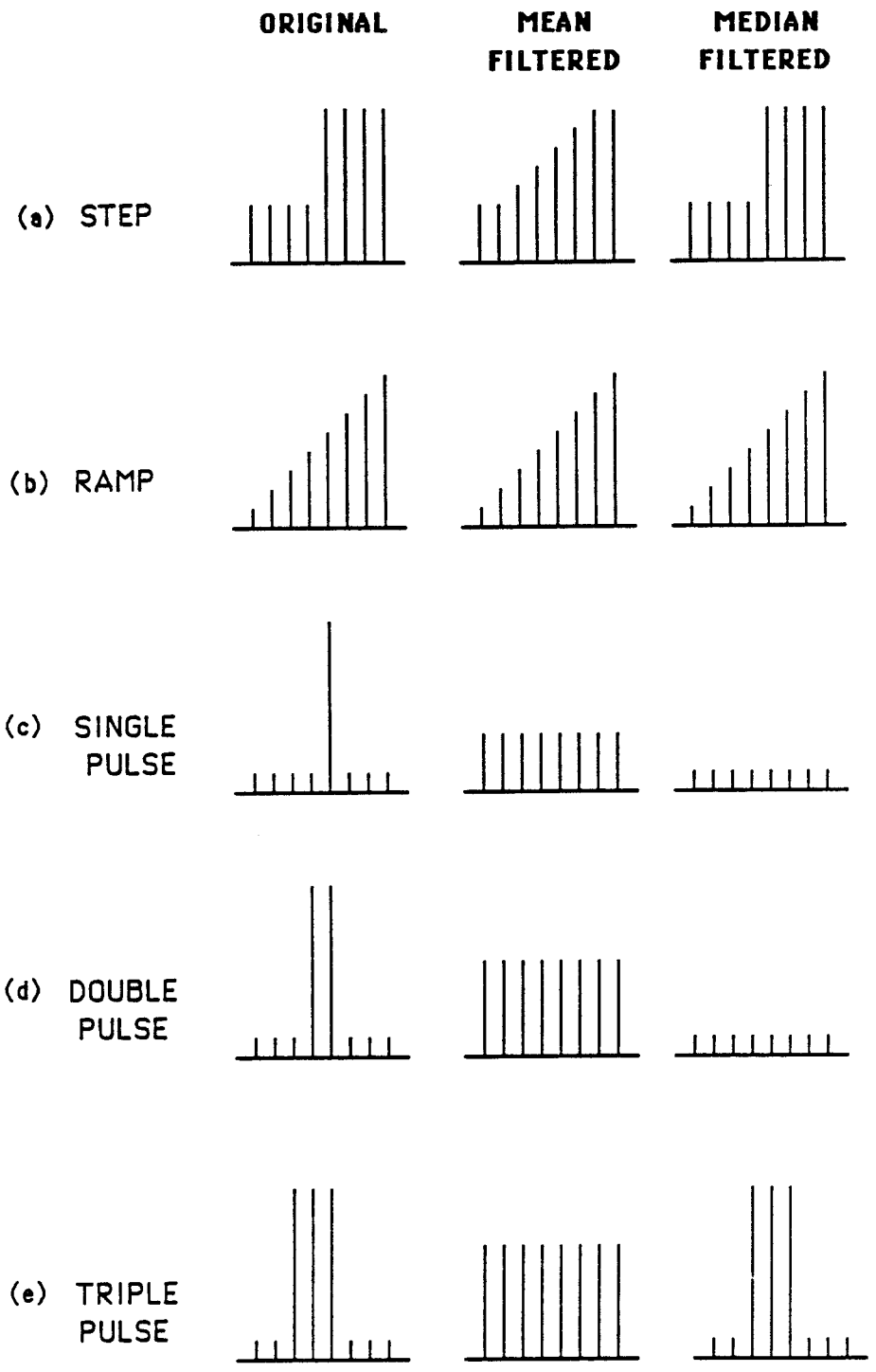

Figure 2.8 Examples of mean and median filtering on simple data streams with a window size of 1 x 5. (From Pratt 1978.)

functions (impulses) are suppressed if the period is less than one-half the window width (i.e., less than or equal to N).

At first glance, the median filter looks far superior to the mean filter. However, when the definitions of edge and constant neighborhoods are carefully examined, it will be seen that 8-bit SAR data rarely will contain true edges due to the high amount of variation within the data. Thus, median filtering of SAR data most likely will cause some blurring of cover type boundaries, (but probably not as much as will be the case with mean filtering). Rosenfeld and Kak (1982) report that a problem with two-dimensional (window) median filtering is that it destroys thin lines as well as isolated points. It also clips (or rounds) sharp corners. The use of a separable filter will reduce these effects if the corner is a right angle oriented along the rows and columns (Narendra 1981).

Filter Examples

This section will provide a brief tutorial on the operation of mean and median filters. Additionally, several filter properties will be illustrated including, separable and non-separable operation, recursive and non-recursive operation, and padding.

Mean filters are an application of a general image processing technique know as convolution. In convolution, a moving window is established which contains an array of coefficients. Such an array is referred to as a kernel which consists of an odd number of pixels. For a mean filter, each coefficient in the kernel is the same and the sum of the coefficients is equal to one. Thus, an arithmetic average of the digital numbers is calculated. Kernels for window sizes of three and five are given in Figure 2.9 for both separable and non-separable mean filters. The kernel is moved throughout the original image and the digital number at the center of the kernel (pixel location highlighted in Figure 2.9) is calculated. This involves multiplying each coefficient in the kernel by the corresponding digital number in the original image and then summing all the resultant products (Lillesand and Kiefer 1987). This sum represents the mean of the digital numbers in the window and it becomes the new value for that pixel location in the output image. This procedure is performed for each pixel in the original image.

To prepare the original image for filtering, the image array must be padded along its edges. Padding normally involves repeating the first (or last) pixel value N times, where the window size is 2N + 1. Figure 2.10 illustrates the padding of an image array in preparation for using a 3 x 3 mean filter kernel. Since the window size is three,

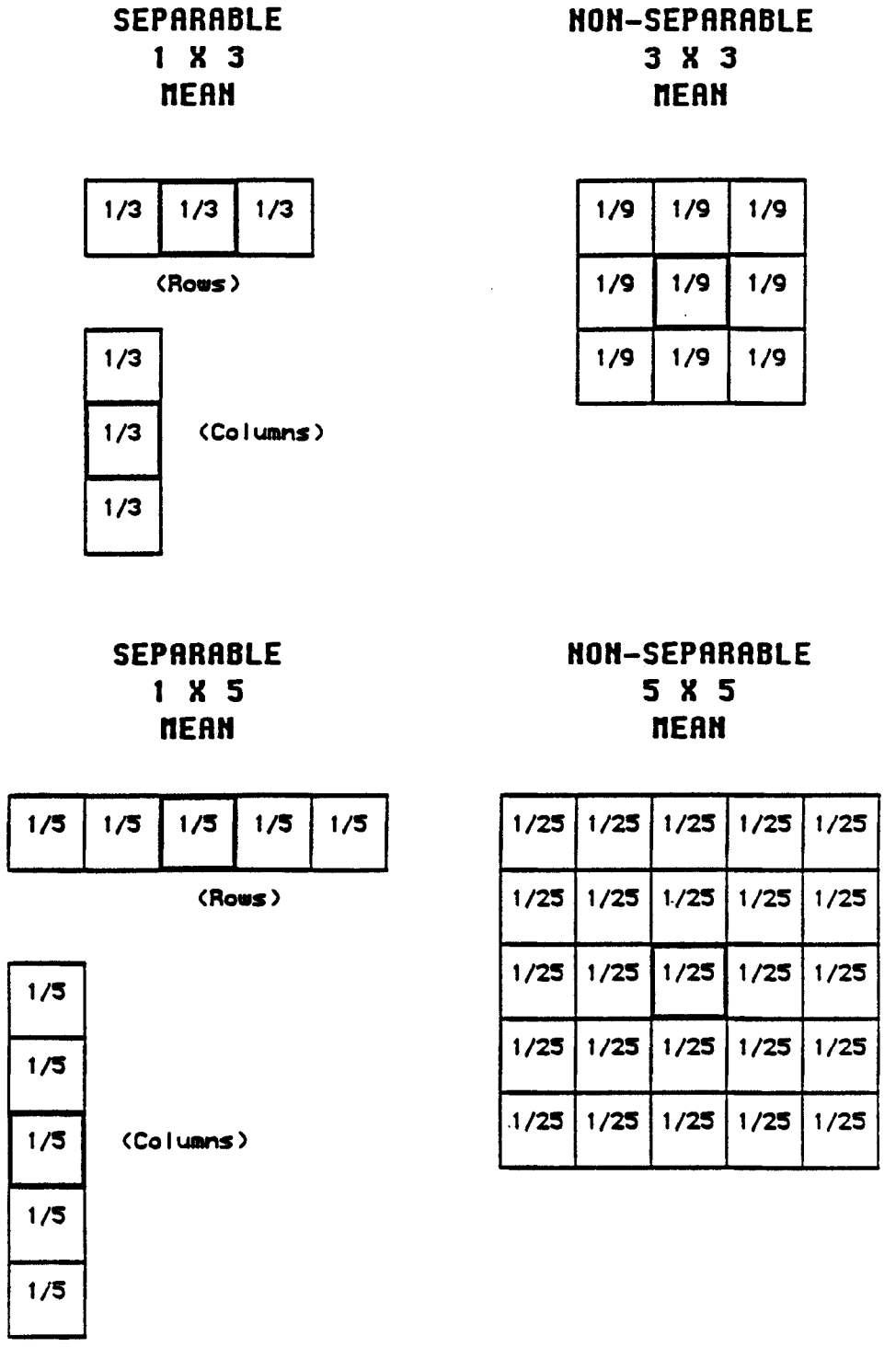

Figure 2.9 Separable and non-separable kernels for the mean filter at window sizes of three and five.

3 x 3 MEAN KERNEL

1/9	1/9	1/9
1/9	1/9	1/9
1/9	1/9	1/9

PADDING CALCULATIONS

Window size = 2 (padding factor) + 1

Where: L = Window size
N = Padding factor

$3 = 2N + 1$

$N = 1$

Therefore, padding factor is 1

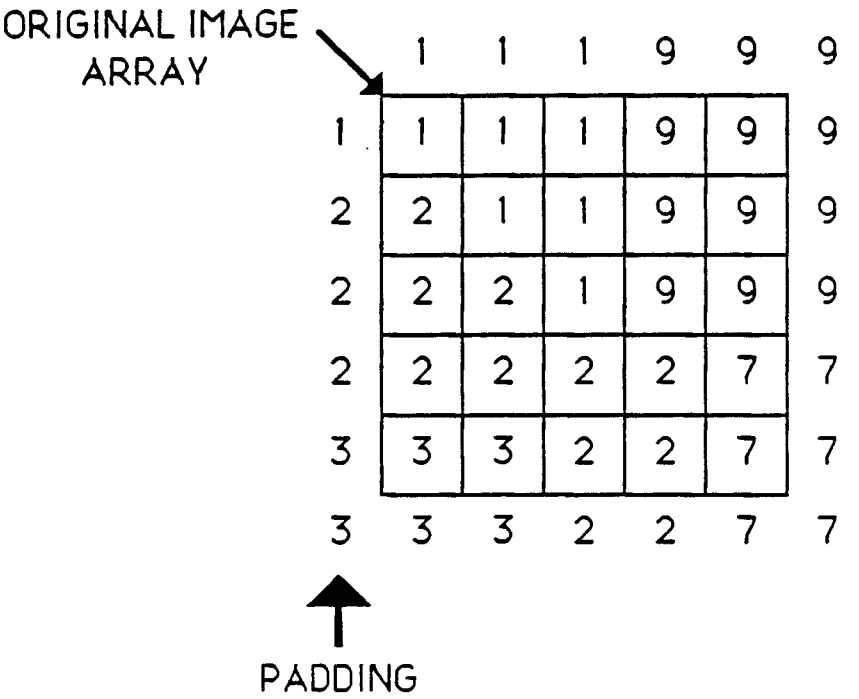

Figure 2.10 Example of padding an image array in preparation for filtering with a non-separable 3 x 3 mean filter.

the padding factor N is calculated to be one. Thus, the perimeter (edge) digital numbers in the original array are repeated once along the boundaries of the image.

Figure 2.11 demonstrates the operation of a 3 x 3 square (non-separable) mean filter. First, the new digital number for the center of the active window is calculated. As was described above, each of the digital numbers in the active window is multiplied by the coefficient in the corresponding position in the filter kernel. These products are summed and this value becomes the digital number in the output image (same position as the center of the active window in the input image). Digital numbers are always integers, so the sum is rounded to the nearest integer. The window is then shifted and the procedure repeated. In subsequent operations, the window is moved across (and down) the image until all output digital numbers have been calculated.

The operation of a 1 x 3 separable mean filter is illustrated in Figure 2.12. As was discussed earlier, a separable filter uses two one-dimensional kernels to filter the columns and rows separately. Thus, a two dimensional window (kernel) is simulated. First, the image array is prepared for filtering of the columns by padding at the top and bottom of the image. Then the column kernel is passed down the columns to create the column output array. This array is then padded at the sides in preparation for the

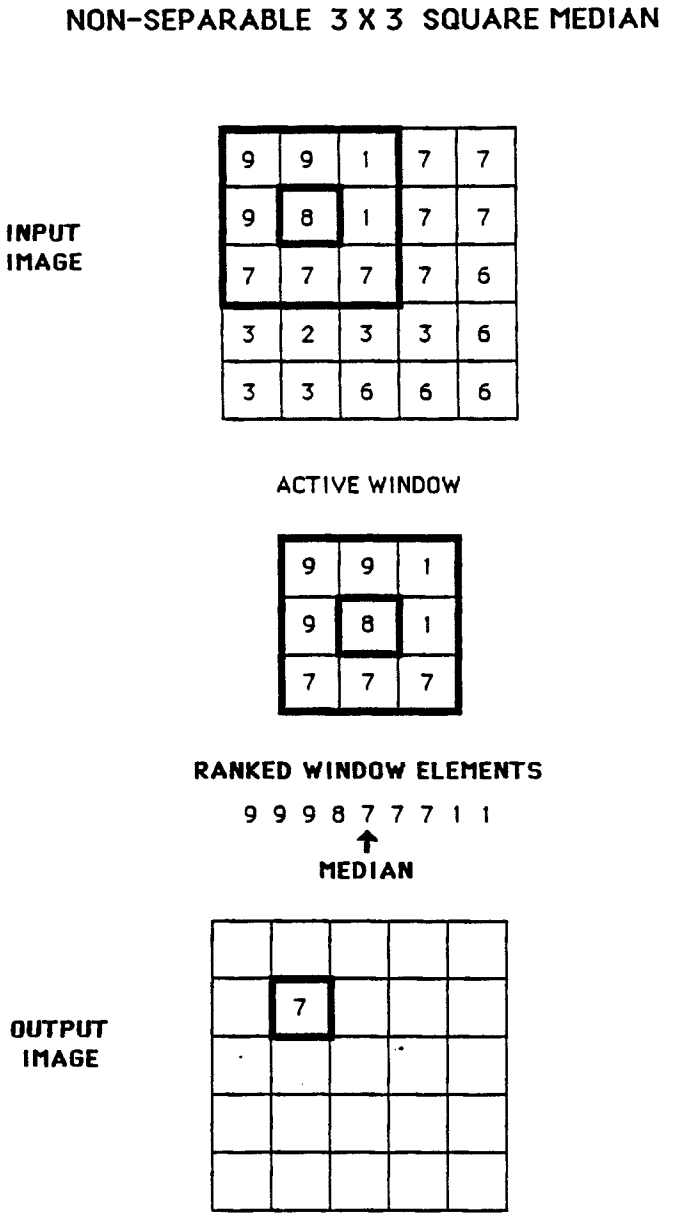

Figure 2.11 Operation of a non-separable 3 x 3 mean filter.

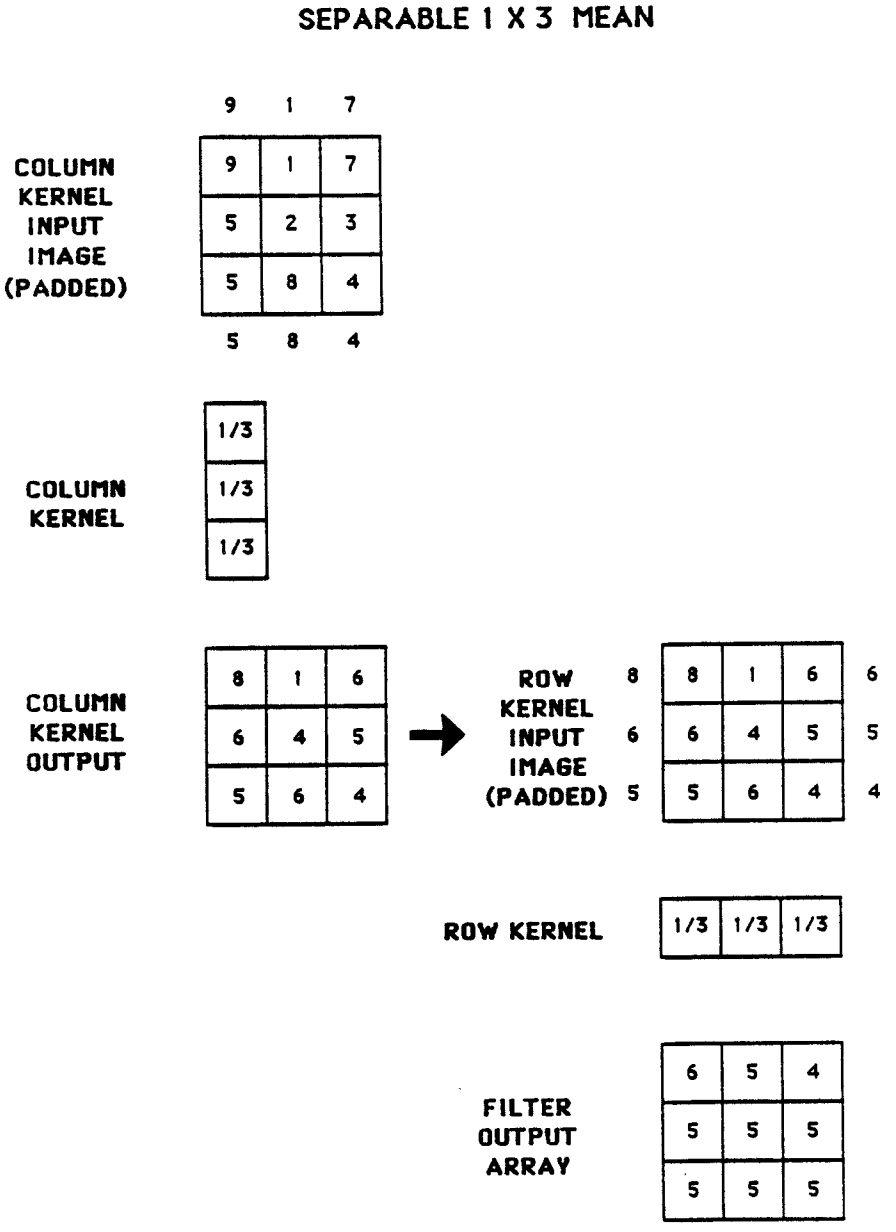

Figure 2.12 Operation of a separable 1 x 3 mean filter

filtering of the rows. The row kernel is passed along the rows of the column output array. This constitutes the first iteration of this filter treatment.

The median filter procedure differs from the process utilized with mean filters. The digital numbers within the active window are ranked and the center value (median) is selected as the new digital number for the output image. As with convolution, the middle digital number within the window is replaced by the new value. This process is illustrated in Figure 2.13 for a 3 x 3 non-separable median filter.

As was mentioned previously, a recursive filter utilizes output feedback. All the filter examples given in the previous figures have been non-recursive. That is, only the digital numbers from the original image array were considered when calculating the new value. Figures 2.14 and 2.15 demonstrate the difference in operation between a non-recursive and recursive 1 x 5 median filter. For simplicity, a one-dimensional window is shown operating on a one-dimensional data stream. The active window shows the five digital numbers that are considered for each operation. The median value of the five digital numbers is selected and it becomes the output digital number indicated at the bottom of the figure. The non-recursive filter in Figure 2.14 operates similar to the filters in the previous Figures. Figure 2.15 illustrates a recursive 1 x 5 median

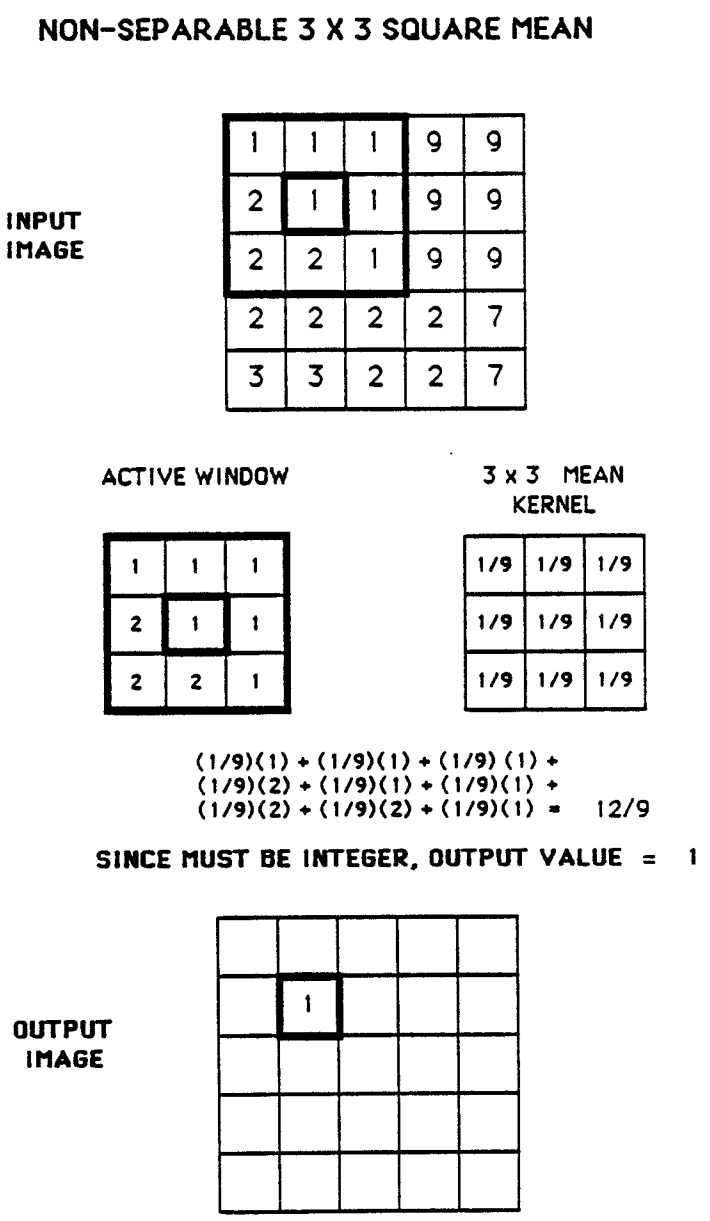

Figure 2.13 Operation of a non-separable 3 x 3 median filter.

NON-RECURSIVE MEDIAN FILTER

(Window Size of 1 x 5)

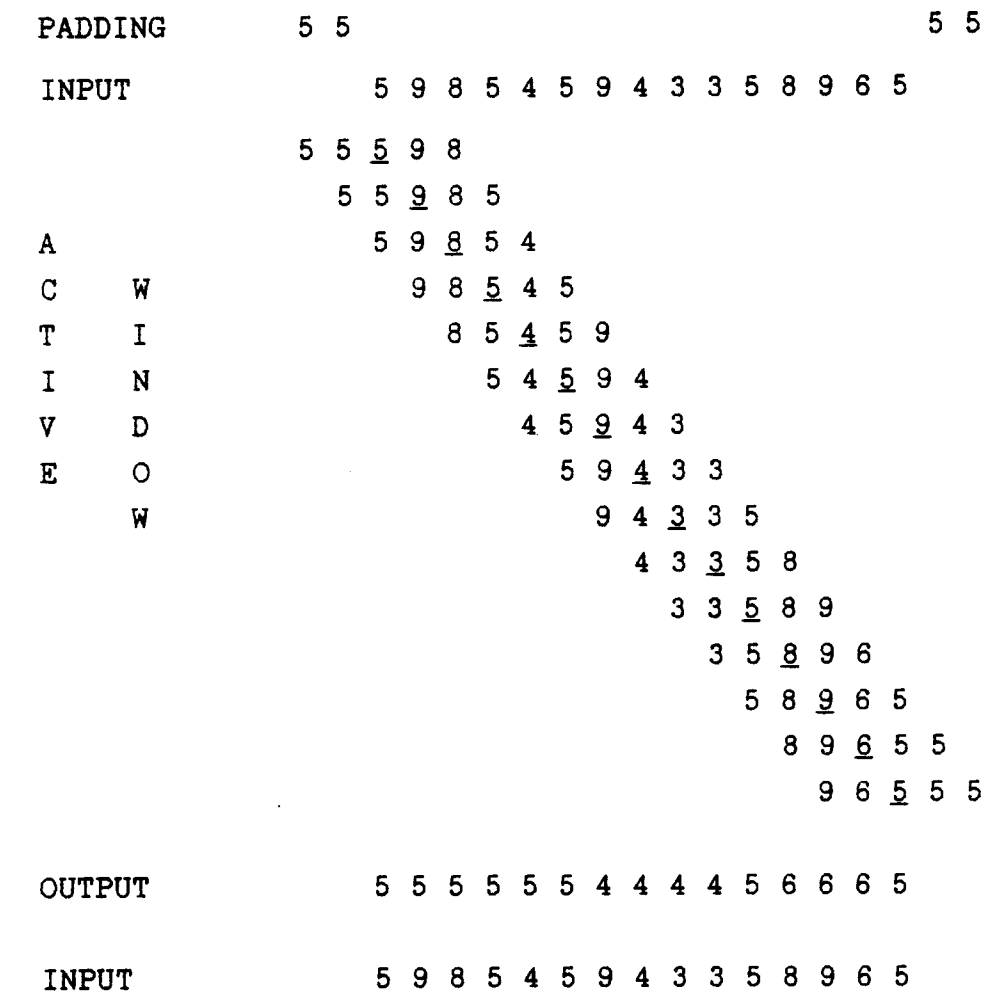

Figure 2.14 Example of a non-recursive median filter with a window size of 1 x 5. The active window shows the data values that are considered for each calculation. The highlighted location in the active window indicates the position for the calculated median value in the output data stream.

RECURSIVE MEDIAN FILTER

(Window Size of 1 x 5)

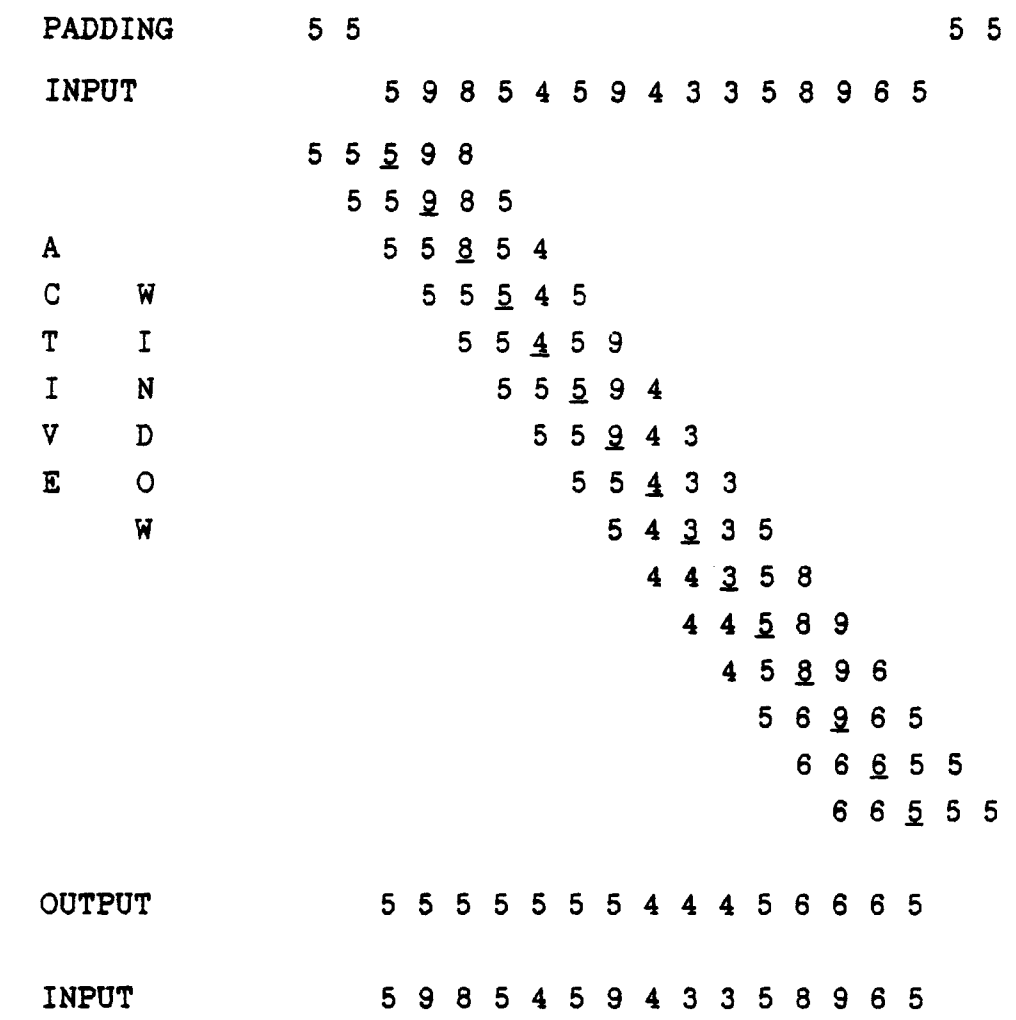

Figure 2.15 Example of a recursive median filter with a window size of 1 x 5. The active window shows the data values that are considered for each calculation. The highlighted location in the active window indicates the position for the calculated median value in the output data stream. In each active window, numbers to the left of the highlighted position are output feedback, while those to the right are from the input data stream.

filter operating on the same data stream as in the previous figure. Once again, the digital numbers in the active window are ranked and the median value selected for the output. It should be noted, though, that not all digital numbers in the window are directly from the input data stream. The numbers that are underlined are output feedback -- that is, they were previously determined to be the median value of a previously active window and they were then utilized in subsequent calculations (retained). An underlined number (output feedback) is only retained as long as the window is positioned over it. When Figures 2.14 and 2.15 are compared, it can be seen that the output differs slightly.

Evaluation

When using digital filtering for smoothing image noise, some method must be utilized for monitoring the filtering process and evaluating the results. Pratt (1978) warns that, "It [median filtering] should not be used blindly, but rather its performance should be monitored to determine if its application is beneficial." Huang (1981) gives additional advice regarding the use of filtering as a preprocessing procedure:

> Although median filtering, or for that matter linear smoothing, often improves the subjective quality of an image, it is by no means clear that they would facilitate further machine analysis of

> the image, such as pattern recognition or metric measurements.

Thus, it is important to use not only qualitative, but also quantitative measures when evaluating the results. The quantitative assessment will be indicative of the classification performance and the qualitative assessment will identify distortions and other major changes. A statistical classification using pattern recognition techniques would be a highly desirable test.

Interpretation and Analysis of L-Band SAR Data

Introduction

The end product of remote sensing is information. According to Lillesand and Kiefer (1987):

> Remote sensing is the science and art of obtaining information about an object, area, or phenomena through the analysis of data acquired by a device that is not in contact with the object, area, or phenomenon under investigation.

Information extraction from remotely sensed data can be accomplished in two ways. The first is an image oriented approach which utilizes qualitative techniques to visually interpret pictorial representations of the data, while a second approach is the quantitative analysis of digital data treating the data as a set of measurements (Landgrebe 1978; Lillesand and Kiefer 1987). Most remote sensing data types, including imaging radar data, can be analyzed by

both techniques. This section describes some of the qualitative studies of radar imagery and then covers some of the quantitative analyses documented in the unclassified published literature.

For vegetation analysis with imaging radar data, mostly qualitative studies have been conducted due to the complex nature of radar data processing since, in the past, more optically correlated images have been available for interpretation. With the development of digital correlation techniques, quantitative analysis of SAR data is increasing.

Image Interpretation

The interpretation of radar imagery is similar to photo interpretation using tone, texture, shape, pattern, size, shadow, and association as interpretive clues (Barr and Miles 1970; Henderson 1985). Three types of information regarding vegetation can be obtained from the analysis of radar data: (1)geographic pattern; (2) gross structure and physiognomy; and (3) type identification (Morain 1980). Regarding the interpretation of radar imagery, Morain (1980) states:

> In all instances interpretations rely on converging evidence derived from principles of geography, biology and ecology; the interpreter's understanding of the principles of radar reflection from vegetation as well as his experience with the local environment; and inference.

Tone and texture are the major factors to consider when developing interpretation keys for forest typing (Knowlton and Hoffer 1981; Morain 1980). Tone on radar imagery refers to the brightness of the gray scale representation of the radar return. The brightness is directly related to the intensity of the return. Texture refers to the degree of homogeneity in tone over an area and degree of speckling.

When interpreting radar data utilizing the principles mentioned above, the analyst should understand the energy-matter (i.e. signal-target) interactions that occur at microwave wavelengths. Such an understanding will assist him in analyzing the data. Energy-matter interactions depend on the operating wavelength and various other radar and target characteristics as discussed earlier. Since the proposed research project will deal with L-band radar data, the following discussion of visual interpretation of SAR imagery is limited to L-band radar imagery. L-band radars operate in the wavelength region of the electromagnetic spectrum between 15 and 30 cm. The three spaceborne SAR's to date have operated at a wavelength of 23.5 cm.

A limited number of studies have been conducted to develop guidelines for interpretation of L-band radar data acquired from space platforms (i.e. Seasat, SIR-A, and SIR-B). Seasat data was primarily utilized for terrain

analysis or oceanographic studies. Terrain analysis was the major emphasis for interpretation of SIR-A data (Elachi et al. 1982a), but some vegetation interpretation observations have been documented. The following discussion will be concentrated on high L-band radar returns from lowland vegetation (including forest) and also L-band returns from other forest conditions and types.

Analysis of spaceborne L-band SAR imagery have shown anomalously high returns (bright tone) from three different cover types: urban, agricultural, and swamp (Waite et al. 1981). Several investigations have noted that spaceborne L-band SAR data can be used to detect standing water under a forest canopy (Hoffer et al. 1985; Krohn et al. 1983; MacDonald et al. 1980; Mueller and Hoffer 1985; Mueller et al. 1985b; Ormsby et al. 1985; Waite et al. 1981). Anomalous returns were observed in Seasat-A SAR imagery for flooded forest stands of pure cypress; mixed stands of white oak, live oak, and hickory; and also mixed stands of cypress and willow with occasional oak, sweetgum, and hickory in Louisiana and Arkansas (MacDonald et al. 1980). In the Atchafalaya Basin of Louisiana, cypress stands with variable water level and an undergrowth of swamp vegetation over the water surface did not yield this anomalous return. Therefore, MacDonald et al. (1980) proposed that the phenomena is not species dependent and the presence of a vegetation understory between the water surface and the

forest canopy prevents this effect. The resultant tone in this case is that characteristic of upland forest (not underlain by water).

Krohn et al. (1983) observed similar phenomena with Seasat SAR data acquired over eastern Virginia and Maryland. A moderate to bright tone was characteristic of upland forest consisting of several oak species, red maple, Virginia pine, loblolly pine, and shortleaf pine, due to diffuse scattering. Radar return from lowland sites with vegetation underlain by water was strong in some cases and vice versa depending on the structure of the canopy. Thin-stemmed coastal marsh plants having heights of approximately one meter and underlain by water had a lower return than the upland forest, whereas a neighboring flooded mature forest of loblolly pine, with some mixed hardwood species and an understory of evergreen bayberry exhibited a stronger return than upland forest. Farther inland, three flooded vegetation associations yielded high returns (stronger than upland forest). Pure stands of water tupelo with an understory of evergreen bayberry had the lowest of the three strong returns. Multi-tiered unevenaged forest stands of red maple, sweetgum, willow oak, and willow had a slightly higher return. The highest return at this second site was from flat-leaved marsh plants having a height of approximately 0.5 m above the water surface. To explain the difference found between the

two marsh areas, Krohn et al. (1983) suggested that the height of the vegetation was not the important parameter influencing the return, but rather some other factor such as vegetation density of morphology was causing the increased backscatter.

Ormsby et al. (1985) investigated radar return from flooded vegetation situations and found that the L-band response from shorter vegetation species, such as marsh grass, in a flooded situation, was minimal unless the vegetation itself was wet. However, with increased vegetation volume and height, the amount of scattering and enhancement increases when the vegetation is underlain by water. The difference in radar return between flooded and non-flooded forest areas using Seasat-A SAR data and L-band (18.75 cm) scatterometer data for an area in Texas and Maryland was quantified by Ormsby et al. (1985). The slight differences in species mix were not considered. Since no precipitation had occurred prior to measurement, it was felt that all variation was due to surface roughness as well as signal enhancement due to the standing water beneath the canopy. They concluded that an increase of approximately 3 to 6 dB can be expected from water under a forest canopy regardless of species mix.

Ford et al. (1983) interpreted four SIR-A images of predominantly forested areas. It was found that forest swamps often have a very strong (bright) radar return.

This was the case for an area of the Lower Coastal Plain of North Carolina, where hardwood swamps characterized by large gums, cypress, maple, and bay trees, produced strong radar returns. Cypress-tupelo swamps in the Savannah River floodplain of the southeastern U.S. also had strong radar returns, while drier regions of oak, ash, and hickory within the swamp forests had a lower (darker) radar return.

Within imagery for the two areas mentioned above, Ford et al. (1983) also found that southern pine forests (loblolly and longleaf pine included) had a light gray appearance, and thus not as strong a radar return as the swamp areas. Clearcuts within the pine forests could be easily delineated by their darker tone and typical linear boundaries. In the North Carolina scene, large pocosins, characterized by open aspect with stunted shrub and vine species associated with a mat of roots over saturated black organic mud, had low radar returns (dark gray).

It was found by Hoffer et al. (1985) and Mueller and Hoffer (1985) that incidence angle has a large influence on radar return from forest vegetation. The analysis of multiple incidence angle SIR-B data obtained over a forested study site in northeastern Florida showed that forest cover had a relatively high backscatter. Slash pine forests had a lower return than the cypress-tupelo and cypress swamps. Forest cover underlain by standing water (swamps) had a very strong return. The steeper the

incidence angle, the more pronounced was this enhanced return. At a shallow angle of incidence (58^0) pine forest and deciduous swamps were not differentiable.

A scene from a coastal swamp area of Irian Jaya, Indonesia, demonstrated that in some cases, different tropical forest types can be separated in the imagery (Ford et al. 1983). Lowland tropical forest, with an associated mangrove swamp understory, was represented by a generally uniform medium-gray tone. The absence of the mangrove understory increased the radar return and the resultant tone was a lighter gray. This is in accordance with findings by MacDonald et al. (1980).

From the above observations, it can be seen that forest cover often has a high L-band radar return. Since the target surface roughness is one of the major factors affecting radar return (Lillesand and Kiefer 1987), it is to be expected that a forest canopy which is varied and rough textured will diffuse the radar signal and cause a relatively high response. The presence of standing water below the forest stand can cause an increase in radar return, in some cases causing an anamolous return. The enhanced return is believed to be caused by a complex scattering phenemenon where the signal penetrates the forest canopy, is reflected in the corner formed by the tree trunks and water surface, and then exits the canopy back to the sensor.

With a shorter wavelength SAR system, the enhancement due to flooding has not been as consistent. Both Krohn et al. (1983) and Ormsby et al. (1985) stated that with flooded tall vegetation such as trees, the enhancement so prevalent with SAR imagery obtained at a 23.5 cm wavelength was absent from imagery obtained at a 3 cm wavelength. However, thin-stemmed coastal marsh plants which had relatively low radar returns in Seasat imagery (L-band) had high return in X-band imagery (Krohn et al. 1983). They attribute this effect to the inability of the shorter wavelength energy to penetrate the forest canopy while the marsh vegetation scatters the X-band signal in a diffuse pattern. Contrary to the findings of Krohn et al. (1983) and Ormsby et al. (1985), it was reported by Wu (1984) that X-band SAR data can be used for detection of standing water beneath forest vegetation.

Quantitative Analysis

The application of quantitative techniques to remotely sensed data as reported by Bartolucci (1979), Colwell (1983), Lillesand and Kiefer (1987), and Phillips and Swain (1978), have been concentrated on the numerical analysis of multispectral optical data. Recent advances in digital computer storage and processing capabilities have enabled the acquisition of high-resolution digital SAR imagery

(ERIM 1986). A radar system is not multispectral since it usually operates at one wavelength only. However, such variables as look-direction, polarization, and angle of incidence can create multiple-parameter data sets for the same ground location.

Classification. Techniques developed for multispectral optical image data have been applied to the classification of digital SAR data acquired for vegetated areas. Dual-polarized (HH and HV) digitized X-band SAR data for a predominantly forested area in South Carolina was quantitatively analyzed using three classification schemes, one using a per-pixel classifier and the other two utilizing spatial classifiers (Knowlton 1982; Knowlton and Hoffer 1983). Spatially based classifiers performed better than the per-point classifier with data of original pixel resolution and also spatially averaged (degraded resolution) data. Spatially degrading the resolution caused the greatest improvement in classification with the per-point classifier. Classification accuracies (based on seven cover types) obtained using spatially based classifiers ranged from 63.3% to 68.4%, while those obtained with the per-pixel classification algorithm were 35.7% and 45.9%, depending on spatial resolution. A supervised training method was utilized in this study.

Wu (1983, 1984) quantitatively analyzed aircraft X-band (three polarizations) and satellite L-band SAR data for areas in South Carolina and Alabama. L-band SIR-A imagery was digitized at 20 m resolution and later filtered with a 3 x 3 averaging window to reduce speckle. A supervised training method was utilized followed by the application of a maximum-likelihood classification technique. Classification accuracies were below 50% for pine forest, pine forest with slash (thinned), clearcut, pasture/fallow field, and cropland classes in the X-band SAR data. To improve classification with SAR data, Wu suggested that a classification algorithm incorporating texture or spatial feature information should be included in the classification scheme. The L-band SIR-A radar classification had the best results (83%) for pine forests over 30 years of age. The L-band analysis also indicated that radar returns from three pine forest classes were highly correlated with tree age.

Spaceborne L-band SAR data acquired by Seasat and SIR-A were digitally analyzed for land cover mapping purposes (Ulaby et al. 1983; Brisco et al. 1983). A supervised maximum-likelihood algorithm was utilzed on a per-pixel basis and also on spatially averaged data. Combined data sets and single data sets were classified for five general cover types (including forest). The best classification accuracy (97.5%) was achieved by combining two Seasat data

sets (one ascending track, one descending track) with a SIR-A data set (all three data sets spatially averaged). Ulaby et al. (1983) felt that this indicates that the effect of different incidence angles can increase classification accuracies. The Seasat-A SAR had an incidence angle of 20° while SIR-A had an incidence angle of 50°.

Ulaby et al. (1980) quantitatively analyzed dual polarized (HH and HV) L-band SAR data to determine its utility for classifying agricultural crops. A higher overall classification accuracy (71.2%) was achieved using both the HH and HV polarization data sets together. Forest could be discriminated using the cross-polarized (HV) data, but was confused with agricultural crops when only the like-polarized (HH) data was utilized.

Spatial Filtering. As mentioned earlier, the coherent averaging of independent looks for each pixel can be used to reduce the speckle from digital radar imagery. However, if this is not a viable option and an alternative is desired or additional smoothing is necessary, spatial filtering is often conducted. This technique was utilized by Brisco et al. (1983), Knowlton and Hoffer (1983), Sader (1987), and Wu (1984). Wu utilized a 3 x 3 pixel cell for averaging L-band SIR-A data, but no comparison was made with non-filtered data. However, Knowlton and Hoffer

(1983) did study the effect of filtration--a 2 x 2 pixel average--on the outcome of three different classification algorithms. Overall performances between the filtered and non-filtered data sets were found to be significantly different for the Gaussian maximum likelihood (GML) and minimum distance PER-FIELD classifier based on the Newman-Keuls Multi-Range test. However, they were not significantly different for the SECHO classifier, a LARSYS contextual classification algorithm which considers both spatial and spectral information. An increase was seen in classification performance for the GML classifier, but a decrease was seen for the PER-FIELD classifier when using the filtered data.

Brisco et al. (1983) investigated the influence of speckle on classification accuracy by degrading the resolution of a Seasat-A SAR and SIR-A image in a step-wise manner and then classifying the data. The spatial averaging did increase classification accuracy rapidly at first, up until about 20 independent samples were averaged, after which the increase was more gradual. Brisco et al. (1983) felt that the rapid increase is due to a reduction in fading (speckle effects). An improvement in overall classification performance was achieved by using a 6 x 6 filter which boosted the SIR-A (single data set) classification from 71.8% to 85.3%. Goodenough et al. (1980) investigated the performance of four classification

techniques with a four channel SAR data set consisting of X-band (HH and HV) and L-band (HH and HV) radar data. They concluded that all SAR data should be median filtered prior to interpretation for crops and forest.

Sader (1987) used a 5 x 5 median filter to remove speckle noise from multipolarized L-band aircraft SAR before determining the relationship between radar return and various forest stand characteristics. No comparison was made between filtered and unfiltered SAR data.

To summarize, it would appear that from an applications standpoint, the use of computer aided analysis techniques applied to SAR data has been very limited in comparison to the extensive analyses conducted with optical data such as Landsat Multispectral Scanner and Thematic Mapper data. This is particularly true in the area of forest vegetation -- few radar studies have concentrated on the use of radar data in forestry, and an even smaller number of studies has utilized digital analysis techniques for mapping and monitoring forest cover. The analyses that have been conducted have dealt with radar data obtained at various wavelengths, polarizations, and incidence angles for a variety of forest types and conditions. Few applications studies have comprehensively addressed the question of how variations in these parameters affect backscatter from a given forest target. Additionally, it was found that although spatial filters have been applied

to SAR data, little applied research has been conducted to select the most appropriate filter treatment. In total, it would appear that the existing knowledge base for interpreting and digitally classifying radar data of forested land is not very extensive and many gaps and questions exist. Additional studies are required to determine the effects and interactions of both the system and target parameters on radar backscatter. Fortunately, a number of satellite radar experiments are being planned that will acquire multi-parameter SAR data sets in the early and mid-1990's. These experiments will allow thorough investigations of the many influences on radar backscatter.

CHAPTER 3

MATERIALS AND METHODS

Study Site Description

The data utilized for this study covers an area of approximately 380 square kilometers (147 mi^2) of Baker County (and a small portion of Union County), Florida, located in the northeastern part of the state (Figure 3.1).[1] The dominant natural feature of the study site is the northern portion of Swift Creek Pond in the southeastern corner of the SIR-B image data, while a dominant cultural feature is the highway intersection of Interstate 10 and US 90, located near the center of the study site. This highway intersection is located approximately thirty kilometers south of the Okefenokee Swamp and thirty kilometers east of Lake City, Florida.

The study site is located in the Central Delta Plain and Tertiary Highlands physiographic subdivision of the Florida Plateau (Puri and Vernon 1959). It is

---

1. The study area indicated here corresponds to a subset of the total SIR-B data obtained for the "Microwave and Optical Remote Sensing of Forest Vegetation" study that was described in Chapter 1.

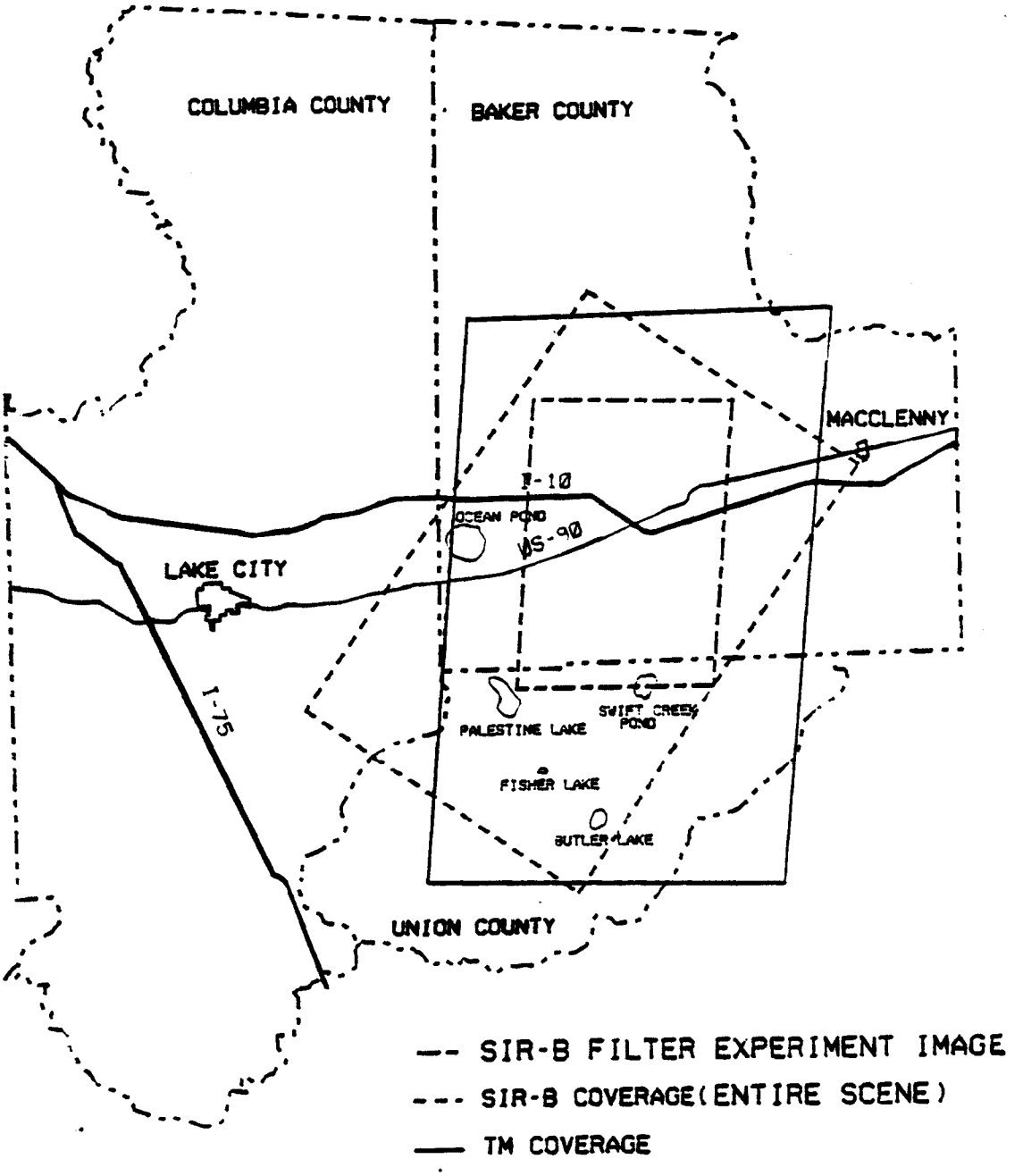

Figure 3.1 Location of the SIR-B data set utilized in this filtering experiment. The boundaries for the entire SIR-B scene of the Florida Forestry Test Site and the registered Thematic Mapper data are indicated.

characterized by swampy plains with lakes in soluble limestone. Soils of the area are predominantly sandy. Elevation within the study site ranges from approximately 27 to 53 meters (90 to 175 feet) above mean sea level.

The nearest official weather station is located at Lake City. The climate is humid, subtropical and is characterized by a mild mean annual temperature of 20.2° C (68.4° F) with mean annual precipitation of 137.62 centimeters (54.18 in) [NOAA 1976].

Ownership of the forested land in the study site is principally divided between Champion International Corporation, Owens-Illinois Corporation, Southern Resin and Chemical Company, and the U.S. Department of Agriculture Forest Service (Osceola National Forest). Forest cover types on the study area according to the classification scheme developed by Avers and Bracy (1974) for the Osceola National Forest are Pine Palmetto Flatwoods, Cypress Swamps, Creek Swamps, and Mixed Bay Swamps. These forest cover types, along with the associated tree and shrub species, are given in Table 3.1. Species present in a particular forest stand include a combination of species associated with the general forest type. The scheme was developed for natural vegetation types associated with the soils of the area. Even under intensive management, the location or composition of these vegetation associations have not greatly changed since most of the Swamps were left

Table 3.1 General forest cover types of Osceola National Forest, Florida, after Avers and Bracy (1974).

FOREST TYPE	COMMON TREE SPECIES	COMMON UNDERSTORY SHRUBS[1]
PINE PALMETTO FLATWOODS[2]	slash pine (*Pinus elliottii*) longleaf pine (*Pinus palustris*)	saw palmetto (*Serenoa repens*) common gallberry (*Ilex glabra*) large gallberry (*Ilex coriacea*) southern bayberry (*Myrica cerifera*) oak (*Quercus* spp.)
CYPRESS SWAMPS[3]	pondcypress (*Taxodium distichum* var. *nutans*) baldcypress (*Taxodium distichum*) swamp tupelo (*Nyssa sylvatica* var. *biflora*) black tupelo (*Nyssa sylvatica*) sweet bay (*Magnolia virginiana*) loblolly bay (*Gordonia lasianthus*) slash pine (*Pinus elliottii*) pond pine (*Pinus serotina*)	Virginia willow (*Itea virginica*) fetterbush (*Lyonia lucida*) buttonbush (*Cephalanthus occidentalis*) evergreen bayberry (*Myrica heterophylla*
CREEK SWAMPS	sweet bay (*Magnolia virginiana*) red maple (*Acer rubrum*) sweetgum (*Liquidambar styraciflua*) loblolly bay (*Gordonia lasianthus*) cabbage palm (*Sabal palmetto*) black tupelo (*Nyssa sylvatica*) water oak (*Quercus nigra*) loblolly pine (*Pinus taeda*)	Virginia willow (*Itea virginica*) sweet pepperbush (*Clethra alnifolia*) flowering dogwood (*Cornus florida*) red bay (*Persea borbonia*)
MIXED BAY SWAMPS	sweet bay (*Magnolia virginiana*) red maple (*Acer rubrum*) slash pine (*Pinus elliottii*) pondcypress (*Taxodium distichum* var. *nutans*) sweet gum (*Liquidambar styraciflua*) water tupelo (*Nyssa aquatica*) pond pine (*Pinus serotina*) water oak (*Quercus nigra*)	sweet pepperbush (*Clethra alnifolia*) southern waxmyrtle (*Myrica cerifera*) buttonbush (*Cephalanthus occidentalis*) yaupon (*Ilex vomitoria*) large gallberry (*Ilex coriacea*) fetterbush (*Lyonia lucida*)

1. Partial listing.
2. Some young loblolly pine (*Pinus taeda*) plantations are present, but their total acreage is minimal.
3. Small cypress ponds often occur as inclusions within Pine Palmetto Flatwoods.

as such, and the Pine Palmetto Flatwoods have remained as such with minor changes such as pine species conversion. Southern pine is managed with a rotation age of 50 years on the Osceola National Forest and from 25 to 30 years on land owned by forest product companies. Longleaf pine is more common on the Osceola National Forest than on company lands. Most company lands have been converted to pine plantations where suitable (mostly land classified as Pine Palmetto Flatwoods), whereas older naturally seeded pine timber is more common on the Osceola National Forest. Pine plantations are almost exclusively slash pine with a low acreage planted in loblolly pine. The two most dominant understory species of the Pine Palmetto Flatwoods are saw palmetto and common gallberry.

Data Utilized

Primary

The primary data analyzed were a multi-angle SAR data set obtained by the Shuttle Imaging Radar-B (SIR-B) during Space Shuttle Flight 41-G in October 1984. The data were collected on October 9, 10, and 11, each day at a different angle of incidence (Table 3.2 and Figure 3.2). These data were digitally processed by the Jet Propulsion Laboratory (JPL) at the California Institute of Technology in

Table 3.2 Characteristics of the digitally correlated SIR-B data acquired over the Florida Forestry Test Site during Space Shuttle Flight 41-G. Characteristics listed pertain to the entire SIR-B scene obtained for the area.

Parameter	Data Set Characteristic		
Center incidence angle	58.4°	45.3°	28.4°
Acquisition data	9 October 1984	10 October 1984	11 October 1984
Center acquisition time: GMT	0934	0917	0900
EDT	0534	0517	0500
Data take scene number	AK-064.2-003	AK-080.2-003	AK-96.2-003
Orbital track (Azimuth from true north)	45.0°	45.0°	45.6°
Platform altitude	229.45 km	230.12 km	225.67 km
Slant range to near edge	409.81 km	311.37 km	249.46 km
Center resolution (ground range x azimuth)	16.5 m x 31.5 m	19.8 m x 34.1 m	29.6 m x 25.5 m
Correlated pixel size	12.5 m x 12.5 m	12.5 m x 12.5 m	12.5 m x 12.5 m
Resampled pixel size	28.5 m x 28.5 m	28.5 m x 28.5 m	28.5 m x 28.5 m
Quantization levels	256	256	256
Wavelength	23.5 cm	23.5 cm	23.5 cm
Polarization	HH	HH	HH

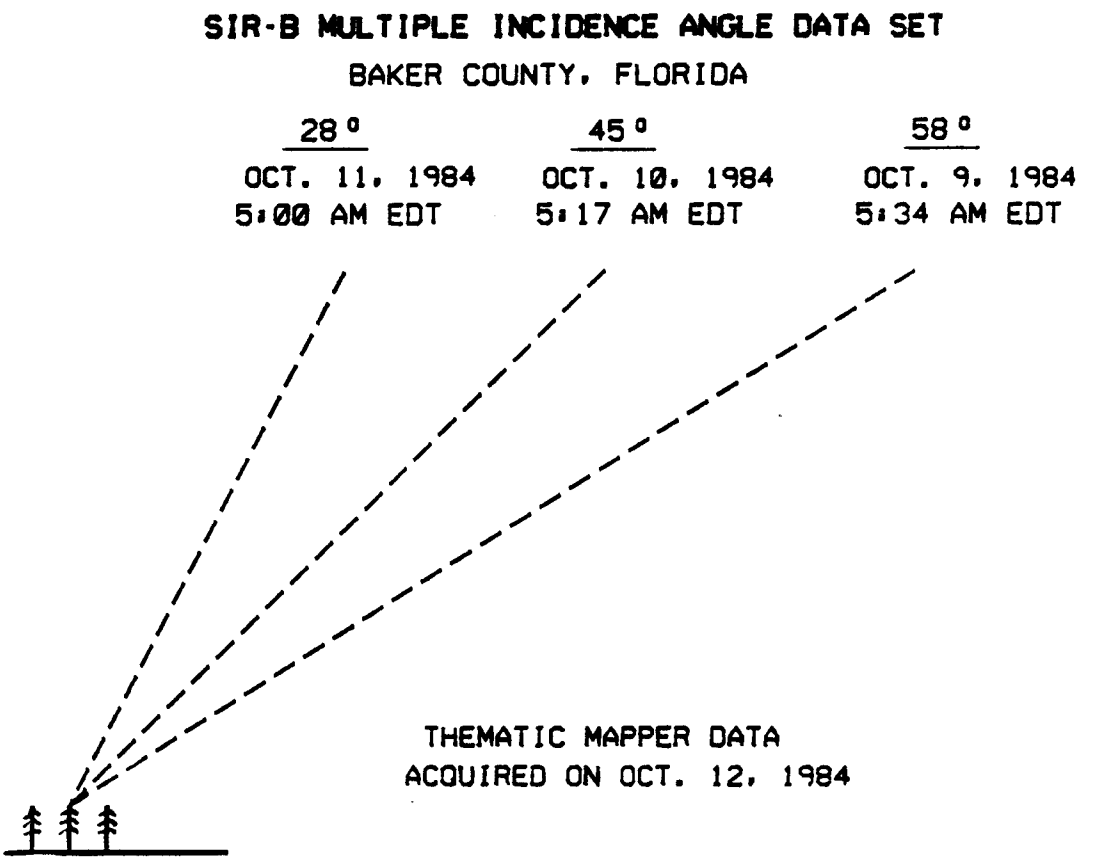

Figure 3.2 SIR-B multiple incidence angle data set for the Florida Forestry Test Site. Thematic Mapper data was acquired for the same area one day later.

Pasadena, California. A description of the SIR-B Digital Processing Subsystem utilized at JPL is given by Curlander (1986). The actual ground resolution varied for each of the three data sets as seen Table 3.2. Not shown in Table 3.2 is the fact that the range resolution varied across the scene in the range direction (image center resolution is listed). For the sake of uniformity, all SIR-B data processed by JPL was digitally correlated to 12.5 m x 12.5 m pixels. The three different data sets corresponding to the different angles of incidence were digitally registered so that each ground pixel would be represented by three digital numbers relating to the three different incidence angles.

One day after the acquisition of the 28° incidence angle SIR-B data, a Landsat Thematic Mapper (TM) scene was acquired for the study site. Characteristics of these data are given in Table 3.3. Since a focus of the overall study by Hoffer (1984) was to investigate the synergistic effects when utilizing SAR and optical data, the registration of the SIR-B and TM data sets was highly desirable. Therefore, the original registered 12.5 m x 12.5 m SIR-B data set was averaged (4 pixels), rotated, and resampled to a ground resolution of 28.5 m x 28.5 m pixels by JPL. This allowed for the digital registration of the SIR-B data to the TM data. The TM data could then be used as reference data directly for the 28.5 m x 28.5 m SIR-B data during the

Table 3.3 Characteristics of the Landsat Thematic Mapper digital data for the Florida Forestry Test Site.[1]

Spectral Band Designation	Wavelength Range (Micrometers)	Spectral Region	Ground IFOV	Pixel Size
TM 1	0.45 - 0.52	Visible blue	30 m	28.5 m
TM 2	0.52 - 0.60	Visible green	30 m	28.5 m
TM 3	0.63 - 0.69	Visible red	30 m	28.5 m
TM 4	0.76 - 0.90	Near infrared	30 m	28.5 m
TM 5	1.55 - 1.75	Middle infrared	30 m	28.5 m
TM 6	2.08 - 2.35	Middle infrared	30 m	28.5 m
TM 7	10.40 - 12.50	Thermal infrared	120 m	28.5 m

Acquisition date	12 October 1984
World Reference System	
Path	17
Row	39
Scene ID number	5022 515311 FL
Platform altitude	705 km
Center incidence angle	0 degrees
Quantization levels	256

1. Sensor characteristics defined by Freden and Gordon (1983).

filtering study. Figure 3.3 shows the SIR-B data set (28° image) utilized in this experiment. For comparison purposes, Figure 3.4 shows the Thematic Mapper Band 5 (1.55 - 1.75 μm) image for the same area.

This study investigated filtering of the 28.5 m pixel size SIR-B data. The 28.5 m data were selected for filtering since the majority of the digital analysis at Purdue has and will continue to depend on usage of the 28.5 m SIR-B data registered to the TM data. The most appropriate filter treatments will be defined for each of the three incidence angle (28°, 45°, and 58°) data sets.

The SIR-B data were recorded on computer compatible tape (CCT) in band sequential format by JPL. Due to requirements of the various image processing systems utilized, the data were converted to various formats (e.g. band sequential and band interleaved) according to the requirements of each system.

Reference

Reference data utilized for interpretation of the SIR-B data included aerial and ground photography, vegetation and soil samples, field notes, and forest stand inventory information provided by the timberland owners. Photography at different scales and formats were also available as reference data. Color infrared (CIR) stereo

Figure 3.3 SIR-B 28^{0} incidence angle image of the data set utilized in the filtering experiment.

Figure 3.4 Landsat Thematic Mapper band 5 (1.55 - 1.75 μm) image corresponding to the SIR-B data in Figure 3.3.

coverage photographs (1:100,000) were acquired for the complete study area in September 1984 by JPL. Complete CIR coverage for the area was also available at a scale of 1:58,000, obtained as part of the National High Altitude Photography program, with different sections of the area photographed in January 1983, February 1984, and March 1984. In addition to the above complete coverage, stereo photographs (1:15,840) obtained in January 1981, were made available by St. Regis Corporation (now a part of Champion International Corporation) for a large portion of the study area. In August and October (during Flight 41-G) 1984, 35 mm reference photographs of various forest stands and features were obtained with both CIR and normal color film types from a light aircraft and also from the ground. The primary and reference data utilized in this study are listed in Table 3.4.

As was mentioned above, the TM and SIR-B data sets were digitally registered by JPL. Given this, and the short time interval (one day) between acquisition of the TM and SIR-B data, the TM data are also considered to be important reference data. As was indicated in Table 3.3, this TM data set consists of measurements collected in seven optical spectral bands covering portions of the visible, near infrared, middle infrared, and thermal infrared portions of the electromagnetic spectrum.

Table 3.4 Digital image and photographic data utilized in the SIR-B spatial filtering experiment.

USE	DATA TYPE	ACQUISITION DATE	PIXEL SIZE	PHOTO FORMAT	PHOTOGRAPHIC DATA SCALE	COVERAGE OF STUDY AREA[1]
PRIMARY ANALYSIS	Shuttle Imaging Radar-B (SIR-B)	9 Oct 1984	28.5 m			C
		10 Oct 1984	28.5 m			C
		11 Oct 1984	28.5 m			C
REFERENCE	Landsat 5 Thematic Mapper (TM)	12 Oct 1984	28.5 m			C
REFERENCE	Vertical Aerial Photography (Color IR)	14 Sep 1984		70 mm	1:100 000	C,S
		Mar 1984		9 in	1: 58 000	P
		5 Feb 1984		9 in	1: 58 000	P
		24 Jan 1983		9 in	1: 58 000	P
		12 Jan 1981		9 in	1: 15 840	P,S
REFERENCE	Oblique Aerial Photography (Color IR and Color)	7 Oct 1984		35 mm	varies	P
		16 Aug 1984		35 mm	varies	P
REFERENCE	Ground Photography (Color and Color IR)	8-11 Oct 1984		35 mm	varies	P
		14-19 Aug 1984		35 mm	varies	P

1. Coverage: C Complete
P Partial
S Stereo pairs

Several maps were used for reference data including USGS 7.5 minute quadrangles (1:24,000), a Baker County Plat Directory, and forest stand maps supplied by the various timberland owners. No Soil Conservation Service Soil Survey has been conducted for Baker County.

Two visits were made to the study area, the first in August 1984 and the second during Space Shuttle Flight 41-G in October 1984 (subsequent visits were made by fellow researchers in February 1986 and June 1987). The first trip facilitated familiarization with the study area and establishment of contacts with timberland owners. Additionally, aerial and ground 35 mm photos were taken and stand descriptions were prepared to document conditions of selected forest stands. During the second field visit, additional forest stands and features were photographed and described, and inventory data and maps were obtained from Champion International, Owens-Illinois, Southern Resin and the USDA Forest Service. Stand inventory data parameters are listed in Table 3.5. Inventory data were organized into a database using dBase III software running on an IBM PC/AT.

SIR-B Data Characteristics

To effectively utilize any type of remote sensing data, the analyst must understand fundamental

Table 3.5 Forest stand timber inventory data provided by cooperating timberland owners.

STAND PARAMETER	OWNERSHIP			
	USFS	Champion	Owens-Illinois	Southern Resin
Stand Designation	x	x	x	x
Species	x	x	x	x
Acreage	x	x	x	x
Age	x	x	x	x
Site Index or Site Quality	x	x	x	x
Volume (Cords)		x	x	x
Volume (Cords/Acre)		x	x	x
Basal Area/Acre		x	x	x
Stems/Acre		x	x	x
Stems/dbh/Acre[1]			x	x
Tree Height			x	

1. Estimated at date (which varies by stand) of cruise and not projected. One-inch dbh classes for Southern Resin and two-inch dbh classes for Owens-Illinois.

characteristics of the sensor system and the associated signal-target interactions. An inherent characteristic of SAR data is speckle noise. The presence of speckle increases the overall variance of the data and also the variance for a particular cover type class. Because of this increased variance, computer-aided analysis techniques developed for use with optical data may not work as well with SAR data. To effectively analyze SAR data, these differences, including speckle noise, must be taken into account.

Table 3.6 illustrates the difference in digital number variance (using identical ground locations) between Landsat Thematic Mapper optical scanner data and SIR-B radar data for several cover types. For comparison, TM band 1 (visible blue) and the SIR-B 28° data sets have been used. TM band 1 is a noisy band for the TM sensor in relative terms, while the 28° SIR-B data set is the least noisy of the SIR-B data sets. It can be seen that in all cases, the standard deviation of the SIR-B pixel values is much greater than those of the TM data (both data sets have 8-bit dynamic range). For pattern recognition techniques to be effective, the cover type classes to be discriminated must be differentiable in the feature space. The ability of a statistical classification algorithm to differentiate classes is highly dependent on the dissimilarity or separability of classes. As the variance for individual

Table 3.6 Comparison of mean and standard deviation of SIR-B (28° incidence angle) and Thematic Mapper (band 1, 0.45-0.52μ) digital numbers for various cover types. Both data sets have an amplitude of 8 bits.

Cover Type	SIR-B		TM		Sample Pixels
	Mean	SD	Mean	SD	
Water	27.15	5.00	70.09	1.32	660
Recent Clearcut	67.53	14.69	87.74	4.34	120
Slash Pine (2 years)	54.33	11.82	78.63	1.42	63
Slash Pine (9 years)	71.11	14.62	74.30	1.55	56
Slash Pine (25 years)	66.76	16.08	72.12	1.44	162
Slash/Longleaf Pine (50 years)	88.16	21.18	73.89	1.61	135
Longleaf Pine (76 years)	95.00	21.15	75.27	1.35	121
Cypress Swamp	130.95	26.26	74.13	1.44	99
Cypress Tupelo	137.13	31.17	75.40	1.54	100
Pasture	29.10	5.20	82.44	1.39	50

classes and the covariance between classes increases, the statistical separability decreases and the chances of misclassification increases. Thus, it can be seen that a reduction of the variance caused by speckle noise is highly desirable.

Digital Analysis Facilities

The SIR-B data were analyzed using the Purdue University Computing Center (PUCC) IBM 3083BX mainframe computer, an IBM 7350 High Level Image Processing System (HLIPS), and an ERDAS (IBM PC/AT-based) system. Software utilized for analyzing the SAR data included the LARSYS System, HLIPS, ERDAS, Statistical Analysis System (SAS), and customized Fortran 77 programs.

In preparation for subsequent digital processing of the SIR-B data, the image data was formatted on computer compatible tapes in both LARSYS MIST (band interleaved) and band sequential formats. This allowed for processing by both the HLIPS and LARSYS software. The tapes containing these image files are listed in Appendix A.

Preliminary Study

Low-pass spatial filtering was selected as the method for reducing variance in the SIR-B imagery. A variety of filter treatments were applied to several of the SIR-B

image data sets (i.e., 12.5 m and 28.5 m pixel size, 3 incidence angles -- all data sets for the same area). The entire digital filtering experiment was divided into two studies in order to fulfill the objectives previously outlined. These two studies included a Preliminary Study which is discussed in this section and the Major Study which is discussed in the following section.

The purpose of the preliminary study was to provide a basis for selecting filter treatments to be utilized in the Major Study and also to demonstrate the value of filtering as applied to SAR data. As was discussed in Chapter 2, the most common arithmetic operations utilized for smoothing of SAR data are mean and median procedures. Therefore, the filter algorithms selected were based on those two arithmetic operations. For both of these operations, a separable and non-separable algorithm was chosen. Thus, both one-dimensional (separable) and two-dimensional (non-separable) windows were included in the selected treatments. The four algorithms selected were square mean (non-separable), separable mean, square median (non-separable), and separable recursive median. By varying the window dimensions[2], a variety of treatments were available

---

2. For purposes of discussion, a separable 1 x n window and a non-separable n x n window are considered to have a window size of n. This is not inappropriate since the two passes (rows and columns separately) of a separable 1 x n filter simulate a n x n non-separable window.

for implementation and evaluation.

The two variables of interest in the preliminary study were algorithm and window size. The median algorithms were expected to preserve edges and boundaries better than the mean algorithms. It was thought that the separable filters might preserve edges and boundaries better than the non-separable filters. The possibility of reaching a root signal was investigated by repeating the same filter treatment (and thus creating a new treatment) by using additional iterations. It was felt that the separable recursive median filter would reduce the variation and reach a root signal in fewer iterations than the non-recursive filters since it utilized filter feedback as discussed in Chapter 2. By using various combinations of these two variables, it was hoped that insight would be gained into the effects of algorithm and window size on filter output. The overriding goal was to select the most appropriate combination of these variables that would constitute the best filter treatment for the SIR-B data.

The square mean, separable mean[3], and square median algorithms were available through the High Level Image Processing System running on the PUCC IBM 3083BX mainframe. The separable recursive median algorithm was originally

---

3. It should be noted that unlike the other three algorithms, the separable mean filter was limited to a maximum size input image of 1024 by 1024 pixels. There was no limit for the other algorithms.

developed within Purdue's School of Electrical Engineering and was subsequently converted for use on the PUCC IBM system (see Appendix B). Modifications of the separable recursive median program included handling of skewed data sets which was foreseen as a need with the rotated 28.5 m SIR-B data sets.

The next step in the Preliminary Study was to develop methodologies for implementation of the various filters. This was particularly important for determining the effects of multiple iterations[4] and the methods of padding. Test images were utilized to study these characteristics for each algorithm. The proper values for controlling padding were determined and it was found that the output image from the separable mean algorithm being utilized was slightly smaller than the input image by one to three lines and columns depending on the window dimension. These missing image lines and columns were replaced by extraneous values that had to be removed before subsequent iterations.

After the procedures of digital filtering were developed, filtering of actual SIR-B data was done. In the preliminary study, a variety of filter treatments were applied to the 12.5 m SIR-B data obtained at an incidence

---

4. The implementation of multiple iterations was investigated. However, in the Preliminary Study, only the first iteration of the algorithms was utilized in the filter evaluation procedures of the Preliminary Study. This variable was later investigated in the Major Study.

angle of 28°. Photographic prints were made for each of the filtered images and the unfiltered image. The photographs utilized in the visual assessment were printed at one scale only and were displayed on the HLIPS electronic display device with a linear histogramming technique. This produced a high contrast image. Interpretation of these photographs did not clearly indicate any one particular treatment as being best. Since the literature had spoken favorably of the separable recursive median filter, two different window sizes were selected for this algorithm. One window size was selected for the square mean and square median algorithms. The separable mean algorithm was not selected because it could not be implemented with data sets larger than 1024 pixels in either dimension. Therefore four treatments were selected for a preliminary evaluation of their effectiveness.

Early work was conducted with the 12.5 m data as it was the first data set made available by the Jet Propulsion Laboratory and this was the standard pixel size for the SIR-B experiment. However, when the 28.5 m data set became available, it became clear that the bulk of the digital processing and analysis would be carried out with the second data set. Therefore, emphasis was switched from the 12.5 m data to the 28.5 m data set.

To verify the merits of spatial filtering with SIR-B data, these four treatments were applied to the entire scene of the 28.5 m SIR-B data (all three incidence angles). Computer classification[5] of these four data sets (each corresponding to a filter treatment) and the unfiltered data was conducted using forty-seven training fields totaling 5214 pixels (Hoffer et al. 1986). Results from this preliminary study indicated that the use of digital filtering could improve classification accuracy as compared to the unfiltered data, and it became clear that a more detailed evaluation of various filtering techniques was needed. The evaluation techniques used had not provided definitive results and it was evident that development of a variety of evaluation techniques was necessary using both qualitative and quantitative methods of assessment.

Major Study

Introduction

After it was determined that a more detailed filtering study should be conducted, the Major Study was initiated. The 28.5 m SIR-B data was utilized in this study. The three variables of interest in this study were the filter

---

5. Using a per-point Gaussian maximum likelihood algorithm.

algorithm, window size or dimension, and the number of iterations (i.e. times that the filter is consecutively applied to data set). Based on the results of the Preliminary Study, a selection of 34 filter treatments was made (Table 3.7). The four algorithms selected in the Preliminary Study were once again used, however, modifications to the window sizes and number of iterations were made.

The range of window sizes that was investigated was from three to seven (odd only) with the separable mean and square mean algorithms. The window size was limited to seven by the HLIPS software. For the square median algorithm, the window size was limited to three by HLIPS. There was no limit on the size of the window for the separable recursive median algorithm. Therefore, a maximum window size of nine was selected. It was felt that such a large window was not necessary, but that the output would give insight into the effects of larger window sizes.

The number of iterations for each algorithm was limited to three with the exception of the square median. For this algorithm a maximum of four iterations was selected since its window size was restricted to three. It was thought that an additional iteration might provide results comparable to increasing the window size.

A 770 line by 610 column portion of the SIR-B scene was selected for filtering (shown previously in Figure

Table 3.7 Filter treatments applied to the SIR-B data in the Major Study.

Window Dimension	Algorithm			
	Square Mean	Separable Mean	Square Median	Separable Recursive Median
3	3SQMN1 3SQMN2 3SQMN3	3SMN1 3SMN2 3SMN3	3SQMD1 3SQMD2 3SQMD3 3SQMD4	3SRMD1 3SRMD2 3SRMD3
5	5SQMN1 5SQMN2 5SQMN3	5SMN1 5SMN2 5SMN3		5SRMD1 5SRMD2 5SRMD3
7	7SQMN1 7SQMN2 7SQMN3	7SMN1 7SMN2 7SMN3		7SRMD1 7SRMD2 7SRMD3
9				9SRMD1 9SRMD2 9SRMD3

KEY

aAAAAn = filter treatment code

Where:

a = window dimension

AAAA = filter algorithm
- SQMN - Square mean
- SMN - Separable mean
- SQMD - Square median
- SRMD - Separable recursive median

n = iterations

3.3). For purposes of discussion, this data set will hereafter be referred to as the SIR-B image. The selected 34 filter treatments (Table 3.7) were applied to each of the three incidence angle data sets of the SIR-B image.

In the Preliminary Study, it was found that visual assessment of the filtered images was not always definitive. With the large number of different treatments involved, it was difficult to sort through and distinguish the differences between the many treatment photos, since visual appearances were often quite similar. For this reason and others discussed in Chapter 2, a combination of both quantitative and qualitative tests was desired. After careful consideration, four evaluation studies were selected. These included: (1) Cover Type Differentiation Study, (2) Edge/Boundary Retention Study, (3) Cover Type Classification Study, and (4) Visual Assessment Study. The first three studies were quantitative in nature, while the last one was a qualitative study. Each of these will be discussed in detail in subsequent sections.

Before conducting the evaluation tests, the selection of blocks of data, called fields, was necessary. These fields were to be utilized in the Cover Type Differentiation Study and the Cover Type Classification Study. Each data block was selected from within the boundaries of a particular cover type unit such as a forest stand, pasture, or water body. Identity of the cover units and boundaries

were determined by relating reference data (e.g. stand maps and aerial photographs) to the SIR-B imagery. The registered TM data was a particularly useful reference for locating and selecting fields. A total of seventy-eight fields of known cover type were selected and their pixel coordinates were recorded. The LARSYS software required each field to be rectangular in shape.

The four evaluation studies that were utilized for assessing the 34 filter treatments will be discussed in detail. The 28° incidence angle SIR-B data was utilized in the Cover Type Differentiation Study and the Edge/Boundary Retention Study. For the Visual Assessment Study and Cover Type Classification Study, all three incidence angles (28°, 45°, and 58°) were utilized in the analysis procedures.

Cover Type Differentiation Study

The purpose of the Cover Type Differentiation Study was to quantitatively measure the differences between various fields representing a variety of different cover types. Pattern recognition techniques utilize the statistical properties of known patterns to develop rules whereby other unidentified patterns can be classified into a limited number of discrete classes (Swain and Davis 1978). In the application of this theory with remote sensing data of the earth's surface, patterns are

associated with each cover type. The nature of the pattern is dependent on the characteristics of the cover type and the electromagnetic energy being measured. It is the statistical differences between these patterns that allows for the various cover types present in a data set to be differentiated in the feature space of the image data. As the separation or statistical distance between the cover type patterns becomes greater, the cover type classes become more distinct. Unidentified data pixels can more accurately be assigned to classes (patterns) that are distinct rather than to those that have overlapping statistical distributions. The variance associated with a given cover type class pattern has a great effect on the differentiability of two classes as illustrated in Figure 3.5 for a one dimensional (channel) situation.

As the variance is reduced, the classes become more distinct and classification accuracy should increase. As mentioned previously, speckle noise increases the variance of SAR data. The purpose of utilizing spatial filters is to reduce the variance. To quantify the differences between the fields, transformed divergence (see Swain 1978) was used as the measure of statistical distance between the classes of interest. The greater the difference (statistically speaking) between two fields, the larger the transformed divergence value for that pair of fields.

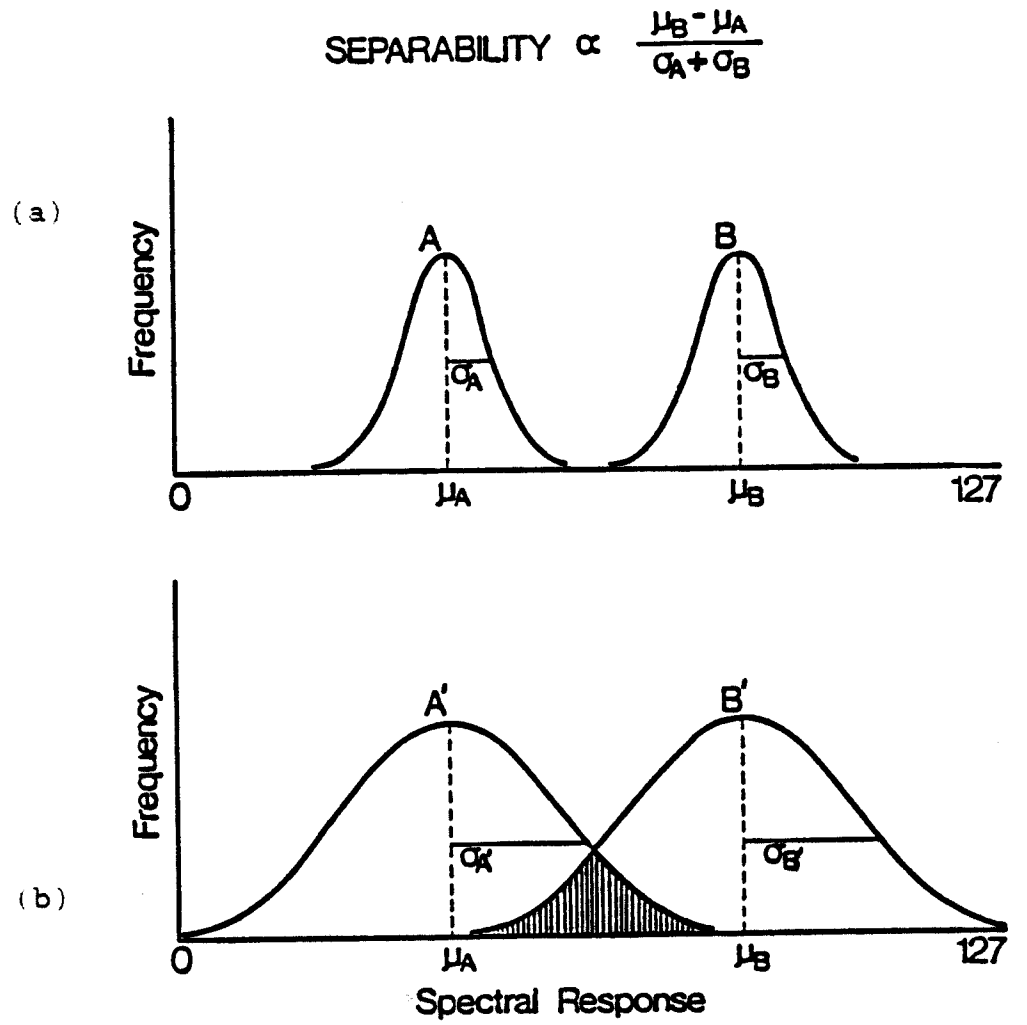

Figure 3.5 Illustration of the effect of increased variance on the differentiability of two cover type classes. In (a), cover types A and B are differentiable in the one-dimensional feature space. In (b), the increased variance associated with classes A' and B' causes overlap of their statistical distributions, even though the means are identical to those found in (a). The shaded area represents the probability of error associated with the classification of these two cover types. (After Swain 1978.)

The desirable outcome of filtering is that as the variance is reduced, the statistical distance, or separability, between two dissimilar classes becomes even greater as illustrated in Figure 3.5. Fields having similar cover type properties were not desired since the statistical distance between them would be low in the unfiltered data and would remain so after filtering. Since it was the change in transformed divergence that was of interest, only dissimilar fields were selected. Sixteen fields (of the available 78) were selected as being representative of the variety of different cover types located in the SIR-B image. The minimum size of the cover type units in which the fields were selected was 9 x 9 pixels. This reduced the likelihood of the cover type unit being obliterated (smoothed beyond recognition as a separate entity from its surrounding cover type units) by even the largest window size of nine.

For each of the 34 treatments and the unfiltered 28° incidence angle data, the class mean vectors and covariance matrices were calculated for the 16 selected fields of different cover type.[6] Next, the transformed divergence between all possible pairs of fields was calculated for

---

6. When the variance for a given field was 0.0 due to the filtering, this caused the covariance matrix elements associated with that field to be zero. To enable further use of such matrices and avoid division by zero, the 0.0 values in the matrices were replaced by the value 0.0000001.

each treatment. An average transformed divergence value was generated for each treatment based on the transformed divergence values between each pair of fields.

The treatments were ranked according to average transformed divergence and a Studentized Newman-Keuls multiple range test was run on the average transformed divergence values ($\alpha = 0.05$). The Studentized Newman-Keuls multiple range test identifies groupings of means according to the statistical differences between the means (Steel and Torrie 1980). The test was used for testing for statistically significant differences between the average transformed divergence values.

Edge/Boundary Retention Study

The purpose of this study was to provide a measure of the edge/boundary retention properties for each of the filter treatments. Low-pass filters are also known as smoothing filters. Smoothing in the sense of reducing the variance in the data was desired, but the blurring of edges and boundaries was not wanted. Therefore, a test was devised to measure the edge/boundary preservation properties of the different filter treatments. As was noted previously, this test was conducted with the 28.5 m, 28^{0} incidence angle SIR-B data set. It involved the selection of transects across boundaries between cover type

units as was done by Cushnie and Atkinson (1985) with Thematic Mapper data. The boundaries were selected such that they would divide cover type units that had distinctly different appearance in the imagery.

Transects were oriented perpendicularly to the boundary. Two vertical (along columns), two horizontal (along lines/rows), and one diagonal (approximately 45^0) transect were selected from a number of potential locations. A variety of orientations was selected to reduce the directional biases, if any, of the filters. Figure 3.6 illustrates the layout of a horizontal transect. The transects were three pixels in width, and at least 10 pixels in length. The length was adjusted so that each end of the transect included at least nine pixels (i.e. three rows or columns depending on orientation) of roughly equivalent digital number value, that were located in the cover type unit on that side of the boundary. Vertical and diagonal transects were similar except for their orientation. The width of the diagonal transect was along the columns, as with the horizontal transect, however, each group of three row pixels was offset from the previous row by one pixel (having a stair-step effect). The vertical transects had length along the columns and width along the rows.

The pixel values of these transects were utilized in two ways. They were utilized to calculate contrast ratios

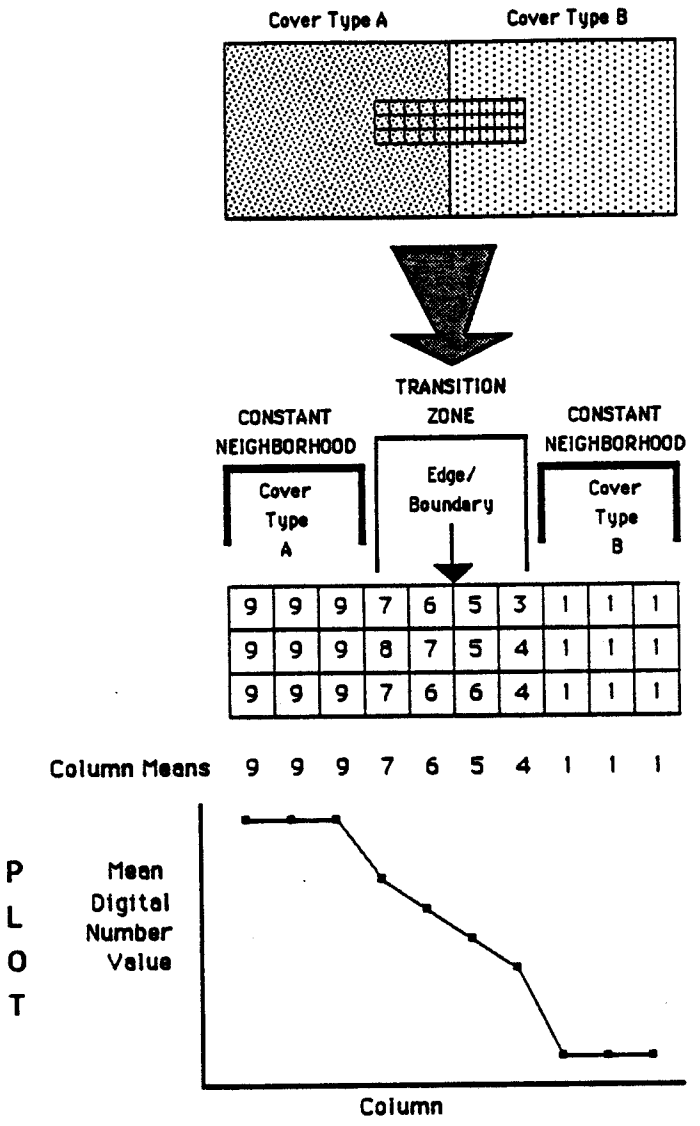

CONTRAST RATIO $\frac{1+1+1}{9+9+9} = 0.111$

Figure 3.6 Example of horizontal transect across the boundary between cover type A and cover type B. Column means are first calculated for the transect digital numbers. These means are then utilized to generate transect plots and also a ratio representing the contrast between the two constant neighborhoods.

and to plot curves depicting the boundary. For each of the filtered and unfiltered 28⁰ data sets, a contrast ratio for the cover types on opposite sides of the boundary was calculated as follows:

$$R = \frac{\sum_{i=1}^{3} \overline{Xi}}{\sum_{i=n-2}^{n} \overline{Xi}} \qquad (3.1)$$

Where:

R = Contrast ratio (reciprocal of quotient taken if necessary so that $0 < R < 1$),

$\overline{Xi}$ = Mean of three pixels located in column or row along the width of the transect,

i = Row or column number,

n = Number of rows or columns in the transect (lengthwise).

Additionally, a plot was made of the average digital number values along the length of the transect as illustrated in Figure 3.6. For each of the five transects, 35 such plots were made (corresponding to the filtered and unfiltered data sets).

The plots and ratios were used to "grade" the boundary/edge retention properties of each of the filter treatments. It was felt that the plots contained the majority of the useful information. Therefore, more emphasis was placed on analysis of the plots rather than the ratio values. For each plot, the shape of the curve

was graded and a score given to it according to the generalized grading procedure given in Figure 3.7. The first step was to determine the shape of the curve. When the boundary/edge was retained, a distinct level or plateau was found at both ends of the transect plot. For purposes of evaluation, a plateau was defined as at least three points with nearly equal value (± 2 digital numbers) found on either side of an edge. A plateau represents a theoretical "constant neighborhood" as discussed in Chapter 2. If two distinct plateaus were discernible, the shape was determined to be a "step." It had a "ramp" shape if only one plateau was discernible. That is, the transect was changed into an incline and the transition zone extended into one or both of the constant neighborhood regions. If no plateau was present nor was there a constant incline, then the shape was called "uncertain." The latter two shapes were given a score of zero.

For those plots judged as having a ramp shape, the number of transition points between the two plateaus was counted. If there was an enhancement in the boundary (e.g. caused by corner reflector effects) and this enhancement was retained, the number of transition points was decreased by one for that treatment. To be considered an enhancement, there had to be an increase of at least 10 digital numbers as compared to the adjacent constant neighborhood (cover type unit). For each filter treatment,

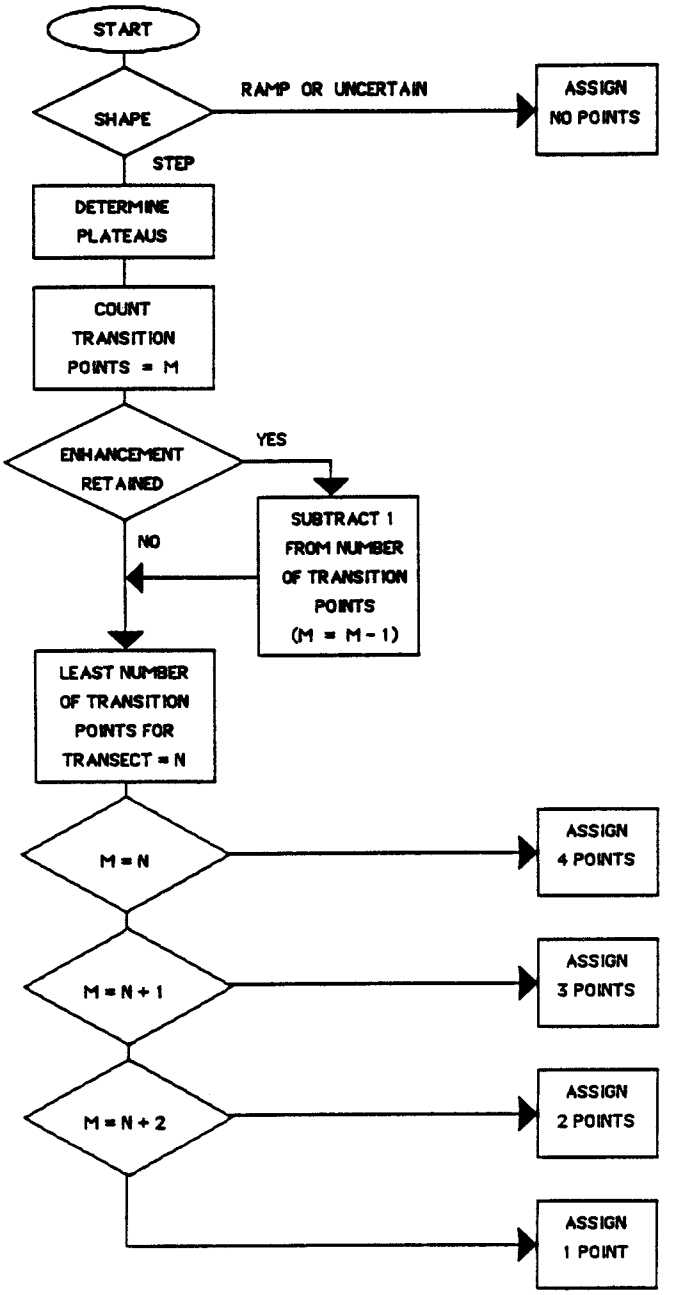

Figure 3.7 Generalized flowchart for the evaluation of transect plots and assignment of a score.

the scores from the five transects were added to yield a aggregate score. The filter treatments were then ranked by their aggregate scores. A high score was the most desirable as this indicated that on the average, the associated filter treatment had the shortest transition zone between the two cover type plateaus.

The ratios were calculated using Equation 3.1 for those curves that had a ramp shape. The ratios for the five transects were then combined, yielding a composite ratio for each filter treatment. For those treatments assigned the same aggregate score, the composite ratio was used to rank the treatments for a given score. A low ratio was desirable as this indicated a high contrast was retained between the two cover types.

Cover Type Classification Study

The 78 fields selected previously were divided into training and test fields for computer classification purposes. Twenty-seven fields considered to be representative of the cover types present and providing representation of classes proportional to their presence in the scene were utilized for training purposes. These training fields and their cover type descriptions are listed in Table 3.8. The means and covariance matrices were calculated for each field using all filtered data sets

Table 3.8 Training fields used for the Cover Type Classification Study, their cover type, field size, and cover class group.

Cover Type	Number of Pixels	Cover Class Group
Forest clearcut	20	PINE1
Forest clearcut	81	PINE1
Slash pine plantation, age 2 years	63	PINE1
Slash pine plantation, age 3 years	72	PINE1
Slash pine plantation, age 3 years	28	PINE1
Slash pine plantation, age 5 years	108	PINE1
Slash pine plantation, age 9 years	81	PINE2
Slash pine plantation, age 17 years	60	PINE2
Slash pine plantation, age 22 years	98	PINE2
Slash pine plantation, age 24 years	108	PINE2
Slash pine plantation, age 26 years	108	PINE2
Slash pine plantation, age 30 years	81	PINE2
Slash pine (natural origin), age 39 years	32	PINE2
Slash pine (natural origin), age 45 years	84	PINE2
Longleaf pine (natural origin), age 62 years	66	PINE2
Longleaf pine (natural origin), age 77 years	110	PINE2
Slash pine - cypress swamp	99	SWAMP1
Tupelo - cypress swamp	24	SWAMP1
Blackgum - sweet bay - maple swamp, age 62 years	81	SWAMP1
Slash pine - hardwood swamp	90	SWAMP2
Slash pine - cypress swamp	66	SWAMP2
Cypress swamp	90	SWAMP2
Bare soil	70	SMOOTH
Bare soil	81	SMOOTH
Pasture	81	SMOOTH
Water	100	SMOOTH
TOTAL	1982	

as well as the unfiltered data for each of the three incidence angles.[7] The training field statistics were not combined by cover type. Rather, each field was treated as a separate class during the classification process, but were later grouped by cover class for evaluation purposes.

The remaining 51 fields were utilized as test fields (totaling 2881 pixels). These fields were classified utilizing the LARSYS processor CLASSIFYPOINTS, a per-point Gaussian Maximum likelihood classifier (Phillips 1973). Thus, 35 classifications were conducted, each consisting of the same filter treatment applied to all three incidence angles. The overall correct classification accuracy was calculated as suggested by Heller and Ulliman (1983):

$$PCC_O = \frac{\sum_{i=1}^{n} N_i}{\sum_{i=1}^{n} T_i} \qquad (3.2)$$

Where:

PCC_O = Overall percentage correct classification performance (all cover types),

N_i = Total number of test pixels correctly classified for i^{th} cover class,

---

7. As in the Cover Type Differentiation Study, the covariance matrix elements with value 0.0 were changed to 0.0000001 to enable use of these statistics data sets.

T_i = Total number of test pixels for i^{th} cover class.

n = number of cover classes

For evaluation purposes, the 27 training fields were grouped into five cover classes as indicated in Table 3.8. The five groups were selected after viewing bispectral plots of the training field statistics and five groupings were found.[8] The 51 test fields were also divided into these cover class groups. The overall classification performances (PCC_o's) were compared to determine differences produced when using filtered versus unfiltered SIR-B data. The statistical significance of these differences based on PCC_o's were then tested using the Studentized Newman-Keuls multiple range test with an α = 0.05. Prior to this calculation, the PCC_o's were transformed with an arc sine transformation to convert the binomially distributed proportions (PCC_o) into a normal distribution (Steel and Torrie 1980).[9] The statistical analysis was conducted on a stratified basis to evaluate

---

8. These bispectral plots consisted of plotting digital number mean from one incidence angle against the mean of another incidence angle for each training field.

9. See pages 184 - 187 of Latty (1981) for an example of transforming the PCC_o's with the arc sine transformation and a demonstration of calculating significant differences using the Studentized Newman-Keuls multiple range test procedure.

the effects of algorithm, window size, and the number of iterations.

In addition to the classification of the test fields, classifications were conducted for a 256 x 256 pixel block centered around the highway intersection of Interstate 10 and US 90. A select number of treatments (as discussed in the next section) were classified. The classifications of this subimage[10] were analyzed in the Visual Assessment Study to assess the effects of filtering on classification for a larger area (rather than only test fields). Also, the visual assessment of the classified image would serve as a check to the tabular PCC_o results based solely on test fields.

Visual Assessment Study

As mentioned in Chapter 2, it was thought that a combination of both quantitative and qualitative evaluation techniques would be required to effectively select the best filter treatment(s) for the 28.5 m SIR-B data set. The three evaluation studies previously discussed were meant to provide quantitative and semi-quantitative measures of filter performance. This section will discuss the visual

---

10. Hereafter, this 256 x 256 pixel block will be referred to simply as the subimage.

assessment study which constitutes the qualitative evaluation.

This study was based on the visual analysis of photographic prints of the various filter treatments. The subimage selected above was utilized for detailed analysis in the Visual Assessment Study. As was stated previously, definitive results were not obtained in the preliminary study when visually assessing the filter treatments. Therefore, for this study, more effective display techniques were investigated and utilized. The improvements included using different display scales and different digital display histogramming techniques. Both black and white and color film types were utilized for taking photos of the 256 by 256 pixel block at full scale and at 1.6 times enlargement. The photos taken are listed in Table 3.9. The visual analysis procedure can be broken down into several steps. The outline of the procedure followed is given in Figure 3.8.

The first step included detailed analysis of the 28° incidence angle subimage. Black and white photos were taken of all treatments of the 28° subimage. Two different histogram techniques were utilized when displaying the data on the electronic display device of the HLIPS system. The first method used a linear stretch technique, while the second applied a standard deviation adjustment.[11] The

---

11. The linear stretch technique was the *H display option

Table 3.9 Image photographs utilized in the Visual Assessment Study.

Data Set					Filter Treatments		Enlargement Factor		Film Type		Print Type	
Individual Incidence Angle			3-Angle Composite	3-Angle Classification[1]	All	Subset	1.0	1.6	Black & White	Color	Contact	Enlargement
28	45	58										
X					X		X	X	X		X	
X						X	X	X	X			X
	X	X				X	X	X	X		X	
			X			X	X	X		X		X
				X		X	X	X		X		X

1. These classification photos were not used in the qualitative filter selection process. Rather, they were used to verify the results obtained in the Cover Type Classification Study.

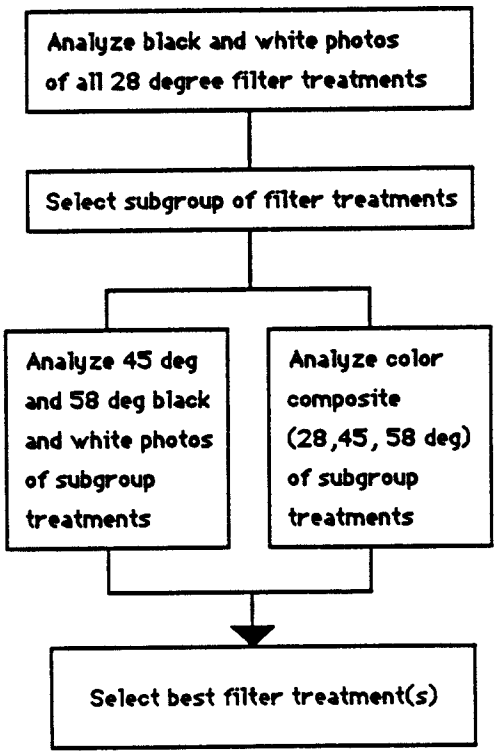

Figure 3.8 Flowchart of the Visual Assessment Study procedure.

former provided a high contrast image which was good for highlighting some of the data characteristics. The latter histogram technique provided a continuum of gray tones which made subtle details more apparent. The combined use of these two different histogram techniques was found to be superior to that used in the Preliminary Study where only the linear stretch technique had been utilized.

For comparison purposes, contact prints were made for the initial evaluation. Enlargements of some of the key treatments were made for more detailed analysis. A qualitative assessment of the filter effects was made. The effects of the algorithm, window size, and number of iterations were studied. A subgroup of filter treatments was selected for more detailed analysis.

In the next step, a variety of photographs were taken for the subgroup of filter treatments, as was indicated in Table 3.9. Single band images were photographed for the 45° and 58° incidence angle SIR-B data. Additionally, color composite images using the three incidence angles

---

of HLIPS. With this display method, a histogram of all pixels in the image was computed. Then a translation table was built in such a way that the image data was level sliced into equally populated levels. The standard deviation adjustment technique was the *S display option of HLIPS. In this method, a translation table was calculated so that the displayed data had a given mean and standard deviation. The default values were utilized for the *S option which were identical for all three color guns as follows: mean = 128.00; standard deviation = 45.00. In the monoband (gray) mode the defaults were: mean = 128.00; standard deviation = 40.00 (IBM 1983).

were photographed for the subgroup of filter treatments that were selected in the first step. The various photographic products developed in this step were analyzed and a decision was made as to which treatments were performing the best. A qualitative selection of the best filters was made based on visual assessment of the photos for the unclassified images.

For the purposes of providing a visual check of the tabular classification results, a visual assessment of subimage classifications was also conducted. For each of the subgroup (selected above) filter treatments, the subimage was classified using the training statistics developed in the Cover Type Classification Study. Color photos were taken of these classified images displayed as five cover type groups. These photos were used to interpret and verify the results obtained in the Cover Type Classification Study.

Filter Selection

The results from the quantitative and qualitative evaluation methods were compared. The initial plan was to give equal weighting to each of the three quantitative evaluation studies and the visual assessment. However, it became apparent that the Visual Assessment Study and the statistical analysis of the classification performances

provided the most useful information. Results collected by the remaining two studies were therefore considered to be of secondary importance and were used primarily to offer additional insight into the effects of the various filter treatments. Besides the selection of the best filter treatment, information on trends related to algorithm, window size, and iterations were obtained through analysis of the data obtained from the various evaluation studies.

CHAPTER 4
RESULTS AND DISCUSSION

Introduction

The results presented will be divided into two sections. First, the results from the Preliminary Study will be briefly discussed. This will be followed by a detailed presentation and discussion of the results from the Major Study.

Preliminary Study

The purpose of the Preliminary Study was to provide a basis for selecting filter treatments to be utilized in the Major Study and also to demonstrate the value of filtering as applied to SAR data. A variety of filter treatments were applied to the 28º incidence angle, 12.5 m SIR-B data. Visual assessment was conducted for photographic prints of uniform scale and displayed using a linear histogram stretch. This histogram technique was later found to be inferior to other techniques. In this assessment, only one iteration of filtering was considered. The four treatments selected using visual interpretation techniques were:

3SQMN1, 3SQMD1, 3SRMD1, and 5SRMD1 (see Table 3.7 for explanation of treatment codes). Visual assessment of these four treatments showed that there were no definitive differences or clear-cut advantages for one treatment over another. This was largely due to the methods utilized in producing the photographic prints.

In order to quantitatively analyze the effects of these filters on the 28.5 m SIR-B data, the four selected treatments were applied to the three incidence angle images (28^0, 45^0, and 58^0). For evaluation purposes, 122 test fields of known cover type were utilized (totaling 8648 pixels). Table 4.1 shows the classification results based on three cover type groups. It can be seen that in all cases, the classification accuracy improved with filtering.

After evaluating both the qualitative and quantitative Preliminary Study results, it became clear that a more detailed analysis of various filter treatments was needed. The assessment techniques utilized in the Preliminary Study did not provide clear-cut differences between treatments. Therefore, additional evaluation techniques were seen as necessary and these were developed and implemented in the Major Study. It was decided that a combination of both quantitative and qualitative assessment techniques should continue to be utilized. Improvements in the visual assessment techniques (i.e., more effective photographic products) were also seen as necessary.

Table 4.1 Classification results for the Preliminary Study given by cover type group and overall percent correctly classified (PCC_o) based on three cover type groups.

Treatment	Cover Type			Overall Performance
	Pine	Swamp	Other	
Unfiltered	87.6	79.9	71.6	79.7
3SQMN1	94.0	90.4	65.2	85.2
3SQMD1	92.5	89.9	65.4	84.6
3SRMD1	92.4	89.2	65.0	84.1
5SRMD1	95.5	92.4	63.8	86.2

Major Study

Introduction

It was seen in the Preliminary Study that filtering was beneficial to the classification process. The reason for this was the reduction of the variance in the data. To provide a better understanding of the effects of filtering on the SIR-B data, Figure 4.1 illustrates the effects of spatial filtering for three different cover types. Transects across three cover type units are plotted for the unfiltered 28° data and the 3 x 3 square mean and 3 x 3 square median treatments, each at two iterations (i.e. 3SQMN2 and 3SQMD2, respectively). It can be seen that the variance in the data has been greatly reduced. This variance reduction is quantitatively documented in Table 4.2 for several filter treatments. The standard deviation associated with all cover types was reduced by all the filter treatments. It should be noted that the filter output represents two-dimensional filtering (i.e., the filter output was influenced by pixels not shown). this is the reason for the large changes from one filter treatment to another in the plots for the swamp transect.

The results from the four evaluation studies (i.e., Cover Type Differentiation Study, Edge/Boundary Retention Study, Cover Type Classification Study, and Visual

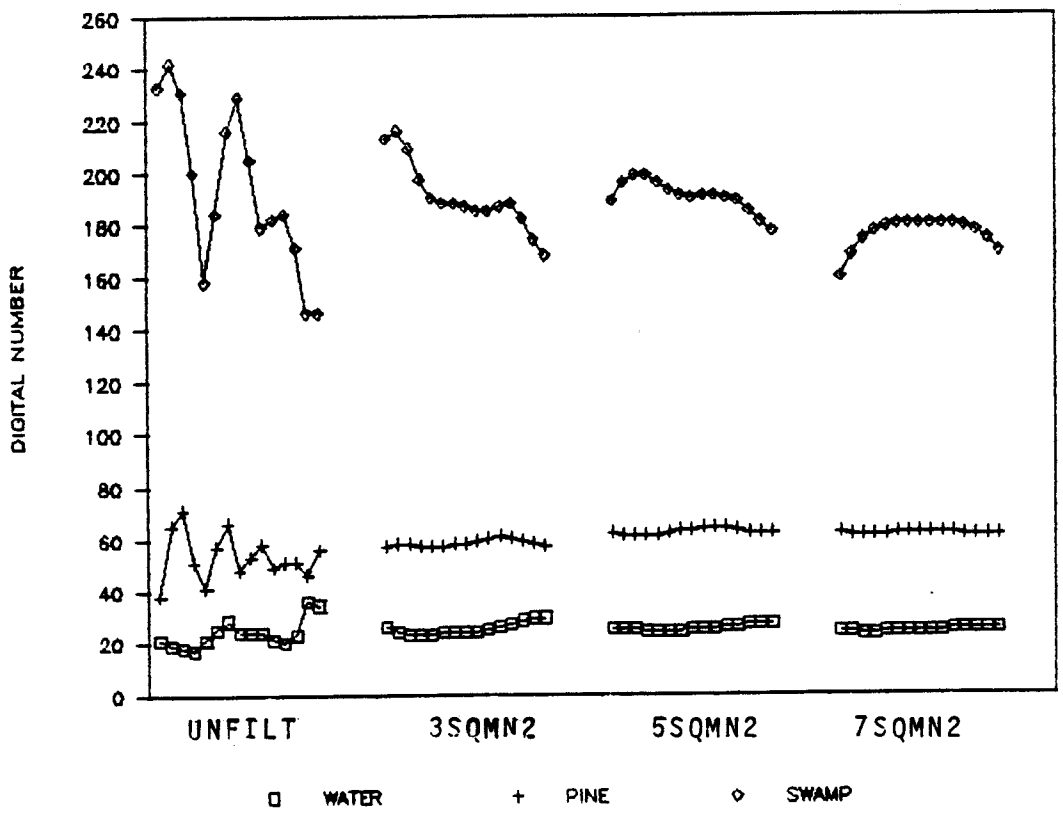

Figure 4.1 Digital number plot showing transects across three cover types for unfiltered and filtered 28° incidence angle SIR-B data. The three treatments shown are 3SQMN2, 5SQMN2, and 7SQMN2. Each transect represents 15 consecutive (along a row or column) digital number values in the respective cover type.

Table 4.2 The effect of spatial filtering on the digital number mean and standard deviation associated with various cover types for 28° incidence angle SIR-B data.

Cover Type	Unfiltered		3SQMN2		5SQMN2		7SQMN2		Sample
	Mean	SD	Mean	SD	Mean	SD	Mean	SD	Pixels
Water	22.87	3.91	22.81	1.43	22.80	1.14	22.12	0.99	100
Recent Clearcut	58.10	14.44	58.79	6.13	59.53	3.41	58.05	3.38	81
Slash Pine (3 years)	63.93	12.35	63.89	6.49	64.47	3.90	62.46	2.39	72
Slash Pine (9 years)	72.11	14.95	73.00	4.99	73.62	2.26	70.44	1.08	81
Slash Pine (22 years)	75.88	15.44	76.66	6.49	77.57	4.82	75.05	3.79	98
Longleaf Pine (62 years)	100.74	17.65	101.79	5.40	101.94	2.68	96.52	2.97	66
Cypress Swamp	131.31	27.12	128.14	9.62	124.97	5.52	116.18	4.21	90
Soil	31.54	7.99	32.14	3.20	33.16	2.37	33.09	2.34	70
Pasture	37.83	7.57	37.64	3.06	37.98	1.70	37.17	1.65	81

Assessment Study) are discussed below. The Cover Type Differentiation Study and Edge/Boundary Retention Study were conducted before a detailed visual assessment was conducted for the various treatments. This was done in the hopes of reducing the number of treatments utilized in the Visual Assessment Study. The Preliminary Study had resulted in a large number of photographic prints corresponding to the different treatments where subtle differences between the treatments could not be easily detected qualitatively. It was hoped that the two initial tests would eliminate some of the treatments from further consideration. After the Visual Assessment Study, the Cover Type Classification Study was conducted to verify the results found in the Visual Assessment Study.

Cover Type Differentiation Study

This study was conducted to quantify the improvement in the filtered SIR-B data from a classification standpoint. Transformed divergence was used as a predictor of classification accuracy. The larger the transformed divergence value, the lower the chance of misclassification between these two classes and the higher the expected classification accuracy. The average transformed divergence values for each of the 34 treatments as applied to the unfiltered 28° data are listed (ranked by average

transformed divergence) in Table 4.3. When these data were ranked, a continuum of average transformed divergence values was obtained. A comparison was made using a Studentized Newman-Keuls multiple range test. All the filter treatments showed a significant improvement over the unfiltered data. However, the groupings of the filter treatments overlapped so much that no statistically significant differences were observed between the average transformed divergence values for any of the treatments. Therefore, the relative ranking of the transformed divergence values was not felt to be useful for comparing the treatments and this study was no longer pursued. It was originally felt that the results of this study could be used to reduce the number of filter treatments evaluated in the subsequent tests. However, since no definitive differences were found, all treatments were used in subsequent evaluation tests.

Although a definitive ranking of the treatments was not obtained, it can be seen from Table 4.3 that, in general, the higher the degree of filtering (i.e. larger window size and/or more iterations), the greater the predicted classification accuracy. This indication of the relationship between window size and number of iterations with classification performance is reasonable.

Table 4.3 Average transformed divergence values for the unfiltered and filtered 28° incidence angle SIR-B data. The maximum transformed divergence value is 2000.

Treatment	TD
9SRMD3	1921.
9SRMD2	1921.
9SRMD1	1889.
7SQMN3	1854.
7SMN3	1847.
7SQMN2	1834.
7SRMD3	1833.
7SRMD2	1833.
5SMN3	1831.
5SQMN3	1817.
7SRMD1	1816.
7SMN2	1814.
7SQMN1	1789.
5SQMN2	1788.
5SMN2	1776.
7SMN1	1775.
5SRMD3	1757.
5SRMD2	1757.
5SQMN1	1700.
3SMN3	1698.
3SQMN3	1698.
5SRMD1	1697.
5SMN1	1695.
3SQMD4	1692.
3SQMD3	1661.
3SQMN2	1646.
3SMN2	1645.
3SQMD2	1615.
3SMN1	1557.
3SQMN1	1557.
3SQMD1	1516.
3SRMD3	1511.
3SRMD2	1510.
3SRMD1	1494.
UNFILTERED	1275.

Edge/Boundary Retention Study

The purpose of this study was to provide a measure of the edge/boundary retention properties of each of the filter treatments. The foundation of this study was the analysis of pixel values along each of the five transects that bisected cover type boundaries. It was hoped that this study would give insight into the effects of the various filter treatments on spatial features -- whether they were retained or they were lost due to blurring. For each transect, plots were generated for each of the 34 filter treatments and the unfiltered 28° SIR-B data. Figure 4.2 is an example plot. Each plot was assigned a score (indicative of the sharpness of the boundary) and a contrast ratio (indicative of the contrast between the two cover types) was calculated as described in Chapter 3. The scores and contrast ratios were totaled for the five transects and the resultant aggregate scores and composite ratios for the 35 data sets are listed in Table 4.4. The data were ordered, first by aggregate score and then within each aggregate score group, by composite ratio. A high composite score was desirable as this indicated preservation of boundaries. Because the contrast ratios only gave an indication of the average contrast since no measure of variation was included in the calculation, they were only of secondary value. Nevertheless, a low score

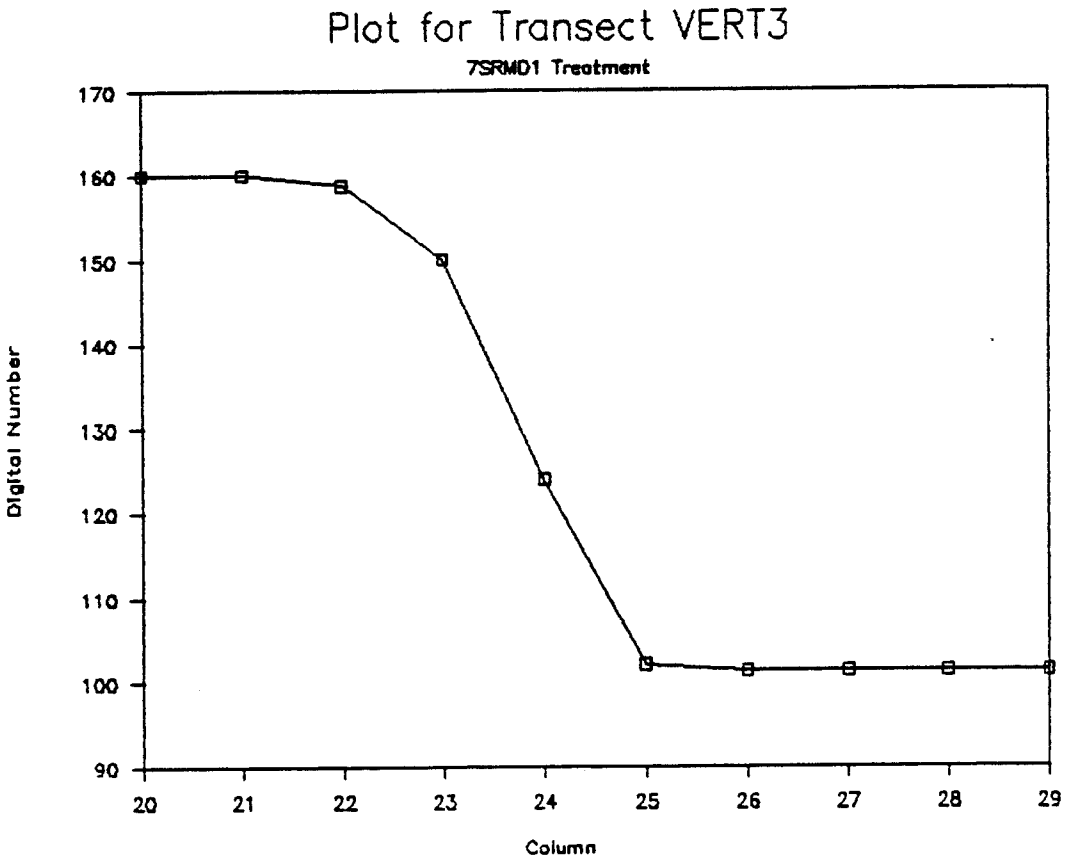

igure 4.2 Example of an edge/boundary plot for the SIR-B 28⁰ incidence angle data, in this case, using the 7SRMD2 treatment.

Table 4.4 Aggregate scores and composite ratios for the transect curves based on five transect locations.

TREATMENT	SCORE	RATIO
7SRMD1	23	2.026
9SRMD1	23	2.332
9SRMD2	23	2.354
9SRMD3	23	2.354
7SRMD2	22	2.047
7SRMD3	22	2.047
5SRMD3	20	1.813
5SRMD2	20	1.813
5SRMD1	19	1.808
3SRMD3	18	1.729
3SRMD2	18	1.729
3SRMD1	18	1.729
3SMN1	12	1.729
3SQMN1	12	1.743
3SQMD1	12	1.743
3SQMD2	9	1.759
3SQMD3	9	1.765
3SQMD4	8	1.766
5SMN1	5	1.760
3SQMN2	5	1.766
3SMN2	4	1.743
5SQMN1	4	1.772
3SQMN3	2	1.792
3SMN3	1	1.753
5SMN2	0	
5SMN3	0	
5SQMN2	0	
5SQMN3	0	
7SQMN1	0	
7SQMN2	0	
7SQMN3	0	
7SMN1	0	
7SMN2	0	
7SMN3	0	
UNFILT	0	

was indicative of a high contrast between the two cover types.

The results showed that the separable recursive median algorithm preserved edge/boundaries much better than either of the two mean algorithms at all window sizes and number of iterations. However, even though the separable recursive median algorithm preserved the edge/boundary, the contrast between the two cover types was lowered. The square median algorithm did not preserve edge/boundaries as well as the separable recursive median algorithm, however, it generally preserved the edge/boundaries better than either of the two mean algorithms. Most mean treatments received an aggregate score of zero. This indicated that the boundaries were turned into ramps and a distinctive edge was lost (blurred). This was especially true when the window dimensions were increased to greater than three. This is in accordance with what was theoretically expected as discussed in Chapter 2. The only mean filter treatments that received any score greater than zero were those with window dimensions of 1 x 3 (separable) or 3 x 3 (non-separable) at all iterations. For the mean algorithms, the next larger window dimension of five only received a positive score at the first iteration.

Visual Assessment Study

Based on experience with visually assessing the filtered images of the Preliminary Study, it was felt that the quantitative tests of the Major Study would provide the most conclusive results. As discussed in Chapter 3, the display and recording techniques used in this Visual Assessment Study proved to be far superior to those employed previously. The improvements included the digital display of data with two different histogramming techniques, and the production of photographic prints at two scales. Figure 4.3 illustrates the two histogram techniques utilized when displaying the data. The two different scales of the photographic images can be seen in Figure 4.4. The combined use of these histogramming techniques and the display of the data at two different scales provided much more effective methods for assessing the filter treatments than had been the case during the Preliminary Study.

When the various photographs were analyzed, it was found that the differences between filter treatments were much more apparent than was found with the quantitative tests. Therefore, contrary to what was expected at the onset of the Major Study, the Visual Assessment Study results were found to be extremely useful. Following is a discussion of the algorithms and their effects on the data.

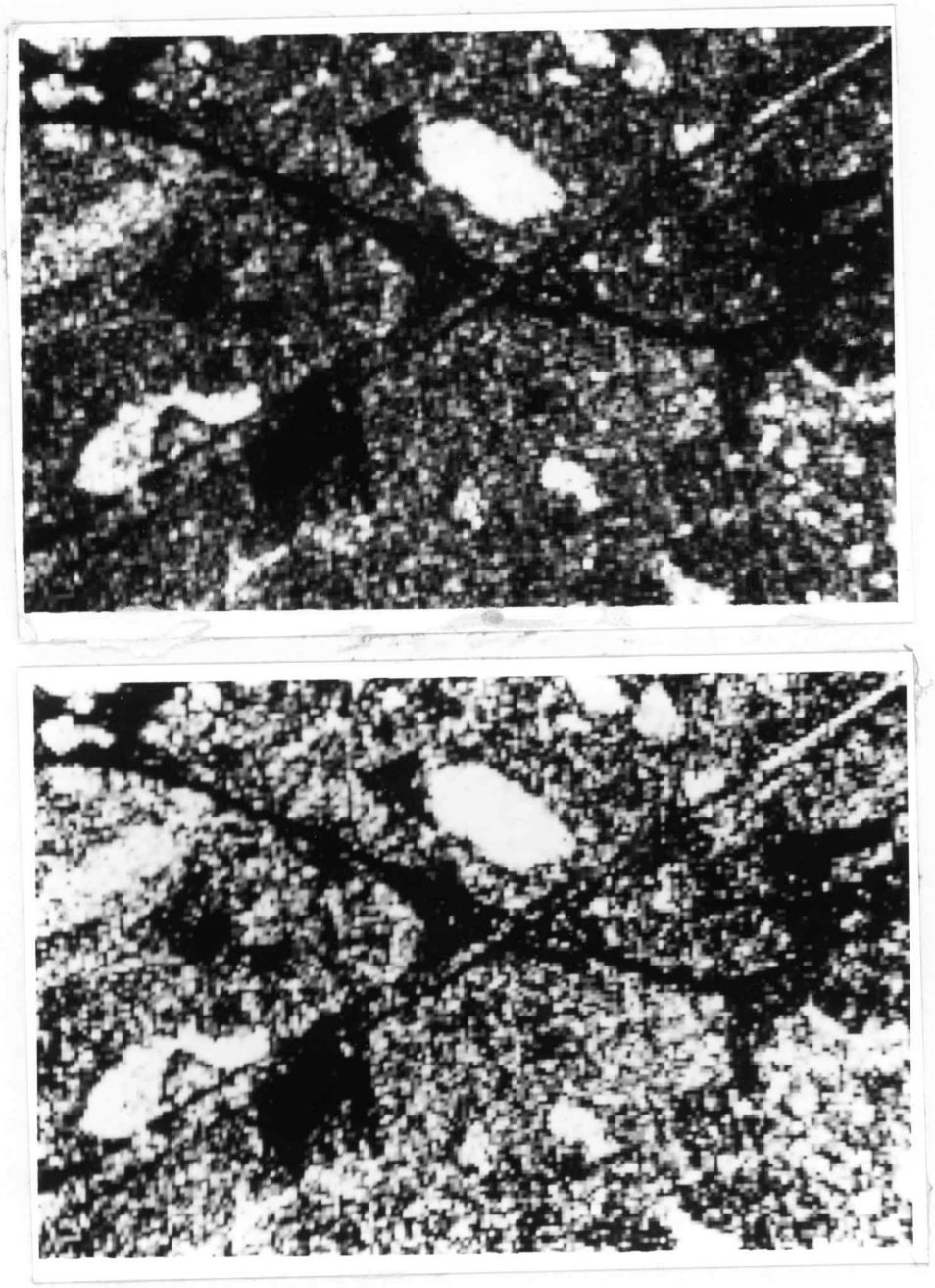

Figure 4.3 Imagery of the unfiltered 28° incidence angle SIR-B data utilizing two different histogram adjustment techniques. The top image was displayed with a standard deviation adjustment technique (*S), while the bottom image was displayed with a linear stretch technique (*H). The accompanying map identifies some of the major features found in these images.

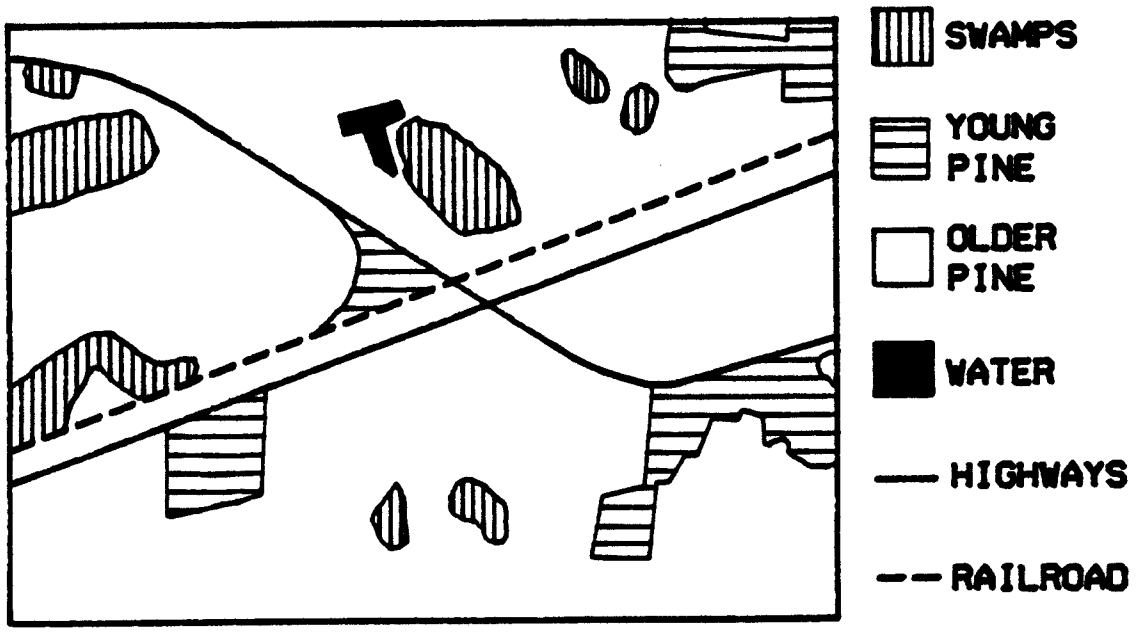

Figure 4.3 (Continued)

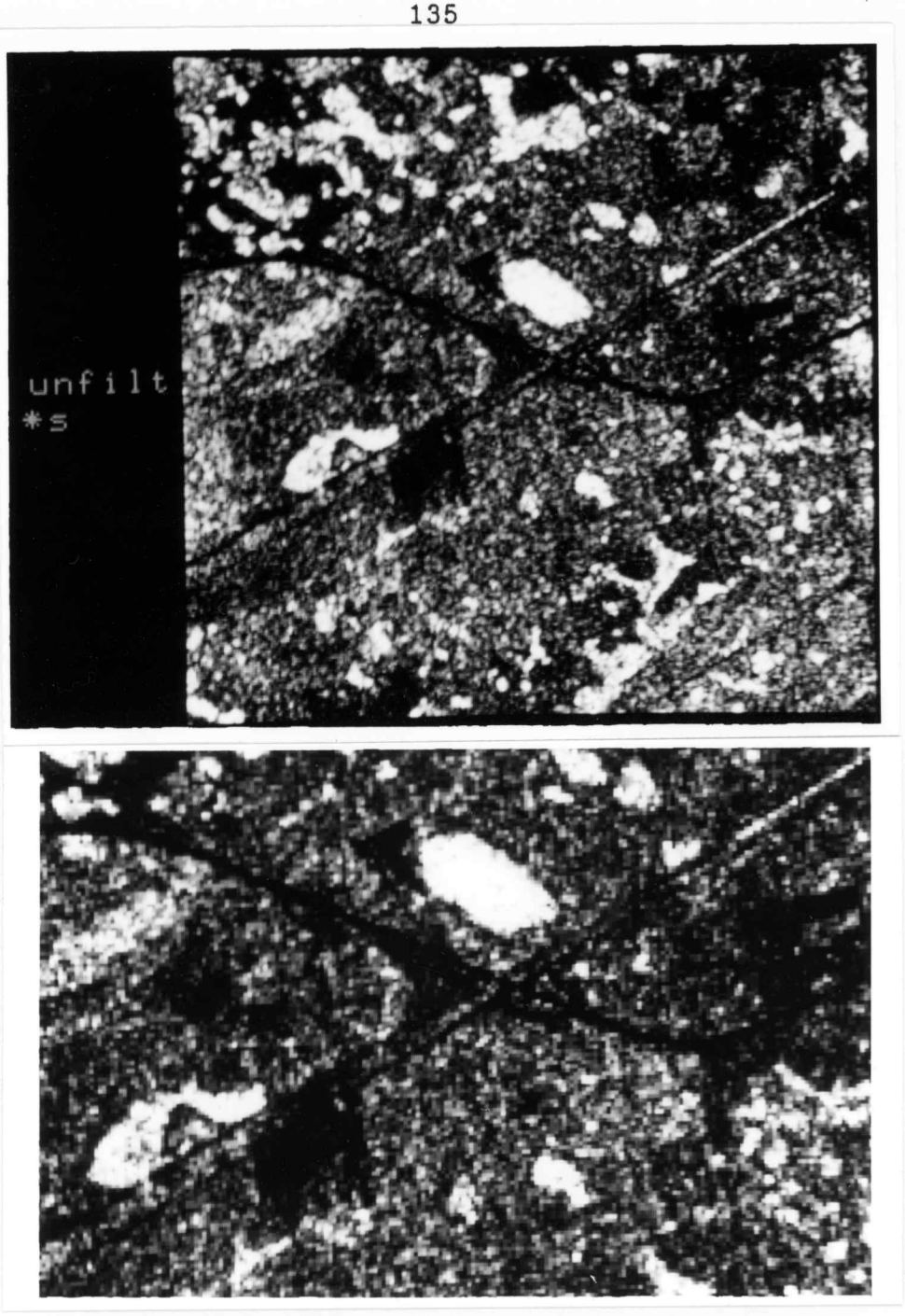

Figure 4.4 Example imagery (unfiltered 28º incidence angle SIR-B data) illustrating the two image scales utilized when visually assessing the filter treatments. The top image (approximately 1:80000) depicts the 256 x 256 pixel subimage, while the bottom image (approximately 1:50000) is an enlargement of the highway intersection area.

Separable Recursive Median. It was found that the output of the first iteration of this filter had a bias along the rows -- features tended to be elongated along the rows. In some cases it appeared as streaking. The separable recursive median algorithm filtered the columns and rows separately, with the rows being filtered last. Evidently, this was causing the elongation. The larger the window the more apparent this effect became. The second iteration greatly reduced this effect. Figure 4.5 shows the first and second iterations of the separable recursive median filter with a window size of 1 x 7 (7SRMD1 and 7SRMD2) on the 28° data set. The elongation and its reduction can be seen clearly in the two images presented.

Although there was an apparent difference between the first and second iterations of the separable recursive median algorithm, there was little difference between the second and third iterations. The differences were so slight that they could not be detected visually for any of the filter treatments. When the two images were digitally subtracted from each other, the differences found were sparsely distributed throughout the image and were of low intensity. This indicated that the second iteration very nearly approached a root signal as defined in Chapter 2. Therefore, a third iteration was not seen as necessary.

It was found that a 1 x 5 was the largest window that should be utilized with 28.5 m data. With all window

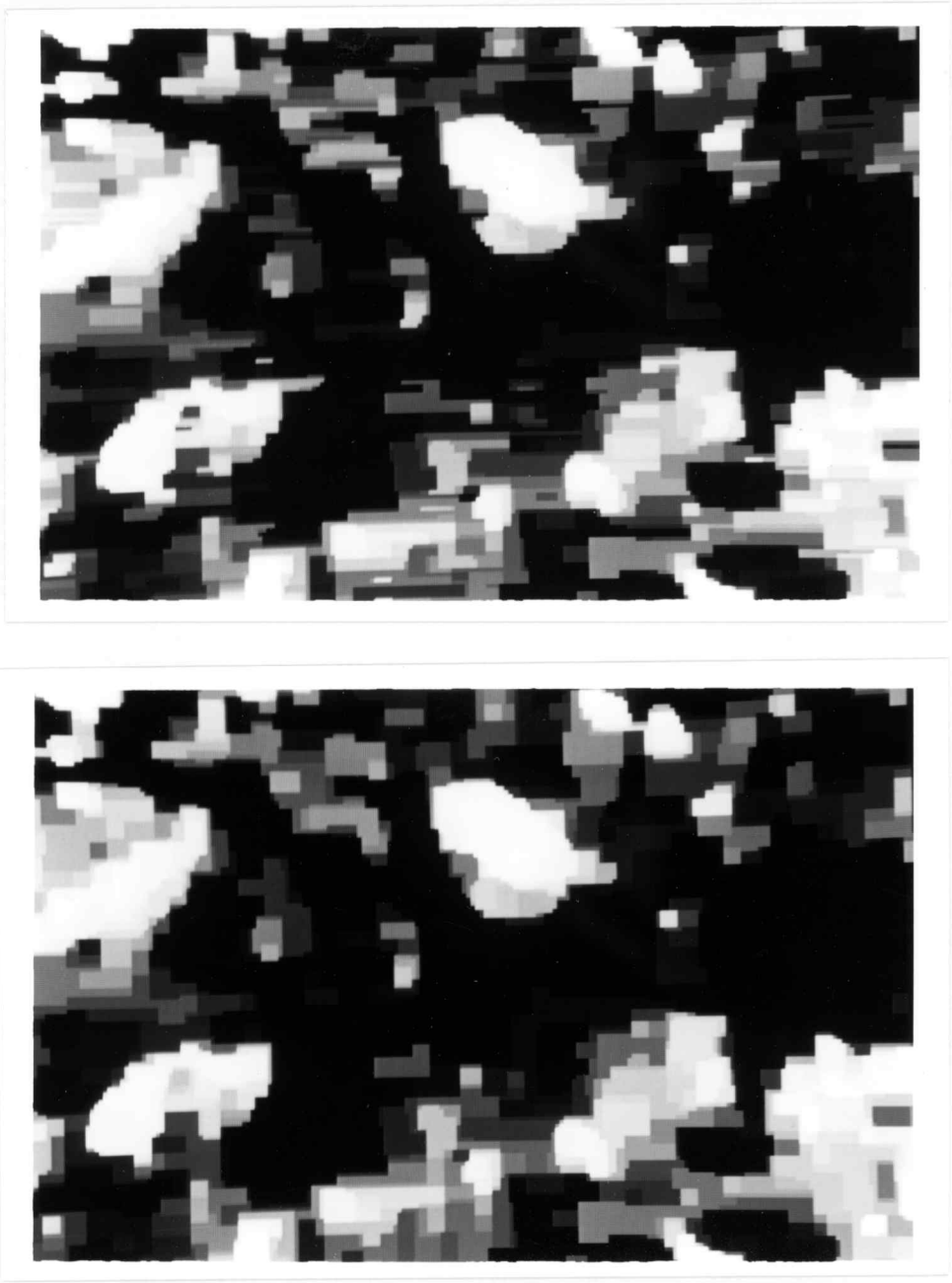

Figure 4.5 The effect of a second iteration with the separable recursive median algorithm. Streaking along the rows is evident in the first iteration image (top), while this problem has been greatly reduced by the second iteration (bottom). These images represent the 7SRMD1 and 7SRMD2 treatments.

sizes, the separable recursive median algorithm gave the filtered image a rather blocky appearance. Figures 4.5 and 4.6 demonstrate this point. At window sizes of 1 x 3 and 1 x 5, the blockiness has not obliterated features (Figure 4.6), whereas at the window size of 1 x 7 (seen previously in Figure 4.5), the only distinguishable features are the swamp areas that appear white and have a very strong return in contrast to the surrounding area. Even at this large window size (1 x 7), however, it appears that the boundaries are maintained around these high contrast features.

Based on these findings, the conclusion is that two iterations should be utilized with the separable recursive median algorithm. A window size of 1 x 3 or 1 x 5 is recommended. From a visual interpretation standpoint, the 1 x 3 window appears to be the best since many linear features such as the highways and railroad were retained. It should be noted, though, that averaging done by the eye decreases the need for a high degree of filtering when visually interpreting the imagery. The variation within the data creates a texture which is also interpreted. Per-point classifiers only consider one pixel at a time and do not consider the area surrounding that particular pixel (i.e. its context). Therefore, digital processing of the data may require a higher degree of filtering. The Cover

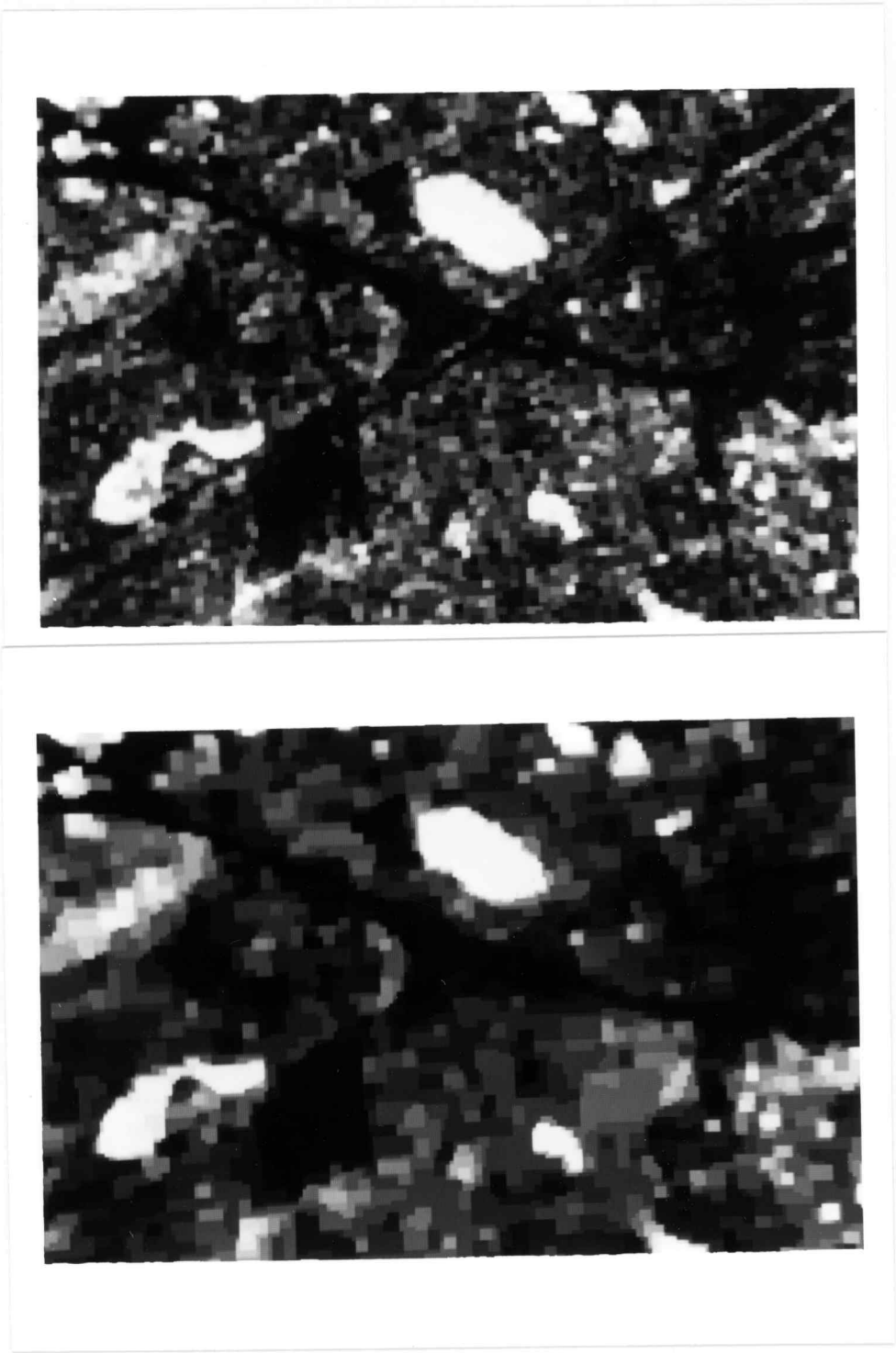

Figure 4.6 SIR-B 28º incidence angle data filtered with the 3SRMD2 treatment (top), and the 5SRMD2 treatment (bottom).

Type Classification Study results will provide answers to this issue.

Square Median. Only one window size was available with the square median algorithm, that being 3 x 3. Therefore, the variable of interest was the number of iterations. The first three iterations of the 3SQMD algorithm for the 28° subimage are shown in Figure 4.7. The second and third iterations have the best appearance. The first iteration does not provide enough smoothing, while by the fourth iteration, some surface features are being lost.

In general, the square median filter provides an image that is slightly blurred as compared to that produced with the separable recursive median filter. However, the blurring is not excessive and actually gives the image a more natural appearance. That is, the transition between gray tones is more gradual and it has a less blocky appearance.

The 3SQMD filter has been utilized commonly for filtering SAR data. However, the use of multiple iterations had not been commonly reported in the literature. The benefits of additional iterations are clearly shown in Figure 4.7.

Separable Mean. There were two variables to consider with the separable mean (SMN) algorithm -- number of iterations and window size. The first iteration tended to give the

(a)

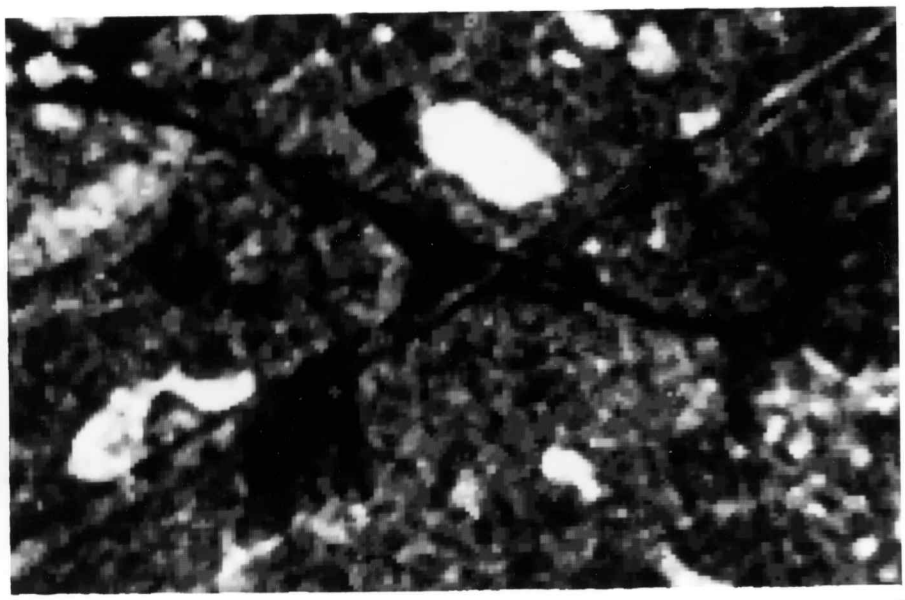

(b)

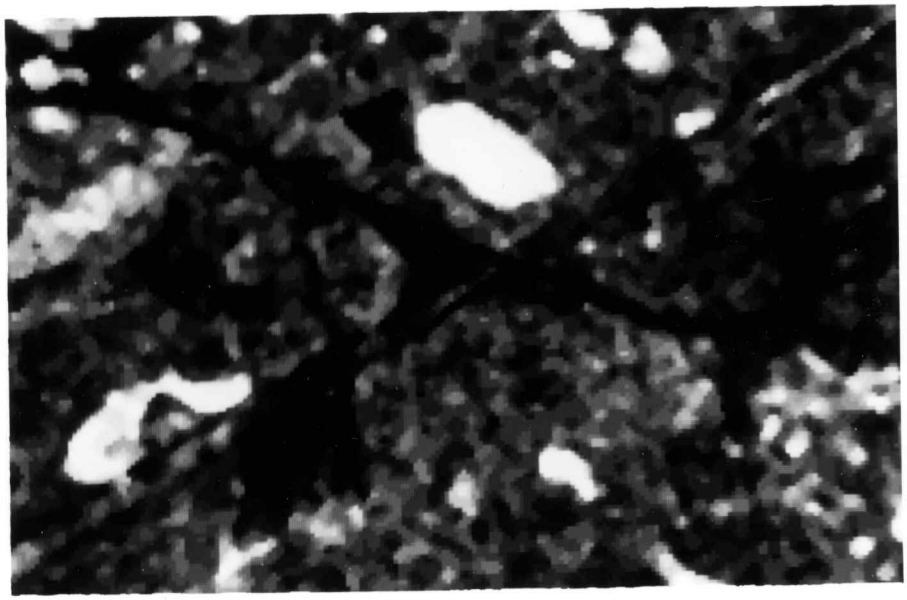

Figure 4.7 SIR-B 28º incidence angle data filtered with the square median algorithm utilizing a window size of 3 x 3 at (a) one iteration, (b) two iterations, and (c) three iterations.

(c)

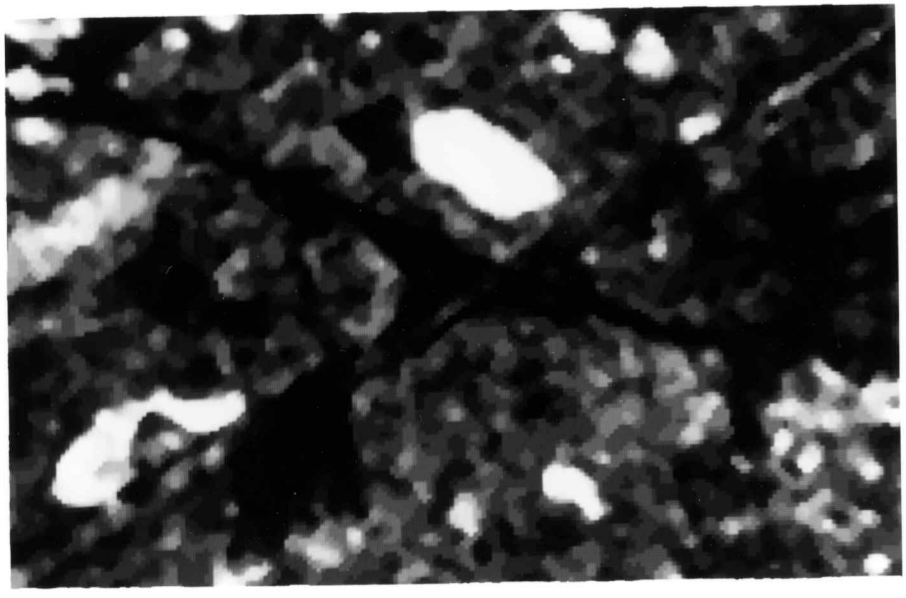

Figure 4.7 (Continued)

image a "gridded" appearance as seen in Figure 4.8 (a). By the second iteration, this effect was greatly reduced as can be seen in Figure 4.8 (b). The separable mean images had an "out-of-focus" appearance due to the blurring caused by the filter. As the number of iterations increased, this effect became more pronounced. Therefore, it was concluded that the optimum number of iterations for the separable mean is two.

The separable mean filter tended to enlarge high contrast features such as swamps. Also, linear features such as highways and railroads tended to be lost at the larger window sizes, especially at window size 1 x 7. Therefore, the best window size with the separable mean filter was visually selected as 1 x 3. Thus, the best treatment for this algorithm was 3SMN2, an example of which is shown in Figure 4.9.

Square Mean. As with the other mean algorithm (separable mean), the square mean produced images that appeared out-of-focus. Thus, the blurring effect seems to be a property of mean filters in general. Additionally, the first iteration produced a gridded effect as was also the case with the separable mean algorithm. The second iteration reduced this effect, as can be seen in Figure 4.10. The third iteration causes the most blurring. Therefore, it was concluded that two iterations was best.

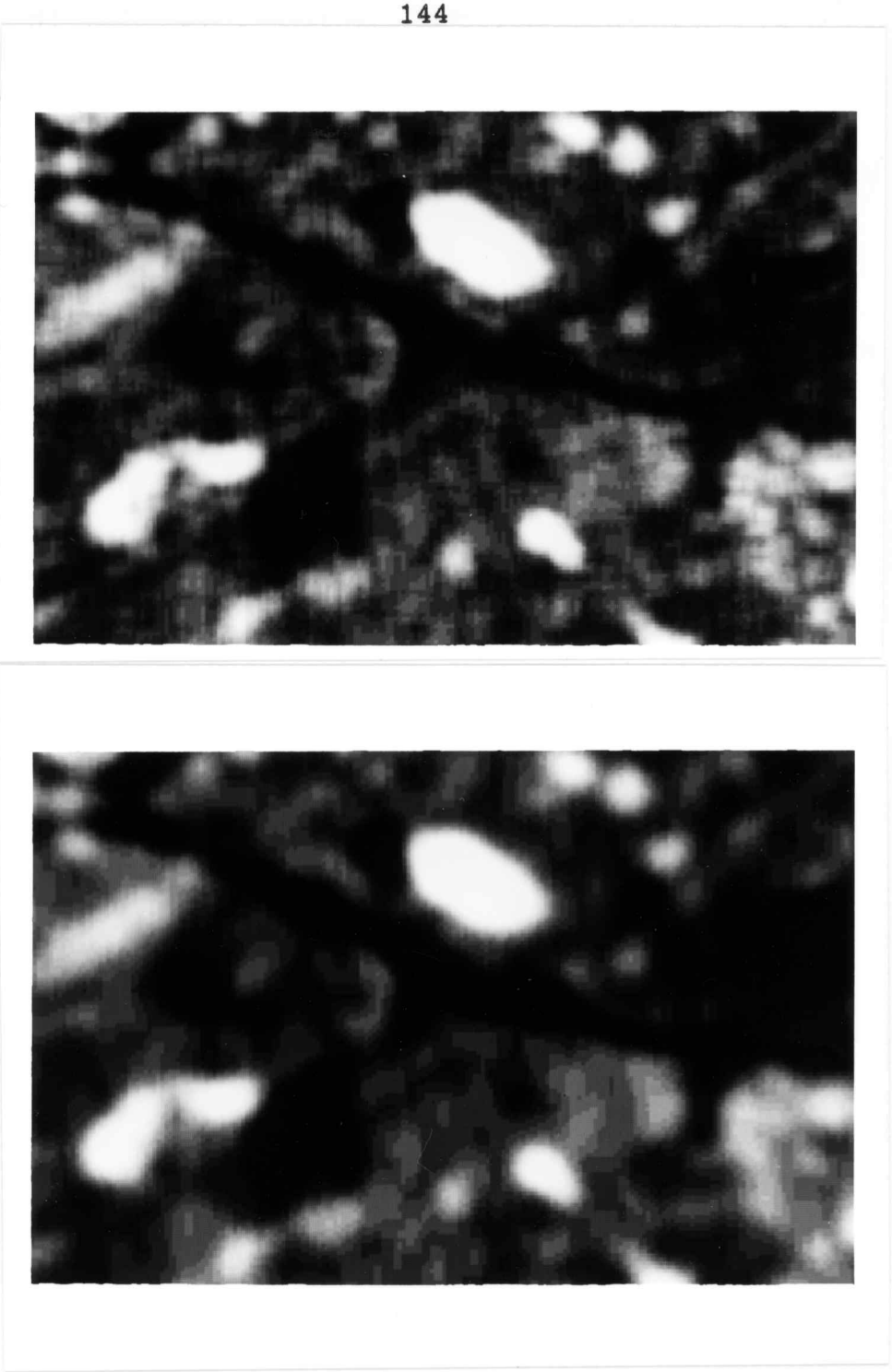

Figure 4.8 The effect of a second iteration with the separable mean algorithm. Gridding seen in the first iteration (top), is greatly reduced by the second iteration (bottom). These images represent the 7SMN1 and 7SMN2 treatments

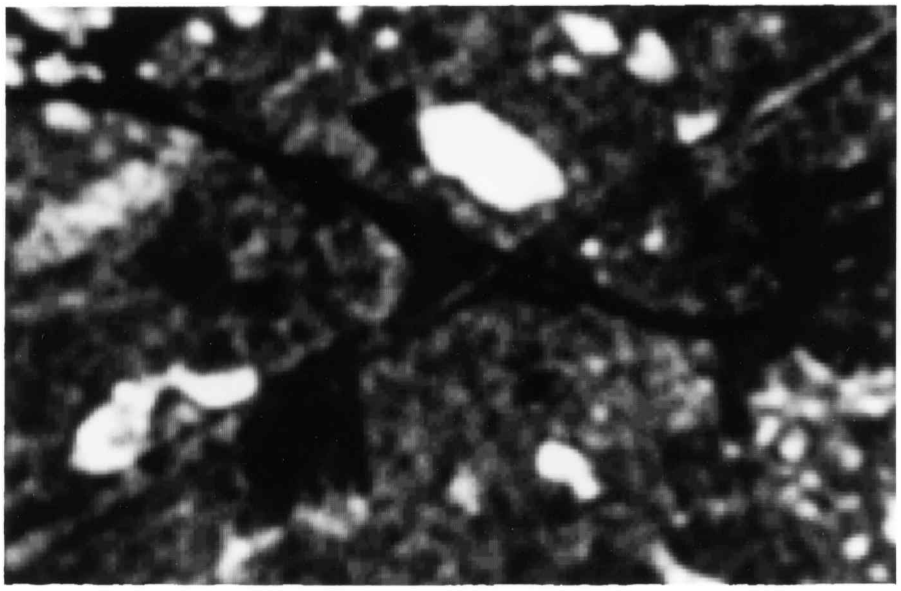

Figure 4.9 SIR-B 28º incidence angle data filtered with the 3SMN2 treatment.

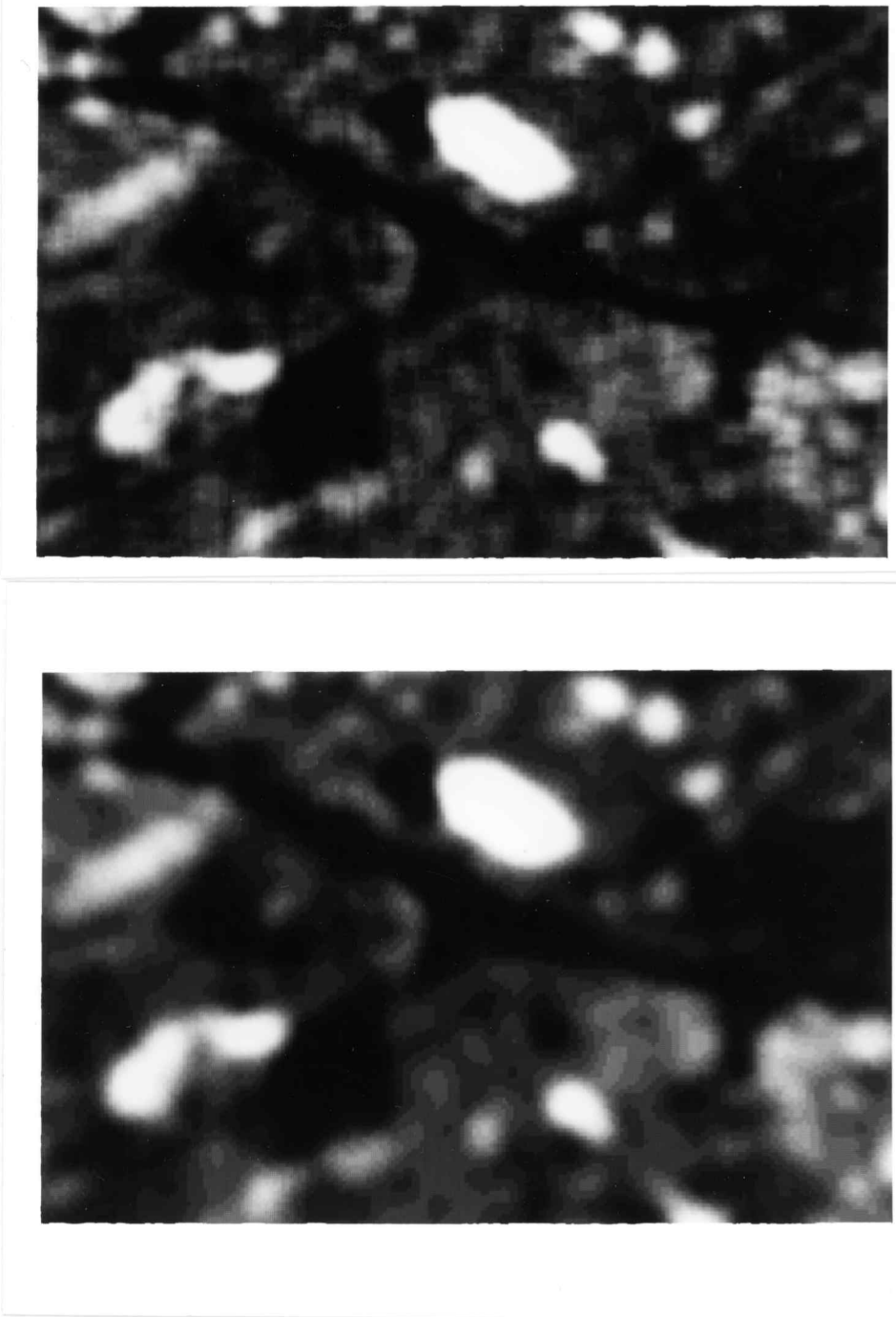

Figure 4.10 The effect of a second iteration with the square mean algorithm. Gridding seen in the first iteration (top), is greatly reduced by the second iteration (bottom). These images represent the 7SQMN1 and 7SQMN2 treatments.

Visually, the window size of three was best. The best square mean treatment is shown in Figure 4.11.

In the Visual Assessment Study, the best treatment was selected for each of the four algorithms. These four treatments are shown in Figure 4.12. When the two mean treatments shown in Figure 4.12 are compared, it can be seen that the separable mean and square mean algorithms produce very similar results. The comparison of Figures 4.10 and 4.8, and also Figures 4.11 and 4.9, confirms this similarity. This similarity was not found between the two median algorithms.

Cover Type Classification Study

Since the predicted classification accuracies obtained in the Cover Type Differentiation Study using transformed divergence did not provide definitive results, 34 treatments and the unfiltered SIR-B data (all three incidence angles) were classified. The results of the 35 classifications are listed in Table 4.5. The filter treatments have been ranked by their overall classification performance (PCC_o) based on five cover type groups (PINE1, PINE2, SWAMP1, SWAMP2, and SMOOTH) that were selected as discussed in Chapter 3. The PCC_o's span a continuum of values and definitive differences could not be determined when all were grouped together for analysis. Therefore,

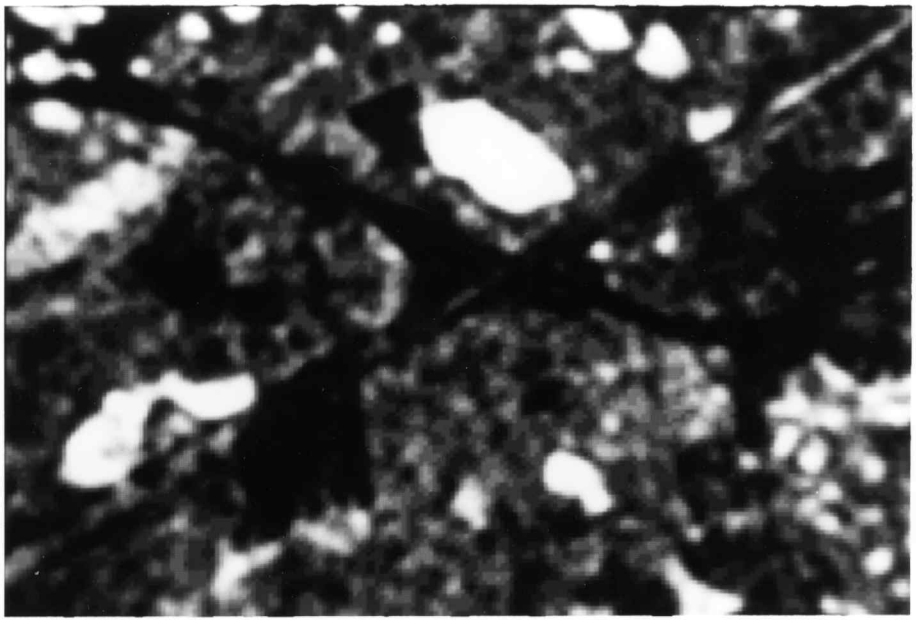

Figure 4.11 SIR-B 28° incidence angle data filtered with the 3SQMN2 treatment.

(a)

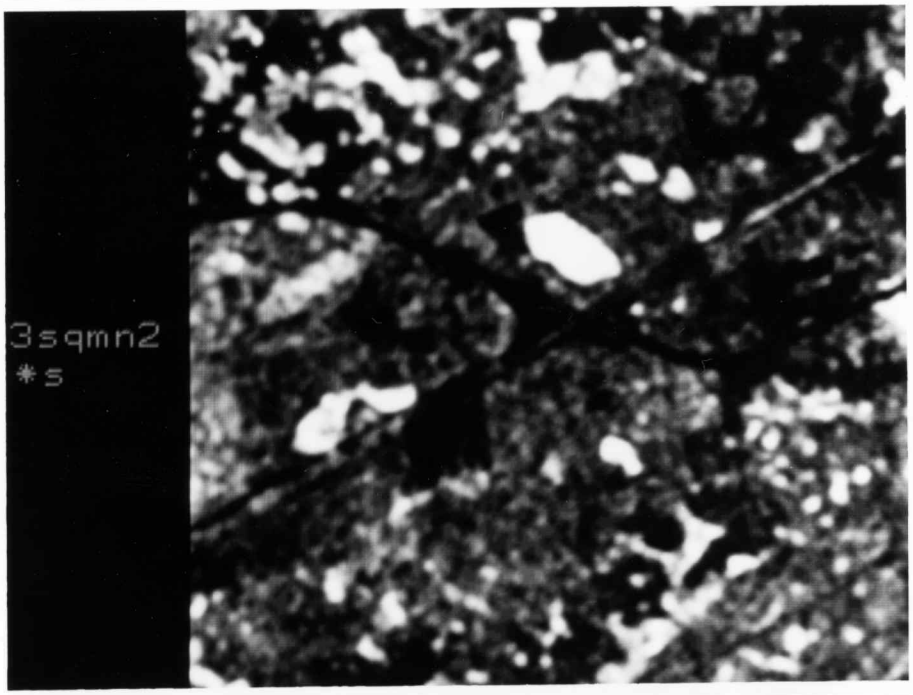

(b)

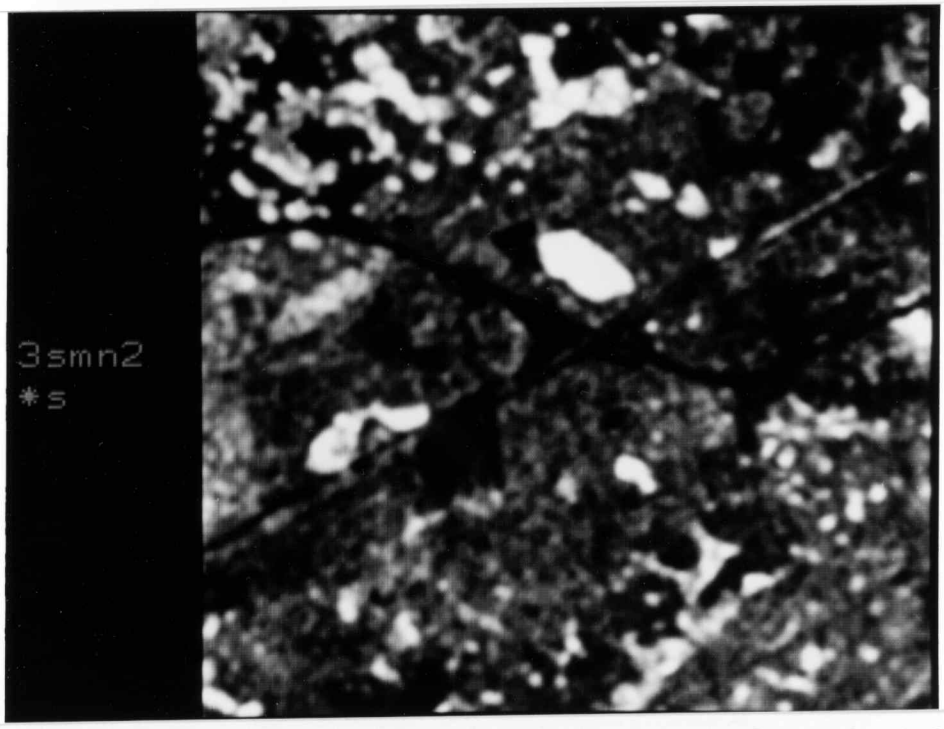

Figure 4.12 SIR-B 28° incidence angle data filtered with the four treatments selected as most appropriate using visual assessment techniques. The treatments are (a) 3SQMN2, (b) 3SMN2, (c) 3SQMD2, and (d) 3SRMD2.

(c)

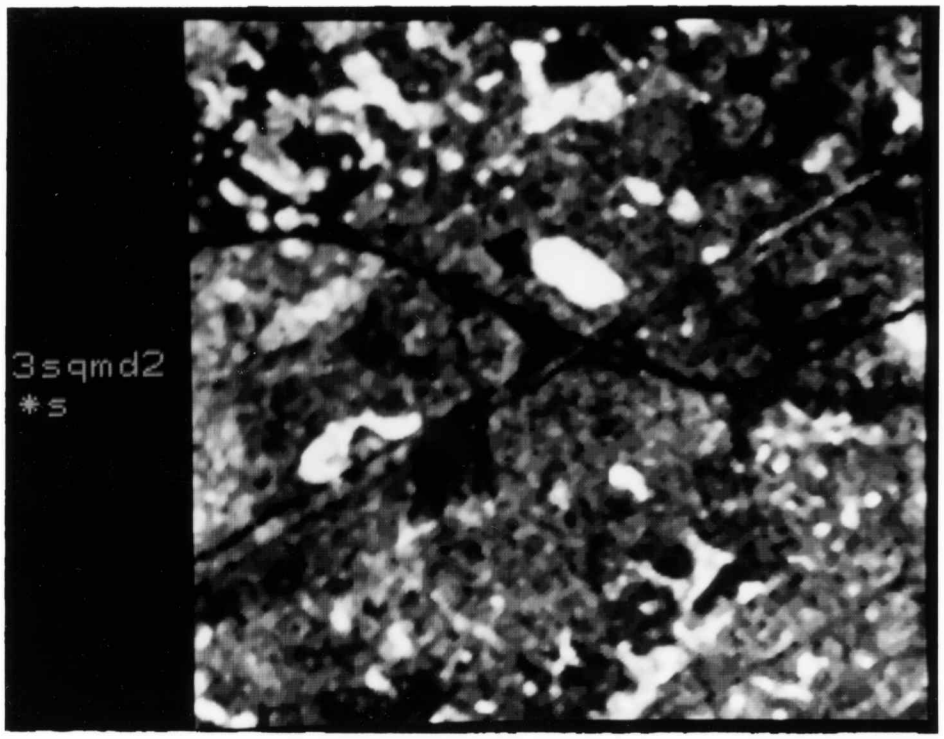

(d)

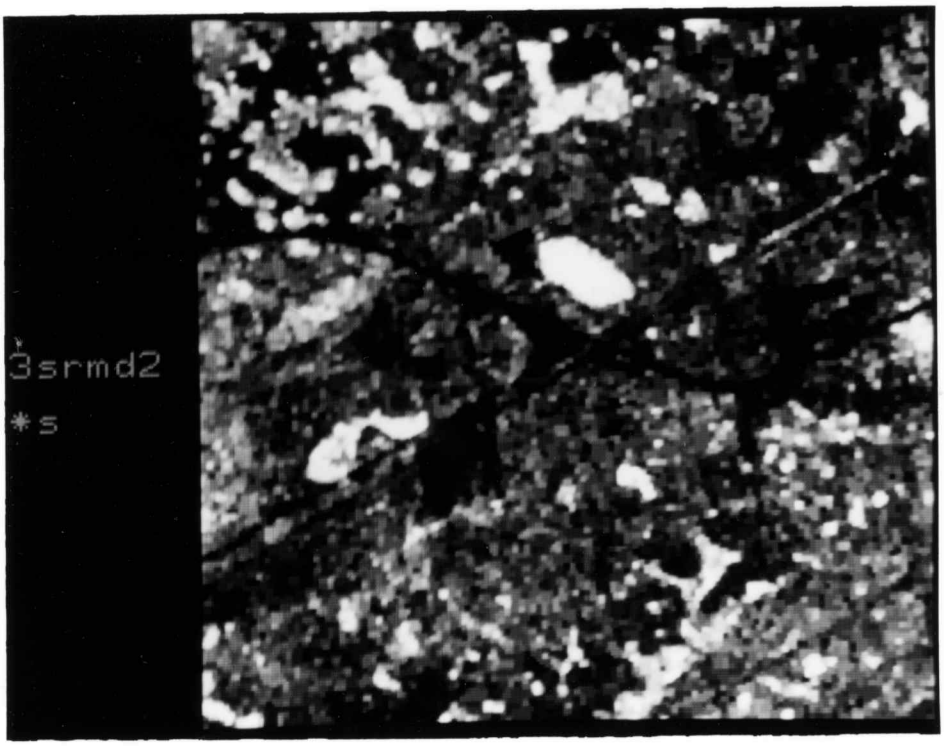

Figure 4.12 (Continued)

Table 4.5 Classification results for the unfiltered and filtered 28.5 meter SIR-B data, given as overall percent correctly classified (PCC_o) based on five cover type groups and 51 test fields.

Treatment	PCC_o
7SQMN2	95.7
5SQMN3	95.6
7SMN2	95.4
5SQMN2	95.1
7SQMN1	94.9
5SMN2	94.9
7SMN1	94.5
5SQMN1	93.6
5SMN3	93.6
3SQMN3	93.4
3SMN3	93.3
5SMN1	93.0
5SRMD3	92.8
5SRMD2	92.8
7SMN3	92.1
5SRMD1	91.0
3SMN2	90.7
3SQMN2	90.7
3SQMD4	90.4
3SQMD3	89.7
7SQMN3	89.2
3SQMD2	88.2
3SMN1	87.6
3SQMN1	87.5
3SRMD2	85.7
3SRMD3	85.6
3SRMD1	85.2
3SQMD1	85.1
7SRMD1	84.0
7SRMD3	83.9
7SRMD2	83.9
9SRMD2	81.1
9SRMD3	81.0
9SRMD1	79.2
UNFILT	72.9

the analysis of these PCC_o's was done on a stratified basis, using the three variables of the treatments as strata. Therefore, results will be presented for each of these strata and then generalizations will be drawn.

Number of Iterations. Table 4.6 contains the results obtained by using the Studentized Newman-Keuls multiple range test to determine the influence of the number of filtering iterations on overall classification performance. For nearly all combinations of algorithm and window size (except window size of seven), the second iteration showed a statistically significant improvement in the classification results. Results from the Visual Assessment Study showed that for the two mean algorithms (SMN and SQMN), gridding was apparent in the first iteration and this effect was greatly reduced by the second iteration. The statistical analysis results are in agreement with these findings.

In the Visual Assessment Study, streaking and linear exaggeration was found with the first iteration of the separable recursive median algorithm. Figure 4.5 clearly demonstrated that the first iteration should not be used. However, the results presented in Table 4.6 do not clearly show an improvement in PCC_o associated with the second iteration for this filter treatment. This illustrates the value of utilizing both quantitative and qualitative

Table 4.6 Statistical evaluation of overall classification performances showing the effect of number of iterations for each algorithm and window size combination. The PCC_o's are based on 51 test fields (8221) points) and 5 cover type groups. Statistical differences were calculated using the Studentized Newman-Keuls multiple range test ($\alpha = 0.05$). Non-significant differences are underlined.

3SQMN1	3SQMN2	3SQMN3
87.5	90.7	93.4

5SQMN1	5SQMN2	5SQMN3
93.6	95.1	95.6

7SQMN3	7SQMN1	7SQMN2
89.2	94.9	95.7

3SMN1	3SMN2	3SMN3
87.6	90.7	93.3

5SMN1	5SMN3	5SMN2
93.0	93.3	94.9

7SMN3	7SMN1	7SMN2
92.1	94.5	95.4

3SQMD1	3SQMD2	3SQMD3	3SQMD4
85.1	88.2	89.7	90.4

3SRMD1	3SRMD3	3SRMD2
85.2	85.6	85.7

5SRMD1	5SRMD2	5SRMD3
91.0	92.8	92.8

7SRMD2	7SRMD3	7SRMD1
83.9	83.9	84.0

9SRMD1	9SRMD3	9SRMD2
79.2	81.0	81.1

evaluation techniques. The dual usage allows for confirmation of results and detection of problems that might go undetected if only one method were used. It is seen that in all cases, the second and third iterations of the separable recursive median algorithm are not significantly different. Thus, the theory of reaching a near root in two iterations is strengthened.

For the two mean algorithms implemented at window size of three, significant improvement in classification accuracy was found with the third iteration. For visual assessment of the images, the second iteration of these algorithms was preferred. At the third iteration, small features such as small swamps were lost in the unclassified imagery. The test fields were not placed in these smaller swamps and therefore their loss was not considered in the calculated PCC_o's. Thus, it was felt that the second iteration was the best choice.

Window Size. The results of the statistical evaluation of the PCC_o's as influenced by window size are given in Table 4.7. Based on the results presented above, only the second iteration was considered. The square median algorithm is not included since it was run at only one window size. The classification accuracy increased when the window size was enlarged from three to five for the three algorithms included in this analysis (i.e., square mean, separable

Table 4.7 Statistical evaluation of overall classification performances showing the effect of window size for each algorithm implemented at two iterations. The PCC_o's are based on 51 test fields (8221) points) and 5 cover type groups. Statistical differences were calculated using the Studentized Newman-Keuls multiple range test ($\alpha = 0.05$). Non-significant differences are underlined.

3SQMN2	5SQMN2	7SQMN2
90.7	95.1	95.7

3SMN2	5SMN2	7SMN2
90.7	94.9	95.4

7SRMD2	3SRMD2	5SRMD2
83.9	85.7	92.8

mean, separable recursive median). The next increase in size showed no significant increase for any of the three algorithms, and in the case of the separable recursive median algorithm, it actually showed a statistically significant decrease. This latter finding is not in agreement with the trend seen in the Cover Type Differentiation Study. However, it should be noted that the previous study was done only with the 28^0 incidence angle image, while the classification was conducted with all three incidence angle images.

Upon inspection of the classified 256 x 256 pixel subimage, it was seen that even though the larger window size of five (versus three) showed an improvement in PCC_o from a quantitative standpoint (Table 4.6), the results were found to be qualitatively inferior. Figures 4.13 and 4.14 show the effects of the larger window size on the classification results. In Figure 4.13, it can be seen that the increased window size caused the loss of linear features such as US 90 and the railroad line running from center to the lower left. Also, many small swamps have been lost. This is consistent with the results found in the Visual Assessment Study. The shape of high contrast features was preserved at the increased window size. This is seen with the swamps and T-shaped borrow pit pond.

Figure 4.14 illustrates the effect of increasing the window size from 3 x 3 to 5 x 5 with the square mean

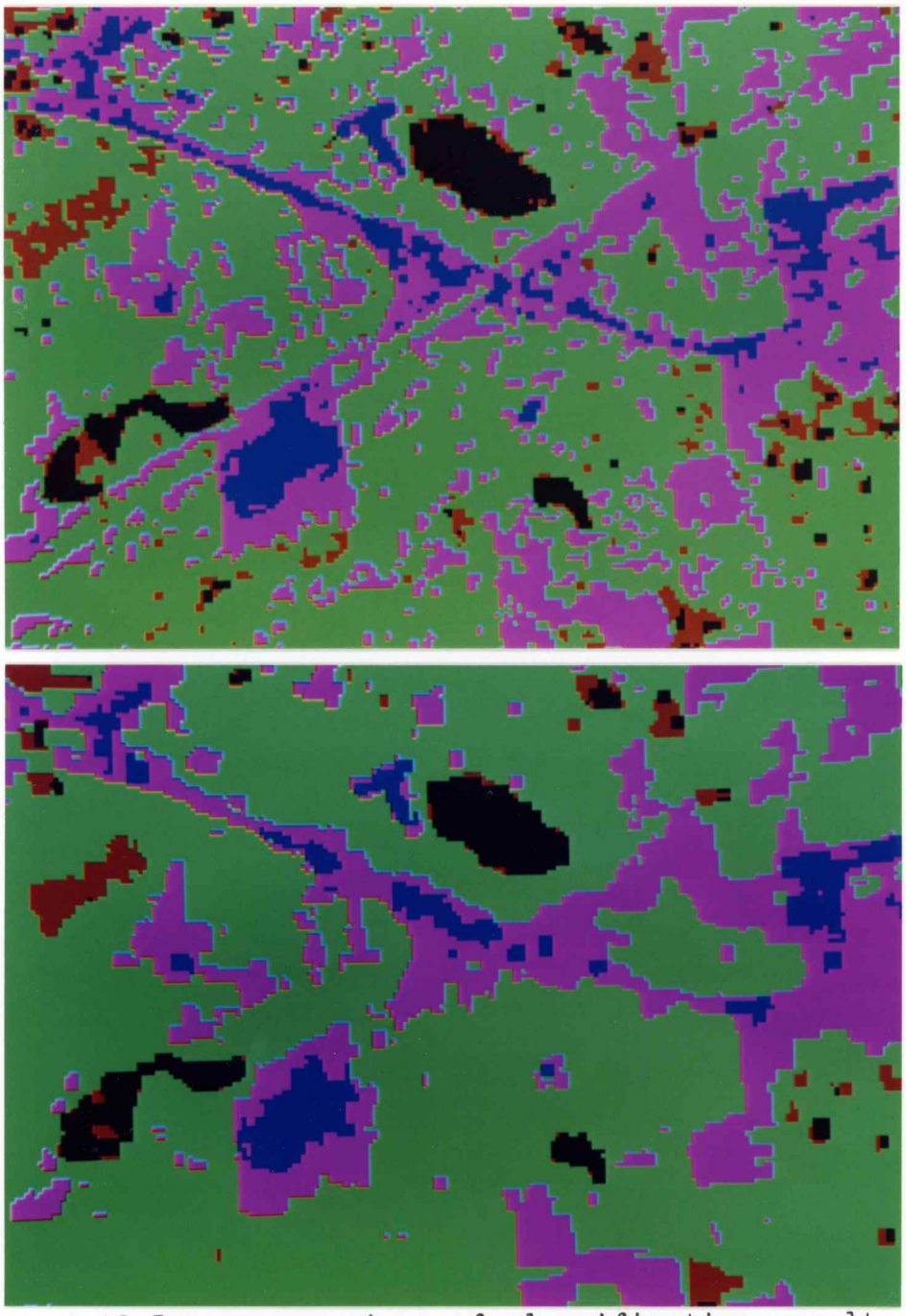

Figure 4.13 Image comparison of classification results for the separable recursive median algorithm at window sizes of 1 x 3 and 1 x 5 (at two iterations). The top image is the 3SRMD2 treatment, while the bottom image is the 5SRMD2 treatment. Five cover type groups are displayed as follows: PINE1 - pink; PINE2 - green; SWAMP1 - black; SWAMP2 - brown; SMOOTH - blue.

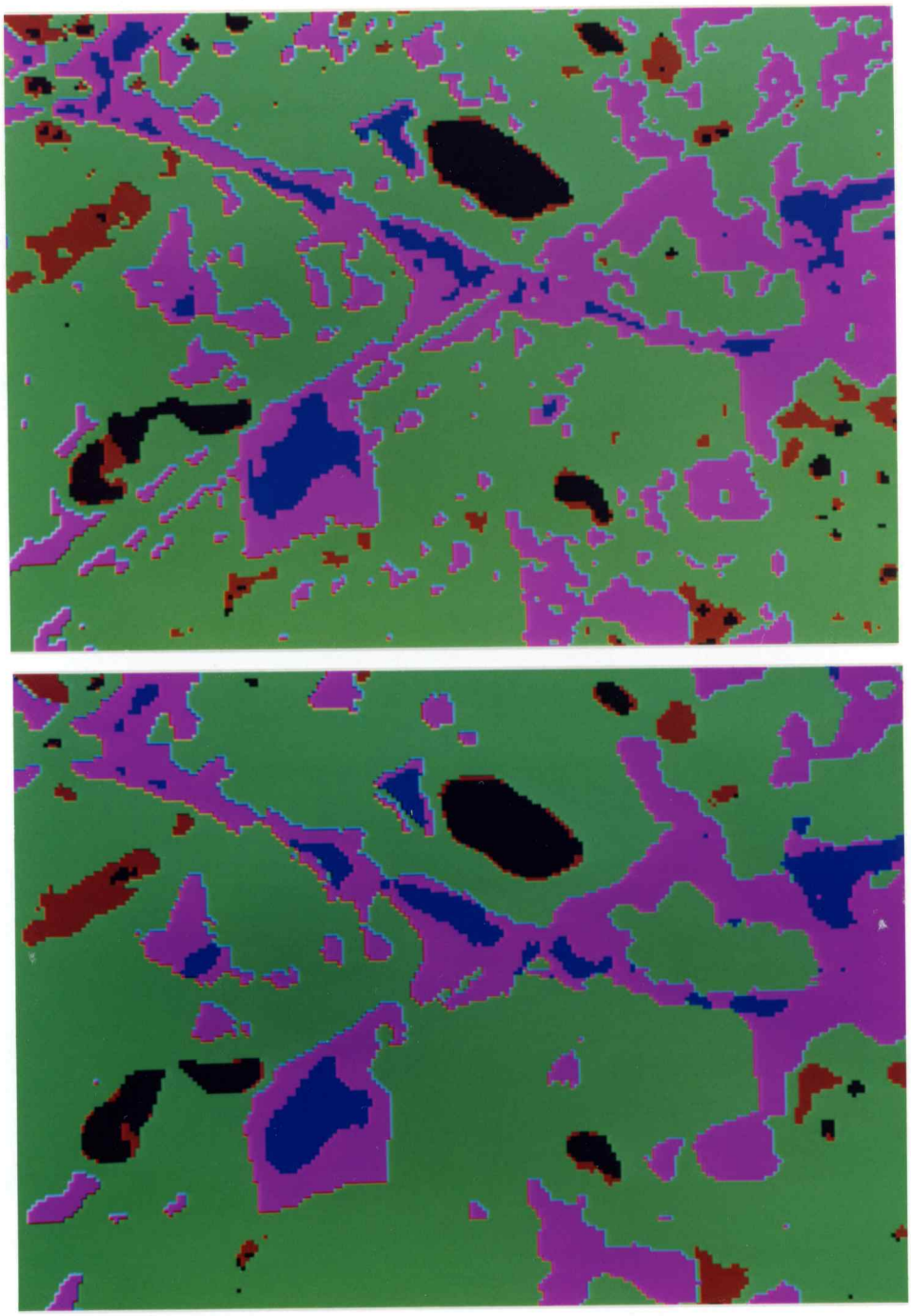

Figure 4.14 Image comparison of classification results for the square mean algorithm at window sizes of 3 x 3 and 5 x 5 (at two iterations). The top image is the 3SQMN2 treatment, while the bottom image is the 5SQMN2 treatment. Five cover type groups are displayed as follows: PINE1 - pink; PINE2 - green; SWAMP1 - black; SWAMP2 - brown; SMOOTH - blue.

algorithm. As was seen with the separable recursive median algorithm in Figure 4.13, the increased window size caused the loss of much of the highway/railroad network and also small swamps and other small cover type units. However, unlike the separable recursive median algorithm, the square mean drastically changed the shape and size of certain features. The arch-shaped swamp in the lower left corner is a continuous unit in the unfiltered image and reference data. Its shape has been retained with the 3SQMN2 treatment. However, it has been broken into two units by the 5SQMN2 treatment. Also note the change in shape of the T-shaped borrow pit pond above the highway intersection. In addition to its shape being altered, there is also an appearance of a row of PINE1 class pixels parallel and to the left of the water.

The basis of the quantitative PCC_o's was the 51 test fields and how they were classified. This method of assessment was a compromise between effectiveness and practicality. The derived PCC_o's provide a measure for comparison, but the limitations must be considered. The fields used in this experiment were rectangular in shape due to the constraints of the LARSYS software that was used for calculation of statistics and classification of the data. Because irregularly shaped polygons could not be utilized, the fields could not conform to the true shape of the cover type units. Thus, the fields tended to be

centered within relatively large cover type units -- there was a bias in the selection of fields due to the constraints of the software. Therefore, the splitting of the swamp as seen in Figure 14.4 (b), was not reflected in the PCC_o's, since no test field was placed in the narrow neck connecting two larger portions. The test field for the swamp was located in the right portion and had a very high classification accuracy.

Another problem with the test field evaluation technique utilized was related to the complexity of the scene. None of the cover type units exhibited true uniformity. Even the slash pine plantations (the most uniform of the forest cover types) had variation in density, height, tree diameters and other stand parameters for a particular stand. This variation was natural and could not (and should not) have been avoided. When selecting test fields, the analyst made a judgment call as to how much variation should be included. Based on reference data such as aerial photography, Thematic Mapper imagery, field knowledge, and forest stand maps and inventory data, the analyst selected what was thought to represent homogeneous fields with some natural variation.

To determine why the larger window sizes were often showing improved classification accuracy quantitatively while qualitatively the trend was the opposite, classification maps of selected test fields were generated

and analyzed in conjunction with the unfiltered SIR-B data and reference data. It was found that in many cases, a small inclusion of another cover type or some variation within the field was causing some of the pixels to be "incorrectly" classified. What was considered normal variation at the time when the test field was selected was found to be statistically similar to another cover type by the classification algorithm. At the larger window sizes (> 5), this variation or the small inclusion was smoothed out and no longer caused a misclassification. The effects of the problems encountered in the classification performance evaluation caused the larger window sizes to seem as if they were producing better results when in fact they were not. Thus when the qualitative and quantitative results were considered in toto, it was felt that the window size of three gave the best actual results.

Algorithm. The results from the statistical evaluation of the algorithms' influence on the overall classification performances are presented in Table 4.8. For the statistical analysis of the algorithms, only the second iteration of each algorithm was considered. The square median was only implemented with a 3 x 3 window size, and therefore could not included in tests for the larger window sizes.

Table 4.8 Statistical evaluation of overall classification performances showing the effect of algorithm for each window size implemented at two iterations. The PCC_o's are based on 51 test fields (8221) points) and 5 cover type groups. Statistical differences were calculated using the Studentized Newman-Keuls multiple range test ($\alpha = 0.05$). Non-significant differences are underlined.

3SRMD2	3SQMD2	3SMN2	3SQMN2
85.7	88.2	90.7	90.7

5SRMD2	5SMN2	5SQMN2
92.8	94.9	95.1

7SRMD2	7SMN2	7SQMN2
83.9	95.4	95.7

The differences in classification accuracy between the two mean algorithms were not statistically significant at any window size. This was in agreement with the findings of the Visual Assessment Study. Only slight differences were detected between the unclassified imagery produced by these two algorithms. Inspection of the classified subimage revealed that the separable mean algorithm tended to have more linear exaggerations (elongations along rows or columns) than was the case for the square mean algorithm. Therefore, the square mean (SQMN2) algorithm was preferred over the separable mean (SMN2) algorithm.

The classification results provided by the median algorithms (SRMD and SQMD) were statistically different from those results obtained with the two mean algorithms. Additionally, it was found that for a window size of three, there were statistically significant differences between the classification accuracies of the two median algorithms (3SRMD2 and 3SQMD2). This could only be tested at a window size of three, and in this case the 3SQMD2 treatment provided better classification results than the 3SRMD2 treatment.

At all three window sizes evaluated (3, 5, 7), the mean algorithms provided higher classification accuracies than those obtained with the median algorithms. These differences were found to be statistically significant.

Filter Selection

Based on the results of both the Visual Assessment Study and the Cover Type Classification Study, the number of candidate treatments to be considered in the final selection process was considerably reduced. The most appropriate number of iterations was found to be two. For the 28.5 m SIR-B data, the best window size was selected to be three (either 1 x 3 separable or 3 x 3 non-separable). Therefore, this left four treatments for further analysis, namely, 3SRMD2, 3SQMD2, 3SMN2, and 3SQMN2.

The Cover Type Classification Study indicated that the differences between the two mean treatments were not statistically significant. However, it was determined through visual assessment of both the unclassified and classified imagery that the 3SQMN2 was preferred over the 3SMN2 treatment, since the latter produced linear exaggerations in the imagery. Therefore, the remaining three treatments were the 1 x 3 separable recursive median filter, the 3 x 3 square median filter, and the 3 x 3 square mean filter, each implemented at two iterations (i.e., the 3SRMD2, 3SQMD2, and 3SQMN2 treatments, respectively). The 28^0 incidence angle image filtered with these three treatments was shown in Figure 4.12. Figure 4.15 shows the classified subimages for these three

treatments. The unfiltered data is also shown for comparison purposes.

All three treatments provided significant improvements in classification accuracy as compared to the unfiltered data and Figure 4.15 provides a visual verification of this fact. Of the two median treatments, the 3SQMD2 provided a significantly better classification accuracy (88.2 % as compared to 85.7% for the 3SRMD2 treatment). Additionally, the appearance of the classified image was less blocky, although the retention of linear features was comparable between the two median treatments. Some of the smaller features were retained better with 3SRMD2 treatment than was true for the 3SQMD2 treatment. In summary, however, the overall appearance of the unclassified and classified imagery obtained with the 3SQMD2 treatment was judged to be better than that obtained with the 3SRMD2 treatment.

The 3SQMN2 treatment provided a statistically significant improvement in classification accuracy over the 3SQMD2 treatment as seen in Table 4.8. However, in arriving at a decision between these two filter treatments, the results of the quantitative and qualitative evaluation tests were reviewed. It was found that in the Edge/Boundary Retention Study, the median algorithms retained edges and boundaries much better than the mean algorithms. More specifically, the 3SQMD2 treatment was found to retain edges and boundaries better than the 3SQMN2

(a)

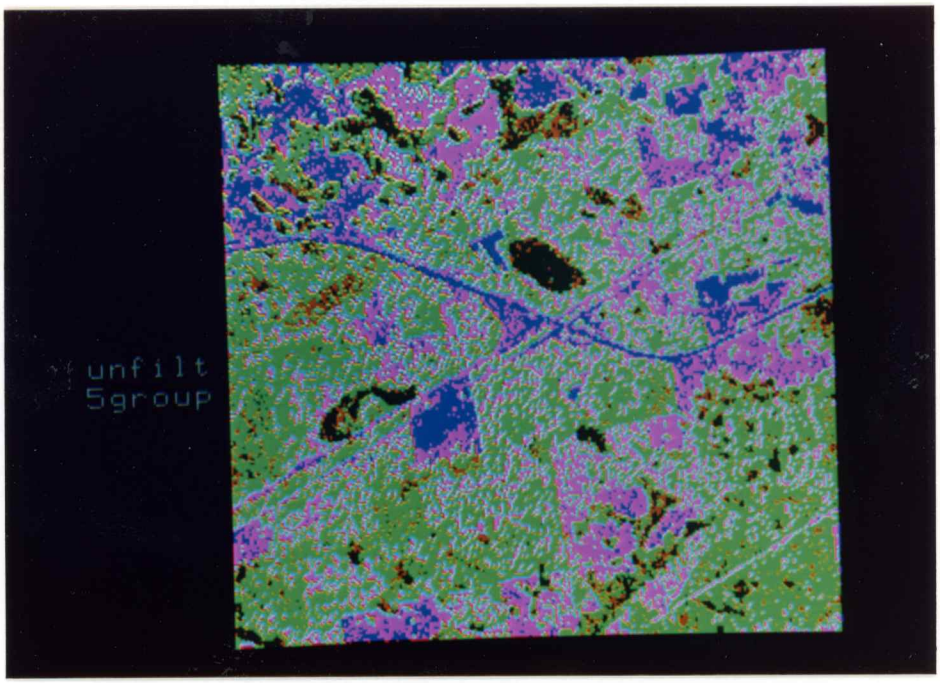

(b)

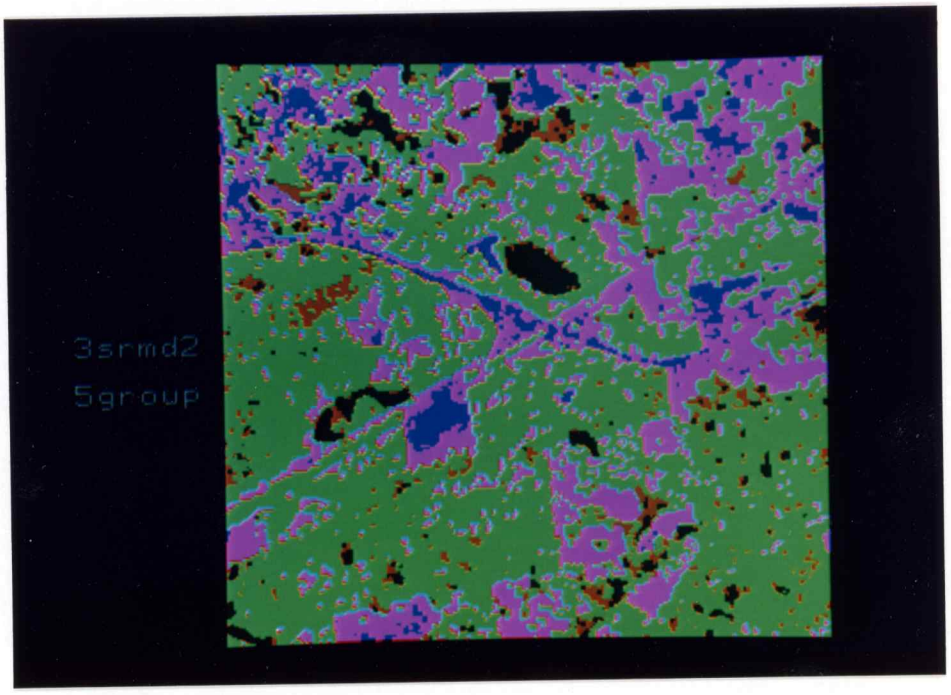

Figure 4.15 Classified imagery for the (a) unfiltered, (b) 3SRMD2, (c) 3SQMD2, and (d) 3SQMN2 SIR-B subimages. Five cover type groups are displayed as follows: PINE1 - pink; PINE2 - green; SWAMP1 - black; SWAMP2 - brown; SMOOTH - blue.

(c)

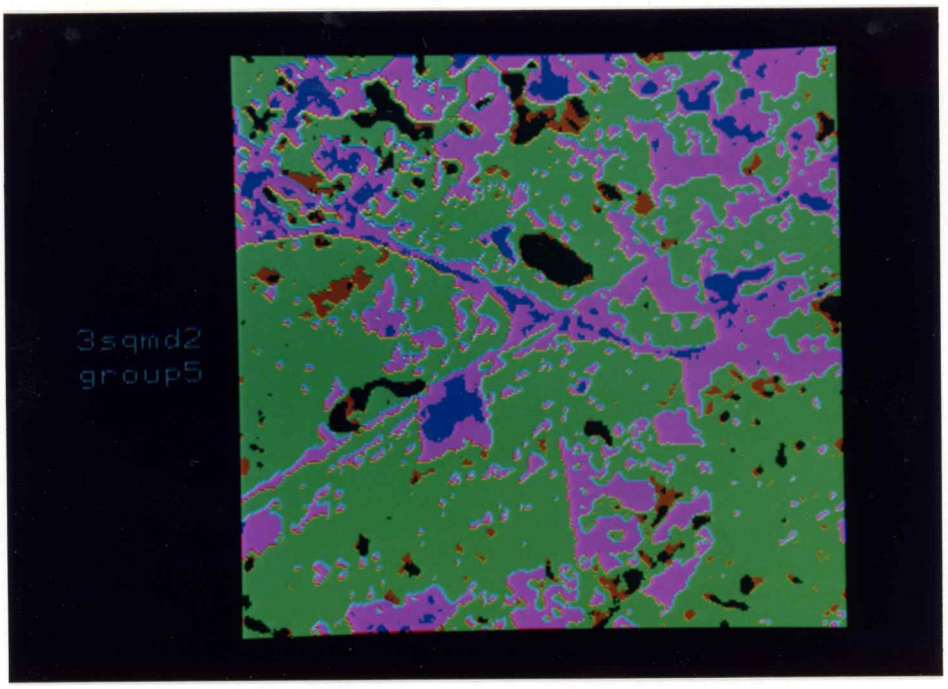

(d)

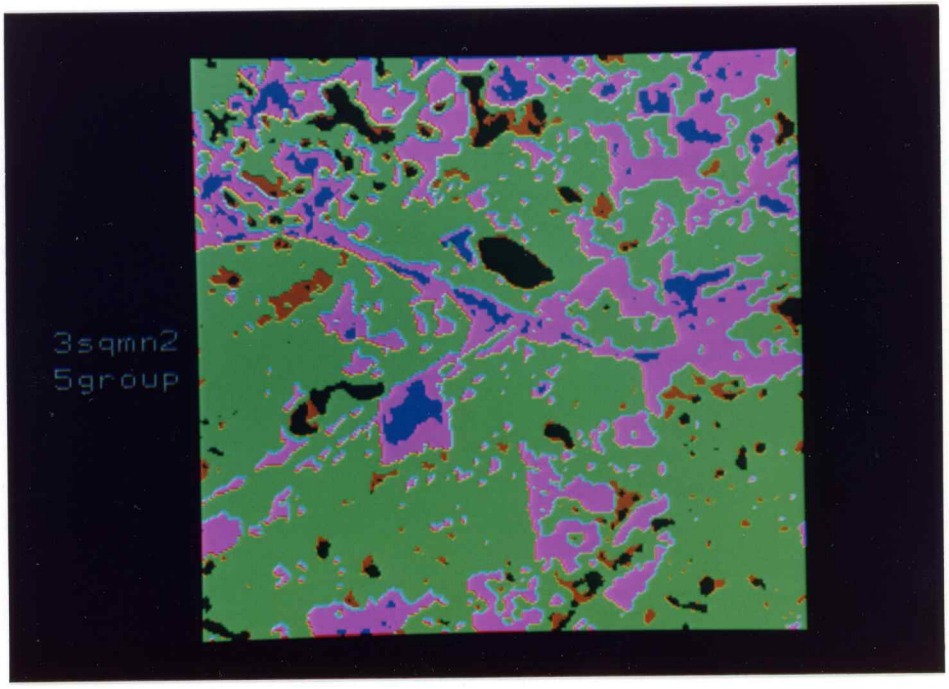

Figure 4.15 (Continued)

treatment. The mean algorithms scored low in edge and boundary retention because the edges were turned into ramp-shaped transitions. This was confirmed in the Visual Assessment Study where it was found that the 3SQMN2 image seemed blurred or out-of-focus when compared to the 3SQMD2 image. When the two classified images are compared visually (Figure 4.15), it is seen that the highway/railroad network has been retained much better with the 3SQMD2 treatment than with the 3SQMN2 treatment.

The results of the evaluation studies point toward the selection of the 3 x 3 square median filter implemented at two iterations (3SQMD2) as the best spatial filter treatment for the 28.5 meter SIR-B multiple incidence angle data set for the Florida Forestry Test Site. The three angle color composites and the classified images for both the unfiltered and filtered (3SQMD2) data are presented in Figure 4.16.

When the classification results were evaluated, it was found that the speckle within the unfiltered radar data caused much spatial variation in the classified image. The cover types are interspersed and highly homogeneous regions are not common. The classification of the 3SQMD2 filtered image provides a much more definitive representation of the cover types present in the area. Cover type units are represented in a much more homogeneous manner. It should be noted though, that some detail has been lost in the

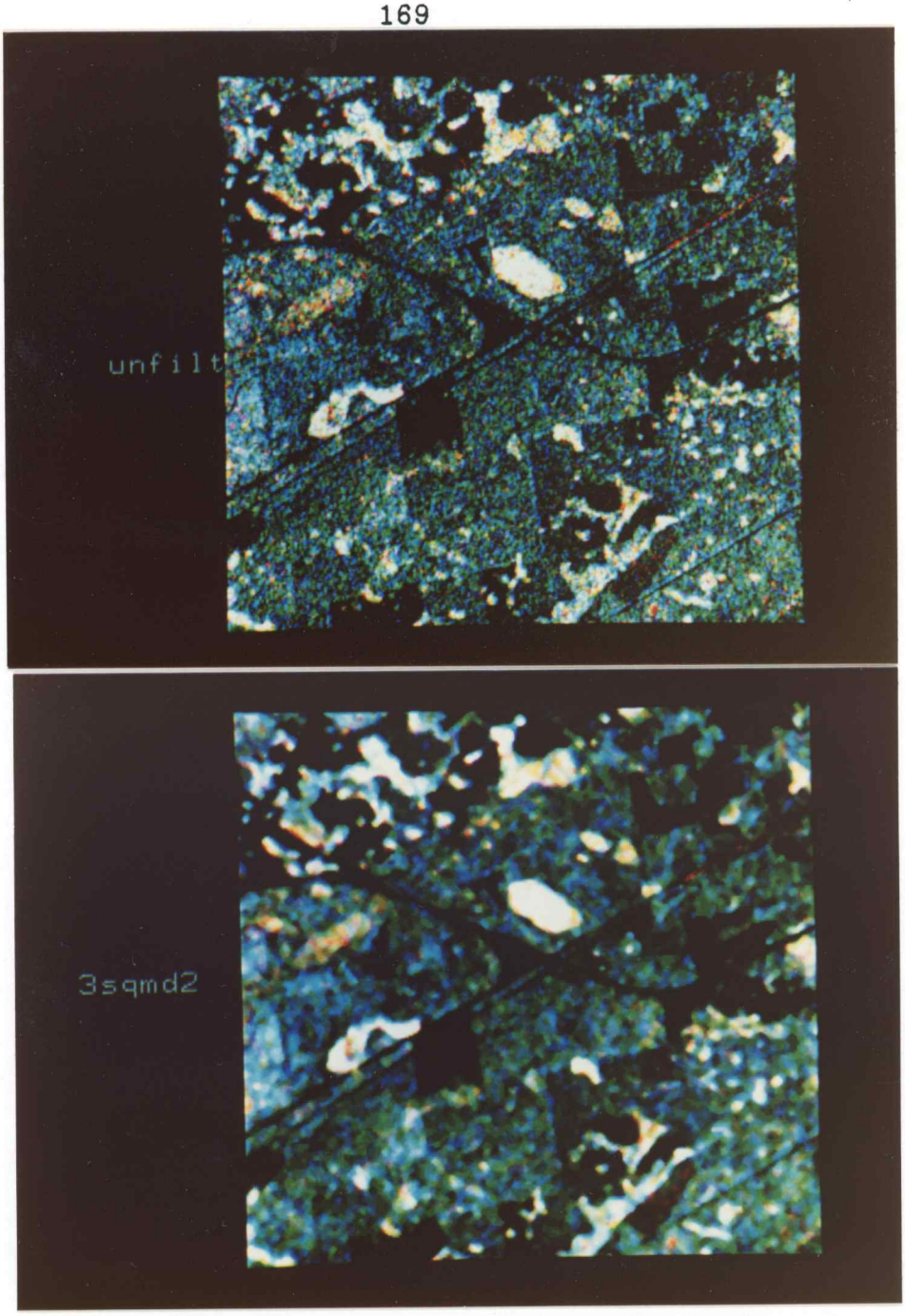

Figure 4.16 Unclassified multiple incidence angle color composites and classified imagery for the unfiltered and 3SQMD2 SIR-B subimages. For the color composites, the incidence angle subimages are displayed as follows: red = 28°; blue = 45°; green = 58°. In the classified imagery, five cover type groups are displayed as follows: PINE1 - pink; PINE2 - green; SWAMP1 - black; SWAMP2 - brown; SMOOTH - blue.

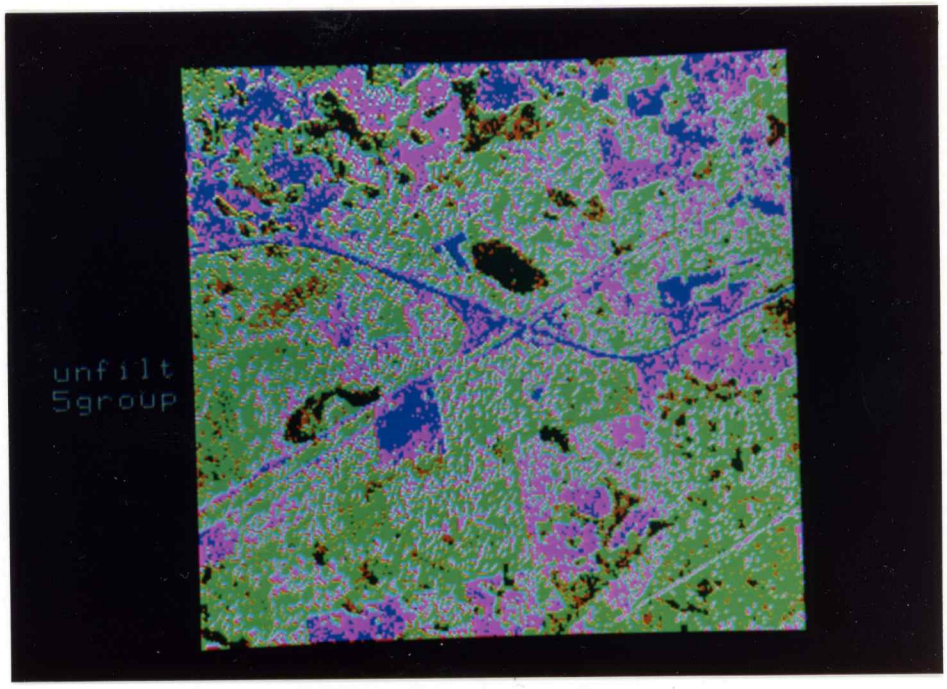

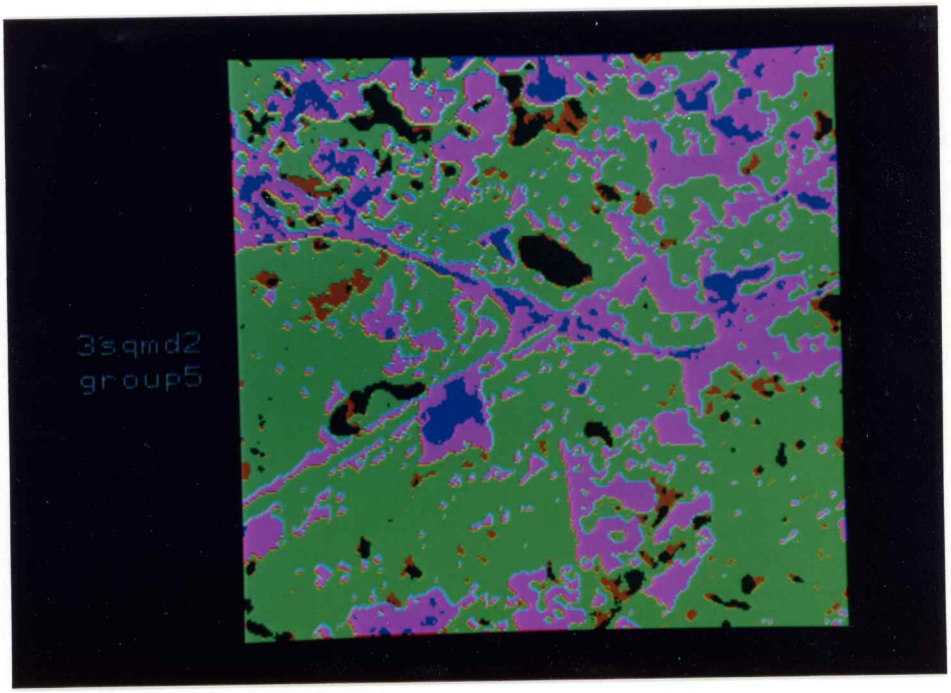

Figure 4.16 (Continued)

filtering process. The linear features such as the highways and railroad have become less distinct. It should be realized, however, that some spatial detail may have to be sacrificed in order to achieve a reduction in the variation within the SAR data.

The results of classifications conducted in this experiment were displayed and evaluated on the basis of five broad cover type groups. These groups consisted of two pine, two swamp, and one smooth cover type group. Within each of these broad groups there was a tremendous variety of more detailed cover type units. For instance the SMOOTH group included water, bare soil, pasture, and roads. The four forest groups included all the forest types (and conditions) described in Chapter 3. This experiment only addressed the question of how filtering could be used to improve the classification of these five cover type groups since a detailed classification of the SIR-B data was not the intent nor objective of this study. For example, the classification accuracy of the more detailed subgroup cover type classes (such as 25 year slash pine versus 60 year old longleaf pine) was not tested between treatments. However, at the level of detail utilized in this experiment, spatial filtering has provided a significant improvement in both the unclassified and the classified SIR-B 28.5 m data.

CHAPTER 5
SUMMARY AND CONCLUSIONS

Summary

The purpose of this study was to determine the most appropriate low pass spatial filter treatments for reducing speckle effects in Shuttle Imaging Radar-B (SIR-B) digital data that is to be utilized for assessing forest resources. The SIR-B data set utilized consisted of multi-angle data collected during Space Shuttle Flight 41-G at center incidence angles of 28.4^0, 45.3^0, and 58.4^0. The pixel size of the unfiltered data was 28.5 meters.

Thirty-four filter treatments were applied to the data. These treatments included the use of square mean, separable mean, square median, and separable recursive median algorithms implemented at 1 to 3 iterations with window sizes ranging from 1 x 3 to 1 x 9 (separable filters) and 3 x 3 to 7 x 7 (square filters).

Both quantitative and qualitative evaluation techniques were utilized. Four specific evaluation studies were conducted: Cover Type Differentiation Study, Edge/Boundary Retention Study, Cover Type Classification

Study, and Visual Assessment Study. The Visual Assessment Study and the Cover Type Classification Study were found to provide the most useful information for evaluating the various treatments. Distinct differences due to type of algorithm, window dimension, and number of iterations were found. The most significant results are summarized as follows:

1) The median filter algorithms were more effective for preserving edges and boundaries than were the mean algorithms (see Table 4.4). The separable recursive median algorithm most effectively preserved edges and boundaries. The square median algorithm did preserve edges also, though not as well. It was found that the two mean algorithms tended to blur the edges and boundaries in the imagery.

2) The use of both quantitative and qualitative evaluation techniques provided an effective approach for selecting the best filter treatment. The qualitative visual assessment of the images often revealed problems that were not detected in the quantitative tests. Conversely, the quantitative tests were helpful in confirming the results derived visually.

3) For visual assessment of the imagery, the most effective presentation was achieved utilizing two

different histogramming techniques for image enhancement and the use of two different print scales (approximately 1:80000 and 1:50000). The different histograms were useful for highlighting subtle details (see Figure 4.3) and the two scales gave an overall view and a more detailed one (see Figure 4.4).

4) For the separable mean, square mean, and separable recursive median algorithms, a single iteration produced visually inferior images. A distinct gridding effect was produced by a single iteration of the first two algorithms, while a single iteration of the separable recursive median algorithm produced streaking.

5) With all algorithms, the second iteration provided the best results. For the three non-recursive filter algorithms (separable mean, square median, and square mean) implemented at window sizes of three and five, the second iteration showed a significant[1] improvement in the classification results (see Table 4.6). Additionally, the second iteration alleviated the gridding and streaking problems encountered in the first iteration with the separable mean, square mean, and separable recursive median algorithms. The

---

1. The term significant, as used in this chapter, refers to statistical significance tested at $\alpha = 0.05$ using the Studentized Newman-Keuls multiple range test.

application of multiple iteration filter treatments to SAR data has not been commonly reported in the literature.

6) The third iteration of the separable recursive median showed little improvement in appearance of the SIR-B imagery as compared to the second iteration. This was confirmed statistically when no significant difference in classification accuracy was found (see Table 4.6). This indicates that a near root image was achieved in two iterations.

7) Visually, the window size of three was selected as providing the best results for all algorithms applied to the SIR-B data with two iterations. The window size of five produced significantly better classification results than the window size of three (see Table 4.7), however visual inspection of the classified images and the classified test fields showed that the window size of three was more appropriate.

8) There was little difference in appearance between the filtered imagery obtained with the two mean algorithms (separable mean and square mean), and statistical analysis showed (see Table 4.8) that there was no significant difference between the classification accuracies achieved with these algorithms (based on the second iteration). However, inspection of the

classified images showed that the square mean algorithm produced more acceptable results.

9) The two median algorithms (3SQMD2 and 3SRMD2) produced images that had distinctly different appearance. The separable recursive median algorithm produced imagery that was blocky in appearance. The square median imagery had a more natural appearance with a more gradual transition between tones. Classification results were significantly better with the 3SQMD2 treatment than with the 3SRMD2 (see Table 4.8). Therefore, the 3SQMD2 treatment was judged to be the better of these two treatments.

10) The best mean treatment (3SQMN2) provided significantly nigher classification results (see Table 4.8) than the best median treatment (3SQMD2), but the Edge/Boundary Retention Study (see Table 4.4) and the Visual Assessment Study evaluations indicated that the median treatment retained edges better and preserved more detail. Although the difference in classification accuracies between the two treatments (90.7% versus 88.2%) is statistically significant, it was decided that this difference was not large enough to outweigh the results obtained in the Edge/Boundary Retention Study and Visual Assessment Study.

11) In evaluating all 34 treatments from both a quantitative and qualitative standpoint, the 3 x 3

square median filter implemented at two iterations (3SQMD2) produced the best overall results with the 28.5 m SIR-B data.

Conclusions

The major conclusions from this research with 28.5 m Shuttle Imaging Radar-B digital data using four filter algorithms (i.e., square mean, separable mean, square median, and separable recursive median) are:

1) The 3 x 3 square median filter implemented at two iterations (3SQMD2 treatment) was the best filter treatment for reducing speckle effects in this data set.
2) The second iteration provided much better results than were obtained with a single iteration.
3) A window size of three was determined to be best.
4) Both quantitative and qualitative evaluation techniques were needed to effectively identify the best filter treatment.

CHAPTER 6

RECOMMENDATIONS

This study has clearly shown the benefits of spatial filtering SAR data. Some interesting insights were gained into the effects of various filter treatments when applied to SAR data. Although many interesting results were obtained, during the experiment many questions arose that remain unanswered. Identified below are some of these areas where future research is believed to be needed. Additionally, problems that were encountered during the experiment are addressed. It is recommended that additional research be pursued in the following areas:

1) The effect of different SAR data pixel sizes and resolutions on filter selection should be studied. The results from this study should provide a good beginning point for work with SAR data of different spatial resolution and pixel size, but these results should be verified with other data sets.
2) The square median algorithm should be tested with larger window sizes. In this experiment, this algorithm was only tested at a window size of three.

Where a higher degree of filtering is necessary, this algorithm implemented with a larger window may be useful.

3) The results of this study should be verified with a more detailed classification study. This experiment did not measure the classification accuracy of subgroup (detailed cover type classes) cover type pixels from one treatment to another.

4) The use of the filtered SAR data should be tested with other uses besides classification. The reduction of the variance in the data may improve statistical analyses such as biomass-signal correlation.

5) The effects of filtering SAR should also be investigated in relation to the use of contextual classifiers. The results should be compared with those obtained with per-point classifiers.

6) The spatial integrity of the filtered SAR data should be tested. Perhaps a graphics map overlay could be used to monitor shrink and swell of surface features. This would also allow for detecting the loss of features. A graphics overlay capability (e.g., a geographic information system) would also provide wall-to-wall reference data that could be used for selecting training and test fields.

7) The use of more sophisticated algorithms should be pursued. More complex arithmetic operations should be

investigated. Adaptive techniques which modify the smoothing operation according to the local statistics would be of interest. The local statistics are calculated based on the pixel and its neighborhood. Reports on two more advanced algorithms are given by Nathan and Curlander (1987) and Azimi-Sadjadi (1987).

A few problem areas were encountered in the experiment. Two of the more significant ones were:

1) The LARSYS program utilized for calculating field statistics was limited to rectangular fields. A capability for utilizing irregular polygons would have allowed the boundaries of the selected fields to correspond more closely to the boundaries of the cover type unit being sampled. This would have allowed the selection of fields from small irregularly shaped cover type units.
2) Throughout the experiment, it was seen that there is a need for developing more effective mechanisms to facilitate integrated use of the image processing systems at Purdue. Software already exists for reformatting image data for use on the various systems, and work has begun on the transferring of statistics from one system to another. This work needs to continue and additional work is needed in such areas as transfer of classification results files

and transfer of field coordinate files. The "system" is functional as it stands, but a number of refinements such as these would streamline the research process.

BIBLIOGRAPHY

BIBLIOGRAPHY

Avers, P.E., and K.C. Bracy. 1974. Soils and Physiography of the Osceola National Forest. U.S. Department of Agriculture Forest Service, Southern Region. 94 p.

Avery, E.A., and G.L Berlin. 1985. Nonphotographic Imaging Systems. Interpretation of Aerial Photographs. Fourth edition. Minneapolis, MN: Burgess Publishing Co. p. 131-233.

Azimi-Sadjadi, M.R. 1987. Speckled Image Restoration by Adaptive Block Kalman Filtering. Proceedings of 1987 International Geoscience and Remote Sensing Symposium; May 18-21, 1987; University of Michigan, Ann Arbor, MI. II:1449-1455.

Barr, D.J., and R.D. Miles. 1970. SLAR Imagery and Site Selection. Photogrammetric Engineering 36(11):1155-1170.

Bartolucci, L.A. 1979. Digital Processing of Remotely Sensed Multispectral Data. LARS Technical Report 040479. Laboratory for Applications of Remote Sensing, Purdue University, West Lafayette, IN. 18 p.

Bennett, J.R., I.G. Cumming, P.R. McConnell, and L. Gutteridge. 1981. Features of a Generalized Digital Synthetic Aperture Radar Processor. Proceedings 15th International Symposium Remote Sensing of Environment; May 11-15, 1981, Ann Arbor, Michigan. 1:271-290.

Brisco, B., F.T. Ulaby, and M.C. Dobson. 1983. Spaceborne SAR Data for Land-cover Classification and Change Detection. Digest 1983 International Geoscience and Remote Sensing Symposium; Aug. 31 - Sept. 2, 1983; San Francisco, CA. Vol. 1, Sect. PS-2, p. 1.1-1.8.

Chin, R.T., and C.L. Yeh. 1983. Quantitative Evaluation of Some Edge-Preserving Noise-Smoothing Techniques. Computer Vision, Graphics, and Image Processing 23:67-91.

Cihlar, J., ed. 1986. The Use of Landsat Data in Forestry. Remote Sensing Reviews 2:1-258.

Colwell, R.N., ed. 1983. Manual of Remote Sensing. Second edition. Falls Church, VA: American Society of Photogrammetry. 2 volumes, 2440 p.

Considine, D.M., ed. 1983. Radar. Van Nostrand's Scientific Encyclopedia. Sixth edition. New York: Van Nostrand Reinhold Co. p. 2376-2378.

Curlander, J.C. 1986. Performance of the SIR-B Digital Image Processing Subsystem. IEEE Transactions on Geoscience and Remote Sensing GE-24(4):649-652.

Curran, P.J. 1985. Principles of Remote Sensing. Essex, England: Longman Group, Ltd. 282 p.

Curtis, W.C. 1977. Synthetic Aperture Fundamentals. In: E. Brookner, ed. Radar Technology. Dedham, Mass.: Artech House, Inc. p. 239-249.

Cushnie, J.L., and P. Atkinson. 1985. Effect of Spatial Filtering on Scene Noise and Boundary Detail in Thematic Mapper Imagery. Photogrammetric Engineering and Remote Sensing 51(9):1483-1493.

de Azevedo, L.H.A. 1971. Radar in the Amazon. Proceedings 7th International Symposium on Remote Sensing of Environment. Ann Arbor, MI. 3:2303-2306.

Duda, R.O., and P.E. Hart. 1973. Pattern Classification and Scene Analysis. New York: John-Wiley & Sons. 482 p.

Elachi, C. 1986. Spaceborne Imaging Radar Research in the 90's. Proceedings of the Second Spaceborne Imaging Radar Symposium; April 28-30, 1986; Jet Propulsion Laboratory, Pasadena, CA. JPL Publication 86-26. p. 45-55.

Elachi, C., W.E. Brown, J.B. Cimino, T. Dixon, D.L. Evans, J.P. Ford, R.S. Saunders, C. Breed, H. Masursky, J.F. McCauley, G. Schaber, L. Dellwig, A. England, H. MacDonald, P. Martin-Kaye, and F. Sabins. 1982a. Shuttle Imaging Radar Experiment. Science 218:996-1003.

Elachi, C., T. Bicknell, R.L. Jordan, and C. Wu. 1982b. Spaceborne Synthetic-Aperture Imaging Radars--Applications, Techniques, and Technology. Proceedings IEEE 70:1174-1209.

English, J.T. 1984. Processing of Synthetic-Aperture-Radar Data. JPL New Technology Report, Case 4815, IR No. 15316. Jet Propulsion Laboratory, California Institute of Technology, Pasadena, CA. 10 p.

ERIM. 1986. Proposal: Investigation of Dual-Polarized, Multifrequency SAR Imagery for Forest Classification. Volume I: Technical and Management Proposal. ERIM Report 618108. Environmental Research Institute of Michigan, Ann Arbor, Michigan.

Ford, J.P., R.G. Blom, M.L. Bryan, M.I. Daily, T.H. Dixon, C. Elachi, and E.L. Xenos. 1980. Seasat Views North America, the Caribbean, and Western Europe with Imaging Radar. JPL Publication 80-67. Jet Propulsion Laboratory, Pasadena, CA. 141 p.

Ford, J.P., J.B. Cimino, and C. Elachi. 1983. Space Shuttle Columbia Views the World with Imaging Radar: The SIR-A Experiment. JPL Publication 82-95. Jet Propulsion Laboratory, Pasadena, CA. 179 p.

Ford, J.P., J.B. Cimino, B. Holt, M.R. Ruzek. 1986. Shuttle Imaging Radar Views the Earth from Challenger: the SIR-B Experiment. JPL Publication 86-29. Jet Propulsion Laboratory, Pasadena, CA. 135 p.

Freden, S.C., and F. Gordon, Jr. 1983. Landsat Satellites. In: R.N. Colwell, ed. Manual of Remote Sensing. Falls Church, VA: American Society of Photogrammetry. p. 517-570.

Fung, A.K., and F.T. Ulaby. 1983. Matter-Energy Interaction in the Microwave Region. R.N. Colwell, ed. Manual of Remote Sensing. Falls Church, VA: American Society of Photogrammetry. p. 115-164.

Gallagher, N.C., Jr., and G.L. Wise. 1981. A Theoretical Analysis of the Properties of Median Filters. IEEE Transactions on Acoustics, Speech, and Signal Processing. ASSP-29(6):1136-1141.

Gonzalez, R.C. 1986. Image Enhancement and Restoration. In: T.Y. Yang and K.S. Fu, eds. Handbook of Pattern Recognition and Image Processing. Academic Press, New York. p. 191-213.

Goodenough, D.G., B. Guindon, and P.M. Teillet. 1980. Correction of Synthetic Aperture Radar and Multispectral Scanner Data Sets. Proceedings 13th International Symposium Remote Sensing of Environment; April 23-27, 1980; Ann Arbor, MI. p. 259-270.

Guignard, J.P. 1981. Overview of Digital Processing of SAR Data. Proceedings 15th International Symposium Remote Sensing of Environment; May 11-15, 1981; Ann Arbor, MI. 1:179-194.

Heller, R.C., and J.J. Ulliman, eds. 1983. Forest Resource Assessments. In: R.N. Colwell, ed. Manual of Remote Sensing. Falls Church, VA: American Society of Photogrammetry. p. 2229-2324.

Henderson, F.M. 1985. Active Microwave Imaging Systems. In: R.K. Holz, ed. The Surveillant Science: Remote Sensing of the Environment. Second edition. New York: John Wiley & Sons. p. 234-247.

Heygster, G. 1982. Rank Filters in Digital Image Processing. Computer Graphics and Image Processing 19:148-164.

Hoffer, R.M. 1984. Microwave and Optical Remote Sensing of Forest Vegetation. The SIR-B Science Investigations Plan. JPL Publication 84-3. Jet Propulsion Laboratory, Pasadena, CA. p. 4:71-4:73.

Hoffer, R.M., D.F. Lozano-Garcia, D.D. Gillespie, P.W. Mueller, and M.J. Ruzek. 1986. Analysis of Multiple Incidence Angle SIR-B Data for Determining Forest Stand Characteristics. Proceedings of the Second Spaceborne Imaging Radar Symposium; April 28-30, 1986; Jet Propulsion Laboratory, Pasadena, CA. p. 159-164.

Hoffer, R.M., P.W. Mueller, D.F. Lozano-Garcia. 1985. Multiple Incidence Angle Shuttle Imaging Radar Data for Discriminating Forest Cover Types. Technical Papers of the ASCM-ASPRS Fall Convention; September 8-13, 1985, Indianapolis, IN. p. 476-485.

Holdermann, F., M. Bohner, M. Bargel, B. Bargel, and H. Kazmierczak. 1978. Review of Automatic Image Processing. Photogrammetria 34:225-258.

Huang, T.S. 1981. Introduction. In: T.S. Huang, ed. Two-Dimensional Digital Signal Processing II: Linear Filters. New York: Springer-Verlag. p. 1-9.

IBM. 1983. IBM 7350 Image Processing System: System Overview. IBM Publication GA19-5433-0, File No. 5370-06. International Business Machines Corporation.

Jenson, H., L.C. Graham, L.J. Porcello, and E.N. Leith. 1977. Side-Looking Airborne Radar. Scientific American 237(4):84-95.

JPL. 1986. Shuttle Image Radar-C Science Plan. JPL Publication 86-29. Jet Propulsion Laboratory, California Institute of Technology Pasadena, CA.

Justusson, B.I. 1981. Median Filtering: Statistical Properties. In: T.S. Huang, ed. Two-Dimensional Digital Signal Processing II: Transforms and Median Filters. New York: Springer-Verlag. p. 161-196.

Keyte, G.E., and M.J. Pearson. 1983. An Assessment of Seasat-SAR. In: Allan, T.D., ed. Satellite Microwave Remote Sensing. West Sussex, England: Ellis Horwood Limited. p. 187-207

Kirk, J.C., Jr. 1975. A Discussion of Digital Processing in Synthetic Aperture Radar. IEEE Transactions on Aerospace Electronic Systems AES-11:326-337.

Knowlton, D.J. 1982. Evaluation of Radar Data for Forest Cover Mapping. West Lafayette, IN: Purdue University. 132 p. Unpublished Master's thesis.

Knowlton, D.J., and R.M. Hoffer. 1981. Radar Imagery for Forest Cover Mapping. Proceedings 7th International Symposium Machine Processing Remotely Sensed Data; June 23-26, 1981; Purdue University, West Lafayette, IN. p. 626-632.

Knowlton, D.J., and R.M. Hoffer. 1983. Computer Analysis of X-Band Radar Data. Proceedings 9th International Symposium Machine Processing Remotely Sensed Data; June 21-23, 1983; Purdue University, West Lafayette, IN. p. 119-127.

Kovaly, J.J. 1977. High Resolution Radar Fundamentals. In: E. Brookner, ed. Radar Technology. Dedham, MA: Artech House, Inc. p. 239-249.

Krohn, M.D., N.M. Milton, and D.B. Segal. 1983. Seasat Synthetic Aperture Radar (SAR) Response to Lowland Vegetation Types in Eastern Maryland and Virginia. Journal of Geophysics Research 88(c36):1937-1952.

Landgrebe, D.A. 1978. The Quantitative Approach: Concept and Rationale. In: P.H. Swain and S.M. Davis, eds. Remote Sensing: The Quantitative Approach. New York: McGraw-Hill Book Co. p. 1-20.

Lang, R.H., A. Schneider, and R. Diaz. 1987. L-band Attenuation in a Trunk-Dominated Forest. Proceedings of the 1987 International Geoscience and Remote Sensing Symposium; May 18-21, 1987; University of Michigan, Ann Arbor, MI. II:815-820.

Latty, R.S. 1981. Computer-Based Forest Cover Classification Using Multispectral Scanner Data of Different Spatial Resolutions. LARS Technical Report 052081. Laboratory for Applications of Remote Sensing, Purdue University, West Lafayette, IN. 187 p.

Lillesand, T.M., and R.W. Kiefer. 1987. Remote Sensing and Image Interpretation. Second Edition. New York: John Wiley & Sons. 721 p.

Lillesand, T.M., and T.H.C. Lo. 1985. The Wisconsin Experimental Program for Satellite Image Mapping Using Thematic Mapper Data. Technical Papers of the ASPRS-ASCM Fall Convention; September 8-13, 1985; Indianapolis, IN. p. 757-769.

Lim, J.S. 1984. Image Enhancement. In: M.P. Ekstrom, ed. Digital Image Techniques. Orlando, FL: Academic Press, Inc. p. 1-51.

Liu, K.Y. 1982. A Comparative Study of Real-Time Spaceborne Synthetic Aperture Radar Processing Techniques. Digest 1982 International Geoscience and Remote Sensing Symposium; June 1-4, 1982; Munich, West Germany. Vol. 2, Sect. FA-1, p. 1.1-1.5

Long, M.W. 1975. Radar Reflectivity of Land and Sea. Lexington, MA: Lexington Books, D.C. Heath and Co. 336 p.

MacDonald, H.C., W.P. Waite, and J.S. Demarcke. 1980. Use of Seasat Satellite Radar Imagery for the Detection of Standing Water Beneath Forest Vegetation. Technical Papers American Society of Photogrammetry Fall Technical Meeting; October 7-10, 1980, Niagara Falls, NY. p. RS-3-B-1 to RS-2-B-13.

Moore, R.K. 1983. Imaging Radar Systems. R.N. Colwell, ed. Manual of Remote Sensing. Falls Church, VA: American Society of Photogrammetry. p. 429-474.

Morain, S.A. 1980. Use of Radar for Vegetation Analysis. Proceedings Seminar on Remote Sensing; October 1980, South Dakota State University, Brookings, SD. p. 40-58.

Morain, S.A., and D.S. Simonett. 1967. K-Band Radar in Vegetation Mapping. Photogrammetric Engineering 33(7):730-740.

Mueller, P.W., and R.M. Hoffer. 1985. Interpretation of Satellite and Aircraft L-band Synthetic Aperture Radar Imagery. Technical Papers of ASCM-ASPRS Fall Convention; September 8-13, 1985, Indianapolis, IN. p. 465-475.

Mueller, P.W., R.M. Hoffer, and J.E. Jacobson. 1985a. Evaluation of Landsat Thematic Mapper Data for Classifying Forest Lands. Proceedings Indiana Academy of Science Centennial Meeting; November 1-3, 1984; Butler University, Indianapolis, IN. 94:297-302.

Mueller, P.W., D.F. Lozano-Garcia, and R.M. Hoffer. 1985b. Interpretation of Forest Cover on Microwave and Optical Satellite Imagery. Proceedings Tenth William T. Pecora Memorial Remote Sensing Symposium; August 20-22, 1985; Colorado State University, Ft. Collins, CO. p. 578-592.

Murata, M., H. Aiba, K. Nakada, T. Tonoike, J. Komai, and H. Hirosawa. 1987. Experimental Results of L-band Microwave Penetration Properties of Trees. Proceedings of 1987 International Geoscience and Remote Sensing Symposium; May 18-21, 1987; University of Michigan, Ann Arbor, MI. II:815-820.

Narendra, P.M. 1981. A Separable Median Filter for Image Noise Smoothing. IEEE Transactions on Pattern Analysis and Machine Intelligence PAMI-3(1):20-29.

Nathan, K.S., and J.C. Curlander. 1987. Speckle Nosie Reduction of 1-Look SAR Imagery. Proceedings of 1987 International Geoscience and Remote Sensing Symposium; May 18-21, 1987; University of Michigan, Ann Arbor, MI. II:1457-1462.

NOAA. 1976. Climate of Lake City Florida. Climatography of the United States No. 20. National Oceanic and Atmospheric Administration, U.S. Department of Commerce. National Climatic Center, Asheville, NC. 4 p.

NOAA. 1984. Imaging Radar: A Companion for Landsat. In: Landsat Data Users Notes. National Oceanic and Atmospheric Administration, U.S. Dept. of Commerce. Sioux Falls, SD. Issue No. 32, p. 1-4.

Nodes, T.A., and N.C. Gallagher, Jr. 1982. Median Filters: Some Modifications and Their Properties. IEEE Transactions on Acoustics, Speech, and Signal Processing ASSP-30(5):739-746.

Nodes, T.A., and N.C. Gallagher, Jr. 1983. Two-Dimensional Root Structures and Convergence Properties of the Separable Median Filter. IEEE Transactions on Acoustics, Speech, and Signal Processing ASSP-31(6):1350-1365.

Ormsby, J.P., B.J. Blanchard, and A.J. Blanchard. 1985. Detection of Lowland Flooding Using Active Microwave Systems. Photogrammetric Engineering and Remote Sensing 51(3):317-328.

Peake, W.H., and T.L. Oliver. 1971. The Response of Terrestial Surfaces at Microwave Frequencies. Technical Report AFAl-TR-70-301. Ohio State University Electroscience Laboratory, Columbus, Ohio. 255 p.

Phillips, T.L., ed. 1973. LARSYS Version 3 User's Manual. Laboratory for Applications of Remote Sensing, Purdue University, West Lafayette, IN. 3 volumes.

Phillips, T.L., and P.H. Swain. 1978. Data-Processing Methods and Systems. In: P.H. Swain and S.M. Davis, eds. Remote Sensing: The Quantitative Approach. New York: McGraw-Hill Book Co. p. 188-226.

Pratt, W.K. 1978. Image Enhancement. In: Digital Image Processing. John Wiley & Sons, New York. p. 307-344.

Puri, H.S., and R.O. Vernon. 1959. Summary of the Geology of Florida and a Guidebook to the Classic Exposures. Special Publication No. 5. Florida State Board of Conservation, Geological Survey, Tallahassee, FL.

Raney, R.K. 1982. Processing Synthetic Aperture Radar Data. International Journal Remote Sensing 3(3):243-257.

Richards, J.A. 1986. Radar Signature Determination: Trends and Limitations. The Second Spaceborne Imaging Radar Symposium; April 28-30, 1986; Jet Propulsion Laboratory, Pasadena, CA. JPL Publication 86-26. p. 184-190.

Rosenfeld, A.R., and A.C. Kak. 1982. Enhancement. In: Digital Picture Processing. Second edition. New York: Academic Press. p. 209-267. (Volume 1)

Sabins, F.F., Jr. 1987. Radar Imagery. In: Remote Sensing: Principles and Interpretation. Second edition. San Francisco: W.H. Freeman and Company. p. 177-233.

Sader, S.A. 1987. Forest Biomass, Canopy Structure, and Species Composition Relationships with Multipolarization L-Band Synthetic Aperture Radar Data. Photogrammetric Engineering and Remote Sensing 53(2):193-202.

Skolnik, M.I. 1980. Introduction to Radar Systems. Second edition. New York: McGraw-Hill Book Co. 581 p.

Steel, R.G.D., and J.H. Torrie. 1980. Principles and Procedures of Statistics: A Biometrical Approach. Second edition. New York: McGraw-Hill Book Co. 633 p.

Swain, P.H. 1978. Fundamentals of Pattern Recognition. In: P.H. Swain and S.M. Davis, eds. Remote Sensing: The Quantitative Approach. New York: McGraw-Hill Book Co. p. 136-187.

Swain, P.H., and S.M. Davis, eds. 1978. Remote Sensing: The Quantitative Approach. New York: McGraw-Hill Book Co. 396 p.

Tomiyasu, K. 1978. Tutorial Review of Synthetic-Aperture Radar (SAR) with Applications to Imaging of the Ocean Surface. Proceedings IEEE 66(5):563-583.

Tukey, J.W. 1971. Exploratory Data Analysis. Reading, MA: Addison-Wesley Publishing Co.

Ulaby, F.T., P.P. Batlivala, and J.E. Bare. 1980. Crop Identification with L-Band Radar. Photogrammetric Engineering and Remote Sensing 46(1):101-105.

Ulaby, F.T., B. Brisco, M.C. Dobson, and S. Moezzi. 1983. Mapping and Monitoring Renewable Resources with Space SAR. Proceedings Spaceborne Imaging Radar Symposium; January 17-20, 1983; Jet Propulsion Laboratory, Pasadena, CA. JPL Publication 83-11; p. 76-78.

Ulaby, F.T., and M.C. Dobson. 1986. SIR-B Measurements and Modeling of Vegetation. Second Spaceborne Imaging Radar Symposium; April 28-30, 1986; Jet Propulsion Laboratory, Pasadena, CA. p. 191-200.

Ulaby, F.T., R.K. Moore, and A.K. Fung. 1981. Microwave Remote Sensing Fundamentals and Radiometry. Reading, MA: Addison-Wesley Publishing Co. 456 p. (Microwave Remote Sensing: Active and Passive; vol. I)

Ulaby, F.T., R.K. Moore, and A.K. Fung. 1982. Radar Remote Sensing and Surface Scattering and Emission Theory. Reading, MA: Addison-Wesley Publishing Co. 608 p. (Microwave Remote Sensing: Active and Passive; vol. II)

van Roessel, J.W., and R.C. de Godoy. 1974. SLAR Mosaics for Project RADAM. Photogrammetric Engineering 40(5):583-595.

Waite, W.P., H.C. MacDonald, V.H. Kaupp, and J.S. Demarcke. 1981. Wetland Mapping with Imaging Radar. Digest 1981 International Geoscience and Remote Sensing Symposium; June 8-10, 1981; Washington, D.C. p. 794-799.

Wu, S. 1983. Analysis of Synthetic Aperture Radar Data Acquired Over a Variety of Land Cover. Digest 1983 International Geoscience and Remote Sensing Symposium; August 31 - September 2, 1983, San Francisco. Vol. 2, Sect. FP-5, p. 6.1-6.6.

Wu, S. 1984. Analysis of Synthetic Aperture Radar Data Acquired Over a Variety of Land Cover. IEEE Transactions on Geoscience and Remote Sensing GE-22(6):550-557.

APPENDICES

Appendix A

LARSYS Multispectral Image Tapes (MIST)

LARSYS Run	Incidence Angle	MIST	Classification	Treatment	Tape/File
84028701	28	X		unfiltered and 29 treatments	2282/1
84028702	28	X		5 treatments	2282/2
84028703	45	X		unfiltered and 29 treatments	2282/3
84028704	45	X		5 treatments	2282/4
84028705	58	X		unfiltered and 29 treatments	2282/5
84028706	58	X		5 treatments	2282/6
84028711	28,45,58	X		unfiltered	2282/7
84028712	28,45,58	X		3SQMN1	2282/8
84028713	28,45,58	X		3SQMN2	2282/9
84028714	28,45,58	X		3SQMN3	2282/10
84028715	28,45,58	X		5SQMN1	2282/11
84028716	28,45,58	X		5SQMN2	2282/12
84028717	28,45,58	X		5SQMN3	2282/13
84028718	28,45,58	X		7SQMN1	2282/14
84028719	28,45,58	X		7SQMN2	2282/15
84028720	28,45,58	X		7SQMN3	2282/16
84028721	28,45,58	X		3SMN1	2282/17
84028722	28,45,58	X		3SMN2	2282/18
84028723	28,45,58	X		3SMN3	2282/19
84028724	28,45,58	X		5SMN1	2282/20
84028725	28,45,58	X		5SMN2	2282/21
84028726	28,45,58	X		5SMN3	2282/22
84028727	28,45,58	X		7SMN1	2282/23
84028728	28,45,58	X		7SMN2	2282/24
84028729	28,45,58	X		7SMN3	2282/25
84028730	28,45,58	X		3SQMD1	2282/26
84028730	28,45,58	X		3SQMD2	2282/27
84028731	28,45,58	X		3SQMD3	2282/28
84028732	28,45,58	X		3SRMD1	4016/1
84028733	28,45,58	X		3SRMD2	4016/2
84028734	28,45,58	X		5SRMD1	4016/3
84028735	28,45,58	X		5SRMD2	4016/4
84028736	28,45,58	X		7SRMD1	4016/5
84028737	28,45,58	X		7SRMD2	4016/6
84028738	28,45,58	X		9SRMD1	4016/7
84028739	28,45,58	X		9SRMD2	4016/8
84028740	28,45,58	X		3SQMD4	4016/9
84028741	28,45,58	X		3SRMD3	4016/10
84028742	28,45,58	X		5SRMD3	4016/11
84028743	28,45,58	X		7SRMD3	4016/12
84028744	28,45,58	X		9SRMD3	4016/13

LARSYS Classification Tapes

LARSYS Run	Incidence Angle	MIST	Classification	Treatment/Area Classified	Tape/File
84028711	28,45,58		X	unfiltered, 51 test fields	1367/1
84028712	28,45,58		X	3SQMN1, 51 test fields	1367/2
84028713	28,45,58		X	3SQMN2, 51 test fields	1367/3
84028714	28,45,58		X	3SQMN3, 51 test fields	1367/4
84028715	28,45,58		X	5SQMN1, 51 test fields	1367/5
84028716	28,45,58		X	5SQMN2, 51 test fields	1367/6
84028717	28,45,58		X	5SQMN3, 51 test fields	1367/7
84028718	28,45,58		X	7SQMN1, 51 test fields	1367/8
84028719	28,45,58		X	7SQMN2, 51 test fields	1367/9
84028720	28,45,58		X	7SQMN3, 51 test fields	1367/10
84028721	28,45,58		X	3SMN1, 51 test fields	1367/11
84028722	28,45,58		X	3SMN2, 51 test fields	1367/12
84028723	28,45,58		X	3SMN3, 51 test fields	1367/13
84028724	28,45,58		X	5SMN1, 51 test fields	1367/14
84028725	28,45,58		X	5SMN2, 51 test fields	1367/15
84028726	28,45,58		X	5SMN3, 51 test fields	1367/16
84028727	28,45,58		X	7SMN1, 51 test fields	1367/17
84028728	28,45,58		X	7SMN2, 51 test fields	1367/18
84028729	28,45,58		X	7SMN3, 51 test fields	1367/19
84028730	28,45,58		X	3SQMD1, 51 test fields	1367/20
84028731	28,45,58		X	3SQMD2, 51 test fields	1367/21
84028732	28,45,58		X	3SQMD3, 51 test fields	1367/22
84028733	28,45,58		X	3SRMD1, 51 test fields	1367/23
84028734	28,45,58		X	3SRMD2, 51 test fields	1367/24
84028735	28,45,58		X	5SRMD1, 51 test fields	1367/25
84028736	28,45,58		X	5SRMD2, 51 test fields	1367/26
84028737	28,45,58		X	7SRMD1, 51 test fields	1367/27
84028738	28,45,58		X	7SRMD2, 51 test fields	1367/28
84028739	28,45,58		X	9SRMD1, 51 test fields	1367/29
84028740	28,45,58		X	9SRMD2, 51 test fields	1367/30
84028741	28,45,58		X	3SQMD4, 51 test fields	1367/31
84028742	28,45,58		X	3SRMD3, 51 test fields	1367/32
84028743	28,45,58		X	5SRMD3, 51 test fields	1367/33
84028744	28,45,58		X	7SRMD3, 51 test fields	1367/34
84028745	28,45,58		X	9SRMD3, 51 test fields	1367/35
84028711	28,45,58		X	unfiltered, 256 x 256 subimage	1367/36
84028713	28,45,58		X	3SQMN2, 256 x 256 subimage	1367/37
84028716	28,45,58		X	5SQMN2, 256 x 256 subimage	1367/38
84028719	28,45,58		X	7SQMN2, 256 x 256 subimage	1367/39
84028722	28,45,58		X	3SMN2, 256 x 256 subimage	1367/40
84028725	28,45,58		X	5SMN2, 256 x 256 subimage	1367/41
84028728	28,45,58		X	7SMN2, 256 x 256 subimage	1367/42
84028730	28,45,58		X	3SQMD1, 256 x 256 subimage	1367/43
84028731	28,45,58		X	3SQMD2, 256 x 256 subimage	1367/44
84028732	28,45,58		X	3SQMD3, 256 x 256 subimage	1367/45
84028734	28,45,58		X	3SRMD2, 256 x 256 subimage	1367/46
84028736	28,45,58		X	5SRMD2, 256 x 256 subimage	1367/47
84028738	28,45,58		X	7SRMD2, 256 x 256 subimage	1367/48
84028727	28,45,58		X	7SMN1, 256 x 256 subimage	1367/49

CMS Backup Format Tapes

Tape/File	Contents
3414/1	TM and SIR-B (unfiltered), Hacienda BSQ format, 770 lines x 610 columns
3414/2	SIR-B (SQMN treatments), Hacienda BSQ format, 770 lines x 610 columns
3414/3	SIR-B (SQMD treatments), Hacienda BSQ format, 770 lines x 610 columns
3414/4	SIR-B (SMN treatments), Hacienda BSQ format, 770 lines x 610 columns
3414/5	SIR-B (SRMD treatments), Hacienda BSQ format, 770 lines x 610 columns
3414/6	SIR-B (SRMD treatments), Hacienda BSQ format, 770 lines x 610 columns
3414/7	SIR-B (SRMD treatments), Hacienda BSQ format, 770 lines x 610 columns
3414/8	SIR-B (SRMD treatments), Hacienda BSQ format, 770 lines x 610 columns
3414/9	SIR-B (28° treatments), Hacienda BSQ format, 770 lines x 610 columns
3414/10	SIR-B (SQMD and SRMD treatments), Hacienda BSQ format, 770 lines x 610 columns
3414/11	SIR-B (SMN treatments), Hacienda BSQ format, 770 lines x 610 columns
3414/12	SIR-B LARSYS stats
3414/13	SIR-B LARSYS stats, CC decks
3414/14	SIR-B LARSYS stats, classification results, cc decks
3414/15	SIR-B (28° treatments), Hacienda BSQ format, 770 lines x 610 columns
3414/16	SIR-B (28° treatments), Hacienda BSQ format, 256 lines x 256 columns
3414/17	SIR-B (45° treatments), Hacienda BSQ format, 256 lines x 256 columns
4153/1-34	Backup of MUELLER account, February 1987 - September 1987; filter work files

Appendix B

```
C  ***********************************************************************
C  *                                                                     *
C  *                        SEPARABLE RECURSIVE                          *
C  *                    MEDIAN FILTER FOR IMAGE DATA                     *
C  *                                                                     *
C  *                                                                     *
C  *                                                                     *
C  *   PROGRAMMERS:  PETER WENDT        ON THE ECN SYSTEM                *
C  *                 CECILIA WEBER      CONVERSION TO PUCC IBM SYSTEM    *
C  *                                    JULY 1985                        *
C  *                 PAUL MUELLER       REVISIONS TO HANDLE SKEWED       *
C  *                                    IMAGES; ADDED COMMENTS;          *
C  *                                    ADDED PROGRESS REPORTS           *
C  *                                    NOVEMBER  1985                   *
C  *                                                                     *
C  *                                                                     *
C  ***********************************************************************
C  ***********************************************************************
C  *                                                                     *
C  *   THIS PROGRAM MEDIAN FILTERS IMAGE DATA RECURSIVELY AND            *
C  *   SEPARABLY.  BOTH SKEWED (SURROUNDED BY ZEROS) AND SQUARED (NO     *
C  *   PADDING OF ZEROS) IMAGE DATA SETS CAN BE FILTERED.  HOWEVER,      *
C  *   WITHIN THE ACTUAL IMAGE DATA, THERE MUST BE NO ZEROS PRESENT      *
C  *   FOR THE FILTER TO OPERATE CORRECTLY.  THE DIAGRAM                 *
C  *   BELOW EXPLAINS THIS POINT GRAPHICALLY.  THE WINDOW                *
C  *   OF THE FILTER IS ONE DIMENSIONAL (1 BY LENGTH).  THIS             *
C  *   WINDOW PROGRESSES ALONG A ROW OR COLUMN OF DATA.  NEW             *
C  *   MEDIAN VALUES REPLACE THE ORIGINAL DATA VALUES (THUS, A           *
C  *   RECURSIVE FILTER).  THIS FILTER IS SEPARABLE IN THAT ROWS AND     *
C  *   COLUMNS ARE FILTERED SEPARATELY.  WHEN BOTH ROWS AND COLUMNS      *
C  *   ARE FILTERED, THE COLUMNS ARE FILTERED FIRST AND THEN THE         *
C  *   ROWS OF PREVIOUSLY FILTERED DATA ARE FILTERED.                    *
C  *                                                                     *
C  ***********************************************************************
C
C     ---       ----------------------
C      ¬        |000000000**000000000|  NOTE:  IT IS ASSUMED THAT NO
C      |        |00000000*    *000000|         0'S ARE CONTAINED WITHIN
C      |        |0000000*       *000|         THE ACTUAL IMAGE DATA,
C      |        |000000*          *|          WHEREAS FOR SKEWED IMAGES,
C               |00000*            *0|         THE AREAS OUTSIDE THE
C    IJ         |0000*   IMAGE    *00|         ACTUAL IMAGE ARE EXPECTED
C               |000*    DATA    *000|         TO BE REPRESENTED BY 0'S.
C      |        |00*            *0000|
C      |        |0*            *00000|
C      |        |0000*        *000000|
C      |        |0000000*    *0000000|
C      V        |0000000000**00000000|
C     ---       ----------------------
C                |<------  IK   ----->|
C
C
C * * * * * * * * * * * * * * * * * * * * * * * * * * * * * * * * * * * *
C
C  VARIABLE   TYPE       DESCRIPTION
C
C * * * * * * * * * * * * * * * * * * * * * * * * * * * * * * * * * * * *
C
```

```
C  COLS        INTEGER    SENTINEL VALUE INDICATING WHETHER ROWS SHOULD
C                         BE FILTERED (1) OR NOT FILTERED (0); FILTERING
C                         WILL PROGRESS FROM TOP TO BOTTOM ALONG EACH
C                         COLUMN OF DATA
C  DATAPT      INTEGER    NUMBER OF IMAGE DATA VALUES (PIXELS) FOR A LINE
C                         (ROW) OR COLUMN TO BE FILTERED
C  FIRST       INTEGER    COORDINATE OF FIRST IMAGE DATA VALUE CONTAINED
C                         IN A LINE (ROW) OR COLUMN TO BE FILTERED
C  FLTCOL      INTEGER    NUMBER OF COLUMNS FILTERED
C  FLTROW      INTEGER    NUMBER OF ROWS (LINES) FILTERED
C  FMTCHR      CHARACTER  FORMAT OF A LINE IN CHARACTER ARRAY
C  I           INTEGER    LOOP CONTROL VARIABLE CORRESPONDING TO LINES
C  IJ          INTEGER    NUMBER OF LINES (ROWS) IN INPUT DATA FILE
C  IK          INTEGER    NUMBER OF COLUMNS (LRECL) IN INPUT DATA FILE
C  IMAGE       CHARACTER  ARRAY REPRESENTING ORIGINAL IMAGE
C  INTRVL      INTEGER    NUMBER OF COLUMNS OR ROWS TO BE FILTERED
C                         BEFORE A REPORT ISSUED
C  IN          REAL       INCOMING PIXEL VALUE (UNFILTERED)
C  J           INTEGER    LOOP CONTROL VARIABLE CORRESPONDING TO COLUMNS
C  LAST        INTEGER    COORDIANTE OF LAST IMAGE DATA VALUE CONTAINED
C                         IN A LINE (ROW) OR COLUMN TO BE FILTERED
C  LENGTH      INTEGER    WINDOW WIDTH (2N + 1)
C  MEDIAN      CHARACTER  ARRAY REPRESENTING FILTERED IMAGE
C  N           INTEGER    N = (LENGTH -1)/2
C  OUT         REAL       PIXEL MEDIAN VALUE
C  RANK        INTEGER    VECTOR OF RANK VALUES CORRESPONDING TO PIXELS
C                         CURRENTLY IN THE FILTER WINDOW; DIMENSION OF
C                         RANK MUST BE GREATER THAN OR EQUAL TO LENGTH
C  REPORT      INTEGER    A PROGRESS REPORT ON NUMBER OF COLUMNS OR ROWS
C                         THAT HAVE BEEN FILTERED WILL BE DISPLAYED ON
C                         TERMINAL SCREEN IF "1" SPECIFIED; IT WILL NOT
C                         IF "0" SPECIFIED
C  ROWS        INTEGER    SENTINEL VALUE INDICATING WHETHER ROWS SHOULD
C                         BE FILTERED (1) OR NOT FILTERED (0); FILTERING
C                         WILL PROGRESS FROM LEFT TO RIGHT ALONG EACH
C                         ROW
C  X           REAL       VECTOR USED IN SUBROUTINE; DIMENSION MUST BE
C                         GREATER THAN OR EQUAL TO LENGTH
C
C * * * * * * * * * * * * * * * * * * * * * * * * * * * * * * * * * * * *
C* * * * * * * * * * * * * * * * * * * * * * * * * * * * * * * * * * * * *
C
C NOTES:  TO CUSTOMIZE THIS PROGRAM TO YOUR IMAGE, THE FOLLOWING TWO
C         PARAMETER STATEMENTS MUST BE CHANGED WITHIN THIS PROGRAM. THE
C         PARAMETERS IJ AND IK MUST BE CHANGED TO MATCH THE NUMBER OF
C         ROWS AND COLUMNS, RESPECTIVELY, IN YOUR INPUT IMAGE.  CHANGE
C         IJ AND IK IN THE PARAMETER STATEMENT FOLLOWING THIS COMMENT
C         BLOCK.  SINCE THE CHARACTER VARIABLE 'FMTCHR' IS USED TO
C         REPRESENT THE FORMAT OF AN LINE (ROW) OF IMAGE DATA, THIS
C         VARIABLE MUST BE CHANGED TO MATCH THE LINE LENGTH (NUMBER
C         OF COLUMNS WHICH IS EQUAL TO IK).  SINCE THE IMAGE ARRAYS
C         ARE CHARACTER ARRAYS, EACH DATA POINT IS OF THE FORMAT OF
C         'A1' ACCORDING TO FORTRAN SYNTAX.  THEREFORE, THERE ARE AS
C         MANY A1'S AS THERE ARE DATA POINTS.  HOWEVER, IN FORTRAN,
C         ONE CANNOT SIMPLY SAY 1024A1 IF THERE ARE 1024 DATA POINTS
C         (COLUMNS, OR IK) IN AN IMAGE LINE.  THE MAXIMUM REPEAT FACTOR
C         IS 255 (I.E., 255A1), SO ONE MUST WRITE THE FORMAT AS
C         A STRING OF CHARACTER FORMATS WHERE THE REPEAT FACTORS
```

```
C         WILL TOTAL THE NUMBER OF DATA POINTS (COLUMNS) IN THE LINE.
C         FOR EXAMPLE:  IF EACH LINE CONSISTS OF 1024 DATA POINTS,
C                       MEANING THAT IK=1024, THEN THE FOLLOWING
C                       PARAMETER STATEMENT SHOULD BE USED
C
C           PARAMETER (FMTCHR = '(255A1,255A1,255A1,255A1,4A1)')
C
C         THIS PARAMETER STATEMENT IS WITHIN THE VARIABLE DECLARATIONS
C         SECTION OF THE PROGRAM.
C
C
C         ALSO NOTE THAT THE TOTAL LENGTH OF FMTCHR CANNOT HAVE A
C         LENGTH OF MORE THAN 60; IF IT DOES, THEN ITS DECLARATION
C         STATEMENT MUST BE CHANGED ACCORDINGLY.
C
C
C         TO RUN THIS PROGRAM, MAKE THE ABOVE MENTIONED CORRECTIONS
C         TO THE PROGRAM CODE, AND THEN EDIT THE FILE
C         'MEDSKEW EXEC' AND CHANGE THE FILEDEF'S ACCORDING TO
C         YOUR INPUT AND OUTPUT FILE NAMES AND DIMENSIONS.  UNIT 2
C         REFERS TO THE INPUT, WHILE UNIT 3 REFERS TO THE OUTPUT FILE.
C
C         THE DIMENSION OF THE VECTORS 'RANK' AND 'X' MUST BE GREATER
C         THAN THE ACTUAL WINDOW SIZE OF THE FILTER BEING USED.  THUS,
C         THEY SHOULD NOT HAVE TO BE REDIMENSIONED UNLESS THE WINDOW
C         IS GREATER THAN 201.
C
C * * * * * * * * * * * * * * * * * * * * * * * * * * * * * * * * * * *
C* * * * * * * * * * * * * * * * * * * * * * * * * * * * * * * * * * *
C
C                         *****************
C                         * MAIN PROGRAM  *
C                         *****************
C
C * * * * * * * * * * * * * * * * * * * * * * * * * * * * * * * * * * *
C
C     VARIABLE DECLARATIONS
C
C * * * * * * * * * * * * * * * * * * * * * * * * * * * * * * * * * * *
C
      PARAMETER (IJ=770,IK=610)
      REAL IN,OUT,X(201)
      INTEGER RANK(201)
      INTEGER ROWS,COLS,LENGTH,FLTCOL,FLTROW,FIRST,LAST,DATAPT,REPORT
      CHARACTER*1 IMAGE(IJ,IK),MEDIAN(IJ,IK)
      CHARACTER*60 FMTCHR
C
C     ***********CHANGE THE FOLLOWING PARAMETER TO MATCH IK************
C       FORMAT OF IMAGE (CHARACTER) ARRAYS BASED ON NUMBER OF COLUMNS
C         ===>  SEE THE NOTES SECTION ABOVE THE PROGRAM CODE  <===
C
      PARAMETER (FMTCHR = '(255A1,255A1,100A1)')
C
C * * * * * * * * * * * * * * * * * * * * * * * * * * * * * * * * * * *
C
C     READ IN THE IMAGE AND INITIALIZE THE MEDIAN ARRAY
C
C * * * * * * * * * * * * * * * * * * * * * * * * * * * * * * * * * * *
```

```
C
      OPEN(UNIT=2)
      DO 100 I=1,IJ
            READ(2,FMT=FMTCHR) (IMAGE(I,J),J=1,IK)
            DO 90 J = 1, IK
                 MEDIAN(I,J)=CHAR(0)
 90         CONTINUE
100   CONTINUE
      CLOSE(2)
C
C * * * * * * * * * * * * * * * * * * * * * * * * * * * * * * * * * * * *
C
C     READ IN THE WINDOW WIDTH FROM USER INPUT
C
C * * * * * * * * * * * * * * * * * * * * * * * * * * * * * * * * * * * *
C
      WRITE(16,140)
140   FORMAT(1X,'ENTER WINDOW WIDTH XX   (IT MUST BE AN ODD NUMBER)')
      READ (15,150) LENGTH
150   FORMAT (I2)
C
C * * * * * * * * * * * * * * * * * * * * * * * * * * * * * * * * * * * *
C
C     DETERMINE IF ROWS AND/OR COLUMNS SHOULD BE FILTERED SEPARABLY
C
C * * * * * * * * * * * * * * * * * * * * * * * * * * * * * * * * * * * *
C
      WRITE(16,160)
160   FORMAT(1X,'SHOULD ROWS AND/OR COLUMNS BE FILTERED?')
      WRITE(16,170)
170   FORMAT(1X,'ENTER ROWS AND COLUMNS XX')
      WRITE(16,171)
171   FORMAT(6X,'WHERE:  10  INDICATES ROWS ONLY WILL BE FILTERED')
      WRITE(16,172)
172   FORMAT(14X,'01  INDICATES COLUMNS ONLY WILL BE FILTERED')
      WRITE(16,173)
173   FORMAT(14X,'11  INDICATES BOTH ROWS AND COLUMNS WILL BE FILTERED',
     2  ' SEPARABLY'/22X,'NOTE THAT WHEN 11 IS SPECIFIED'/22X,'COLUMNS',
     3  ' WILL BE FILTERED FIRST')
      READ (15,175) ROWS,COLS
175   FORMAT (I1,I1)
C
C * * * * * * * * * * * * * * * * * * * * * * * * * * * * * * * * * * * *
C
C     QUERY IF PROGRESS REPORTS WANTED
C
C * * * * * * * * * * * * * * * * * * * * * * * * * * * * * * * * * * * *
C
      WRITE(16,180)
180   FORMAT(1X,'WOULD YOU LIKE A PERIODIC PROGRESS REPORT ON THE ',
     Z    'FILTRATION PROCESS?')
      WRITE(16,181)
181   FORMAT(6X,'ENTER A 0 FOR NO REPORT'/9X,'OR A 1 FOR A REPORT')
      READ(15,182) REPORT
182   FORMAT(I1)
      IF (REPORT .EQ. 1) THEN
           WRITE(16,183)
183        FORMAT(6X,'ENTER INTEGER (I3) INTERVAL FOR REPORTS TO BE',
```

```
     Z        ' ISSUED'/9X, '(EVERY XXX ROWS OR COLUMNS)')
              READ(15,184) INTRVL
184           FORMAT(I3)
          ENDIF
          N=LENGTH/2
          IF (COLS .EQ. 0) GO TO 330
C
C * * * * * * * * * * * * * * * * * * * * * * * * * * * * * * * * * * * *
C
C         MEDIAN FILTER THE COLUMNS (TOP TO BOTTOM ON EACH COLUMN)
C
C * * * * * * * * * * * * * * * * * * * * * * * * * * * * * * * * * * * *
C
          FLTCOL = 0
          DO 240 J=1,IK
C
C * * * * * * * * * * * * * * * * * * * * * * * * * * * * * * * * * * * *
C
C       ASSIGN THE FIRST IMAGE DATA VALUE LINE COORDINATE TO FIRST AND
C       ASSIGN THE LAST DATA VALUE COORDINATE TO LAST
C
C * * * * * * * * * * * * * * * * * * * * * * * * * * * * * * * * * * * *
C
              DO 185 I = 1, IJ
                   IF (ICHAR(IMAGE(I,J)) .GT. 0) GO TO 187
185           CONTINUE
187           FIRST = I
              DATAPT = 0
              IF (FIRST .EQ. IJ) THEN
                   LAST = FIRST
              ELSE
                   DO 190 I = FIRST, IJ
                        IF (ICHAR(IMAGE(I,J)) .EQ. 0)  THEN
                             LAST = I - 1
                             GO TO 195
                        ELSE
                             DATAPT = DATAPT + 1
                        ENDIF
190                CONTINUE
C
C                  * * * * * * * * * * * * * * * * * * * * * * * * * * *
C
C                  CHECK TO SEE IF IJ WAS REACHED AND IS THE LAST IMAGE
C                  PIXEL
C
C                  * * * * * * * * * * * * * * * * * * * * * * * * * * *
C
                   IF(I-1 .EQ. IJ) LAST = IJ
              ENDIF
C
C             * * * * * * * * * * * * * * * * * * * * * * * * * * * * * *
C
C             DETERMINE IF THERE ARE ENOUGH PIXELS TO FILTER; IF NOT, KEEP
C             SAME DATA VALUES
C
C             * * * * * * * * * * * * * * * * * * * * * * * * * * * * * *
C
195           IF ((LAST - FIRST) .LT. LENGTH-1) THEN
```

```
                DO 197 I = FIRST, LAST
                     MEDIAN(I,J) = IMAGE(I,J)
197             CONTINUE
                WRITE(16,199) DATAPT
199             FORMAT ('COLUMN NOT FILTERED.  ONLY ',I6,' IMAGE ',
     Z               'PIXELS IN COLUMN.')
           ELSE
C
C               * * * * * * * * * * * * * * * * * * * * * * * * * * * * *
C
C               INITIALIZE THE WINDOW  (PADDING AT START OF EACH COLUMN)
C
C               * * * * * * * * * * * * * * * * * * * * * * * * * * * * *
C
                DO 200 K= 1, LENGTH
                     RANK(K)=K
                     X(K)=FLOAT(ICHAR(IMAGE(FIRST, J)))
200             CONTINUE
                DO 210 K=FIRST, N+FIRST-1
                     IN=FLOAT(ICHAR(IMAGE(K,J)))
                     CALL RECURS (N,IN,OUT,RANK,X)
210             CONTINUE
C
C               * * * * * * * * * * * * * * * * * * * * * * * * * * * * *
C
C               FILTER A COLUMN
C
C               * * * * * * * * * * * * * * * * * * * * * * * * * * * * *
C
                DO 230 K=FIRST, LAST
                     IF (K .GE. LAST-N) THEN
                        IN=FLOAT(ICHAR(IMAGE(LAST,J)))
                     ELSE
                        IN=FLOAT(ICHAR(IMAGE(K+N,J)))
                     END IF
                     CALL RECURS (N,IN,OUT,RANK,X)
                     MEDIAN(K,J)=CHAR(INT(OUT))
230             CONTINUE
C
C               * * * * * * * * * * * * * * * * * * * * * * * * * * * * *
C
C               GIVE A PROGRESS REPORT IF REQUESTED
C
C               * * * * * * * * * * * * * * * * * * * * * * * * * * * * *
C
                IF (REPORT .EQ. 1) THEN
                     FLTCOL = FLTCOL + 1
                     IF (MOD(FLTCOL,INTRVL) .EQ. 0) THEN
                          WRITE(16,235) FLTCOL
235                       FORMAT(1X,I6,1X,'COLUMNS HAVE BEEN FILTERED')
                     ENDIF
                ENDIF
           ENDIF
240   CONTINUE
C
C * * * * * * * * * * * * * * * * * * * * * * * * * * * * * * * * * * * * *
C
C     IF ROWS NOT TO BE FILTERED, SKIP TO WRITING OF FILTERED DATA
```

```
C
C * * * * * * * * * * * * * * * * * * * * * * * * * * * * * * * * * * * *
C
      IF (ROWS .EQ. 0) GO TO 489
C
C * * * * * * * * * * * * * * * * * * * * * * * * * * * * * * * * * * * *
C
C     READ MEDIAN ARRAY INTO IMAGE ARRAY
C
C * * * * * * * * * * * * * * * * * * * * * * * * * * * * * * * * * * * *
C
      DO 250 I=1,IJ
           DO 250 J=1,IK
                IMAGE(I,J)=MEDIAN(I,J)
250   CONTINUE
C
C * * * * * * * * * * * * * * * * * * * * * * * * * * * * * * * * * * * *
C
C     MEDIAN FILTER THE ROWS (LEFT TO RIGHT ON EACH ROW)
C
C * * * * * * * * * * * * * * * * * * * * * * * * * * * * * * * * * * * *
C
330   IF (ROWS .EQ. 0) GO TO 489
      FLTROW = 0
      DO 450 I=1,IJ
C
C     * * * * * * * * * * * * * * * * * * * * * * * * * * * * * * * * * * *
C
C     ASSIGN THE FIRST IMAGE DATA VALUE COLUMN COORDINATE TO FIRST AND
C     ASSIGN THE LAST IMAGE DATA VALUE COORDINATE TO LAST
C
C     * * * * * * * * * * * * * * * * * * * * * * * * * * * * * * * * * * *
C
           DO 340 J = 1, IK
                IF (ICHAR(IMAGE(I,J)) .GT. 0) GO TO 343
340        CONTINUE
343        FIRST = J
           DATAPT = 0
           IF (FIRST .EQ. IK) THEN
                LAST = FIRST
           ELSE
                DO 346 J = FIRST, IK
                     IF (ICHAR(IMAGE(I,J)) .EQ. 0) THEN
                          LAST = J - 1
                          GO TO 348
                     ELSE
                          DATAPT = DATAPT + 1
                     ENDIF
346             CONTINUE
C
C               * * * * * * * * * * * * * * * * * * * * * * * * * * * * *
C
C               CHECK TO SEE IF IK WAS REACHED AND IS THE LAST IMAGE
C               PIXEL
C
C               * * * * * * * * * * * * * * * * * * * * * * * * * * * * *
C
                IF (J-1 .EQ. IK) LAST = IK
```

```
      ENDIF
C
C     * * * * * * * * * * * * * * * * * * * * * * * * * * * * * * * *
C
C     DETERMINE IF THERE ARE ENOUGH PIXELS TO FILTER; IF NOT, KEEP
C     SAME DATA VALUES
C
C     * * * * * * * * * * * * * * * * * * * * * * * * * * * * * * * *
C
348   IF ((LAST - FIRST) .LT. LENGTH-1) THEN
        DO 349 J = FIRST, LAST
          MEDIAN(I,J) = IMAGE(I,J)
349     CONTINUE
        WRITE(16,360) DATAPT
360     FORMAT ('ROW NOT FILTERED.  ONLY ', I6, ' IMAGE PIXELS',
     Z      ' IN ROW.')
      ELSE
C
C       * * * * * * * * * * * * * * * * * * * * * * * * * * * * * *
C
C       INITIALIZE THE WINDOW (PADDING AT START OF EACH ROW)
C
C       * * * * * * * * * * * * * * * * * * * * * * * * * * * * * *
C
        DO 380 K=1, LENGTH
          RANK(K)=K
          X(K)=FLOAT(ICHAR(IMAGE(I, FIRST)))
380     CONTINUE
        DO 400 K=FIRST, N+FIRST-1
          IN=FLOAT(ICHAR(IMAGE(I,K)))
          CALL RECURS (N,IN,OUT,RANK,X)
400     CONTINUE
C
C       * * * * * * * * * * * * * * * * * * * * * * * * * * * * * *
C
C       FILTER A ROW
C
C       * * * * * * * * * * * * * * * * * * * * * * * * * * * * * *
C
        DO 440 K=FIRST, LAST
          IF (K .GE. LAST-N) THEN
            IN=FLOAT(ICHAR(IMAGE(I,LAST)))
          ELSE
            IN=FLOAT(ICHAR(IMAGE(I,K+N)))
          END IF
          CALL RECURS (N,IN,OUT,RANK,X)
          MEDIAN(I,K)=CHAR(INT(OUT))
440     CONTINUE
C
C       * * * * * * * * * * * * * * * * * * * * * * * * * * * * * *
C
C       GIVE A PROGRESS REPORT IF REQUESTED
C
C       * * * * * * * * * * * * * * * * * * * * * * * * * * * * * *
C
        IF (REPORT .EQ. 1) THEN
          FLTROW = FLTROW + 1
          IF (MOD(FLTROW, INTRVL) .EQ. 0) THEN
```

```
                        WRITE(16,445) FLTROW
445                     FORMAT(1X, I6, 1X, 'ROWS HAVE BEEN FILTERED')
                    ENDIF
                ENDIF
            ENDIF
450   CONTINUE
C
C * * * * * * * * * * * * * * * * * * * * * * * * * * * * * * * * * * * *
C
C     WRITE THE MEDIAN IMAGE
C
C * * * * * * * * * * * * * * * * * * * * * * * * * * * * * * * * * * * *
C
489   OPEN(UNIT=3)
      DO 500 I=1,IJ
         WRITE(3,FMT=FMTCHR)(MEDIAN(I,J),J=1,IK)
500   CONTINUE
      CLOSE(3)
      STOP
      END
C
C
C     RECURSIVE MEDIAN FILTER SUBROUTINE
C
      SUBROUTINE RECURS (N,IN,OUT,RANK,X)
      REAL IN,OUT,X(201)
      INTEGER N,WW,RO,RANK(201)
C
C     SET THE WINDOW WIDTH
C
      WW=2*N+1
C
C     INCREMENT RANKS AND CALCULATE THE RANK OF THE INCOMING SAMPLE
C
      RO=1
      N1=2*N
      DO 10 I=1,N1
         IF (X(WW) .LT. X(I)) RANK(I)=RANK(I)-1
         IF (X(WW) .EQ. X(I) .AND. RANK(WW) .LT. RANK(I)) THEN
              RANK(I)=RANK(I)-1
         ENDIF
         IF (IN .GE. X(I)) THEN
              RO=RO+1
         ELSE
              RANK(I)=RANK(I)+1
         END IF
10    CONTINUE
C
C     UPDATE SEQUENCES
C
      DO 15 I=1,N1
         X(WW-I+1)=X(WW-I)
         RANK(WW-I+1)=RANK(WW-I)
15    CONTINUE
C
      X(1)=IN
      RANK(1)=RO
C
```

```
C      FIND THE OUTPUT SAMPLE
C
       DO 20 I=1,WW
          IF (RANK(I) .EQ. N+1) OUT=X(I)
20     CONTINUE
C
C      RECURSION - REPLACE THE CENTRAL (TIME) SAMPLE IN THE WINDOW
C      BY THE MEDIAN
C
C      *****FOR A NON-RECURSIVE FILTER, DISCARD THIS SECTION*****
C
       RO=1
       DO 25 I=1,WW
          IF (I .EQ. N+1) GO TO 25
          IF (X(N+1) .LT. X(I)) RANK(I)=RANK(I)-1
          IF (X(N+1) .EQ. X(I) .AND. RANK(N+1) .LT. RANK(I)) THEN
               RANK(I)=RANK(I)-1
          ENDIF
          IF (OUT .GE. X(I)) THEN
               RO=RO+1
          ELSE
               RANK(I)=RANK(I)+1
          ENDIF
25     CONTINUE
C
       RANK(N+1)=RO
       X(N+1)=OUT
       RETURN
       END
```